

Voltage Oriented Control of Three-Phase Boost PWM Converters

Design, simulation and implementation of a 3-phase boost battery charger

Master of Science Thesis in Electric Power Engineering

Sylvain LECHAT SANJUAN

Department of Energy and Environment
Division of Electric Power Engineering
CHALMERS UNIVERSITY OF TECHNOLOGY
Göteborg, Sweden, 2010

Voltage Oriented Control of Three-Phase Boost PWM Converters

Design, simulation and implementation of a 3-phase boost battery
charger

By

Sylvain LECHAT SANJUAN

Supervisor

Saeid Haghbin, PhD Student

Examiner

Ola Carlson, Associate Professor

Department of Energy and Environment
Division of Electric Power Engineering
CHALMERS UNIVERSITY OF TECHNOLOGY
Göteborg, Sweden, 2010

VOLTAGE ORIENTED CONTROL OF THREE-PHASE BOOST PWM CONVERTERS
DESIGN, SIMULATION AND IMPLEMENTATION OF A 3-PHASE BOOST BATTERY CHARGER
SYLVAIN LECHAT SANJUAN

© SYLVAIN LECHAT SANJUAN, 2010

Department of Energy and Environment
Division of Electric Power Engineering
CHALMERS UNIVERSITY OF TECHNOLOGY
SE-412 96 Göteborg
Sweden
Telephone : + 46 (0)31-772 1000

Göteborg, 2010

ABSTRACT

Voltage Oriented Control of Three-Phase Boost PWM Converters

Design, simulation and implementation of a 3-phase boost battery charger

Sylvain LECHAT SANJUAN

Department of Energy and Environment

Division of Electric Power Engineering

Chalmers University of Technology

In a plug-in hybrid electric vehicle, the utility grid will charge the vehicle battery through the battery charger. For a three-phase grid supply voltage, three-phase boost rectifiers are a commonly used scheme for chargers. Bi-directional power transfer capability and unit power factor operation are interesting features that can be achieved by the method proposed in this thesis. Different control strategies have been proposed to control the converter. The Voltage Oriented Control is one of these methods based on high performance dq-coordinate controllers.

The Voltage Oriented Control method for a three-phase boost rectifier have been designed and simulated. Moreover, an implementation of the system has been started. The system simulation has been done using Matlab/Simulink software. Feedforward decoupled current controller has been designed along with Pulse Width Modulation scheme to control the battery charging. The controller, that is, a current controller and a DC-link voltage controller, have been designed using a method called Internal Model Control. The simulation results have been presented and the control system performance evaluated in response to the load and dc-bus voltage step changes. dSpace system have been used for practical implementation. The system is directly running a Simulink model as a controller. The Simulink files have been developed for this purpose. A brief explanation of the system configuration has been provided for the experimental system.

Key words : battery charger, decoupled controller, dSpace, Internal Model Control (IMC), Pulse Width Modulation (PWM), three-phase boost PWM rectifier, Voltage Oriented Control (VOC).

ACKNOWLEDGEMENTS

First of all, I would like to express my sincere gratitude to Saeid Haghbin, my supervisor, for his total availability during the thesis, for his understanding, technical guidance and friendliness.

My gratitude also goes to Ola Carlson, for giving me the opportunity to do this Master's Thesis work in the Electric Power division of Chalmers University of Technology.

A very special thanks to Stefan Lundberg and Massimo Bongiorno, for all help, their availability, technical guidance and nice discussions.

Thanks to all the employees and staff in the division who made my thesis work such a pleasant stay. Furthermore, I would like to thank Magnus Ellsen for his availability and help for laboratory set-up.

Finally, many thanks to my fellow Master's Thesis students with Saman Babaei, Thinley Gyeltshen, Francisco Montes Venero, Peng Hou, Sergio Garcia Collino and Johan Andersson. Thanks for their support, guidance and nice discussions. They also made my stay in Sweden an unforgettable experience.

*Sylvain Lechat Sanjuan
Göteborg, Sweden
Wednesday, June 16, 2010*

LIST OF SYMBOLS, SUPERSCRIPTS, SUBSCRIPTS AND ABBREVIATIONS

ABBREVIATIONS

DPC	Direct Power Control
IC	Initial Condition
IGBT	Insulated Gate Bipolar Transistor
IM	Induction Machine
IMC	Internal Model Control
PWM	Pulse Width Modulation
PLL	Phase Locked Loop
PMSM	Permanent Magnet Synchronous Machine
SVM	Space Vector Modulation
VF-DPC	Virtual Flux Direct Power Control
VFOC	Virtual Flux Oriented Control
VOC	Voltage Oriented Control

SYMBOL

U	Line voltage
E	Line voltage
E_g	Grid phase-to-ground voltage amplitude
E_d and E_q	dq-coordinates of line or grid voltage (amplitude invariant transformation)
V_{pcc}	Voltage at the point of common connection
U_s	Converter voltage
V	Converter voltage
V^*	Converter voltage reference from current controller
V_{LL}	Line-to-Line voltage
V_{LN}	Line-to-Neutral voltage
$V_{LN(peak)}$	Amplitude of Line-to-Neutral voltage
E_m	Amplitude of Line-to-Neutral voltage
v_{dc}, V_{DC}	DC-link voltage
v_c	Voltage across AC-side capacitor
i_L	Line current
i	Line current
i_{conv}	Line current, current flowing into the converter
i_{DC}	DC-link current
i_{LOAD}	Load current
R	Line resistance
L	Line inductance
C	DC-link capacitor
R_g	Grid resistance
L_g	Grid inductance
R_b	Breaker SW1 resistance
C_{ac}	AC capacitor
C_{dc}	DC capacitor
R_{LOAD}	Load resistance
R_{LOAD_TEMP}	Temporary load resistance
θ	Voltage angle
F_S	Sampling frequency
T_S	Sampling time

F_{SW}	Switching frequency
F_C	Triangular wave frequency (PWM)
$F_{Triangle}$	Triangular wave frequency (PWM)
α_i	Current controller bandwidth (rad/s)
α_v	Voltage controller bandwidth (rad/s)
G_a	Active damping conductance
Ki_v	Voltage controller integrator coefficient
Kp_v	Voltage controller proportional coefficient
Ki_i	Current controller integrator coefficient
Kp_i	Current controller proportional coefficient
γ_1	PLL Integrator coefficient
γ_2	PLL proportional coefficient
ρ	PLL bandwidth
$F(s)$	Controller transfer function (PI)
$G(s)$	Process transfer function
$L(s)$	Open-loop transfer function
$S(s)$	Closed-loop transfer function
W	v_{dc}^2
P_g	Grid power
P_{load}	Load power

SUPERSCRIPT, ACCENTS

$\hat{E}_g, \hat{C}, \hat{L}, \hat{R}$	Estimated values
x^s	Space vector
x^{dq}	dq-coordinate system
x^*	Reference value of x

SUBSCRIPT, UNDERLINE

x_{dq}	dq-coordinate system
\underline{x}	dq-coordinate system, complex value

TABLE OF CONTENTS

ABSTRACT	IV
ACKNOWLEDGEMENTS	V
LIST OF SYMBOLS, SUPERSCRIPTS, SUBSCRIPTS AND ABBREVIATIONS	VI
1 INTRODUCTION AND SCOPE	1
2 THREE PHASE CONTROLLED RECTIFIERS	3
2.1 Introduction	3
2.2 Universal bridge topology	5
2.2.1 Steady state operation	5
2.2.2 Mathematical model	5
2.2.3 Limitations	9
2.3 Control strategies	11
2.3.1 Introduction	11
2.3.2 Direct Power Control and Virtual Flux Direct Power Control	12
2.3.3 Voltage and Virtual Flux Oriented Control	13
2.3.4 Comparison and discussion	14
2.4 Pulse Width Modulation	15
2.4.1 Sinusoidal PWM	15
2.4.2 Digital implementation	16
2.4.3 Dead time effect	16
3 VOLTAGE ORIENTED CONTROL – SIMULATION	18
3.1 Introduction – References chosen	18
3.2 System block diagram	19
3.3 PWM Simulation	20
3.3.1 Simulink implementation of PWM	20
3.4 Current controller	22
3.4.1 Internal Model Control	22
3.4.2 Synchronous PI control	22
3.4.3 Design of the synchronous PI controller	23
3.4.4 Active damping, voltage saturation, anti-windup	25
3.4.5 Current controller simulation	27
3.5 DC-link voltage controller	30
3.5.1 DC-link model and linearization	30
3.5.2 Design of voltage controller	30
3.5.3 Voltage saturation, anti-windup, active damping	31
3.5.4 Voltage controller simulation	33
3.5.5 Simulation with current controller	36
3.5.6 Controller improvements	39
3.6 Stability analysis	41

3.6.1	Current controller	41
3.6.2	Voltage controller	41
3.6.3	Complete controller	42
3.6.4	Nyquist and Bode diagram	43
3.6.5	Conclusion	46
3.7	Phase Locked Loop (PLL)	48
3.7.1	Design	48
3.7.2	Simulations	48
3.7.3	Improvements and conclusion	52
3.8	Grid modeling	53
3.9	Grid connected converter simulation	55
3.9.1	Simulation steps, Simulink block diagram	55
3.9.2	Verification	56
3.9.3	Simulation results	58
4	VOLTAGE ORIENTED CONTROL – IMPLEMENTATION	63
4.1	Block diagram	63
4.2	Principle	63
4.3	Simulink model modification	64
4.4	Running an experiment	67
5	CONCLUSIONS AND FUTURE WORK	70
	REFERENCES	71
	APPENDICES	74
A.	Three-phase system – Coordinate transformations	74
A.1	Voltage and current definition	74
A.2	Equivalent two-phase system, $\alpha\beta$ -transformation (Clarke)	74
A.3	Synchronous coordinate, dq-transformation (Park)	75
A.4	Simulation	76
A.5	Impedance in synchronous coordinates	77
B.	Voltage and current control, continuous simulation	79
B.1	Simulink current control tests – Block diagram	79
B.2	Continuous voltage controller, simulation with saturation, anti-windup, active damping	80
C.	Digital simulation	81
D.	Voltage and current control, discrete time simulation	82
E.	Stability analysis cont.	83
E.1	Simulations	83
F.	Grid connected converter simulation cont.	91
F.1	Data and simulations	91
F.2	Matlab Script (Vdc Step)	102
G.	Implementation	104

1 INTRODUCTION AND SCOPE

PHD PROJECT

The master thesis is part of a PHD project titled *“Integrated charger for plug-in Hybrid Electric Vehicles”*.

The PHD project is funded by the Swedish Hybrid Vehicle Centre (SHC¹) and is done by the PHD student Saeid Haghbin under supervision of Associate Professor Ola Carlson. Moreover, Assistant Professor Sonja Lundmark is the project co-supervisor.

The scope of the PhD project is :

- Investigating and evaluating existing plug-in HEV’s in general and especially the charging systems. This collection of available information also includes listing all as well as the most interesting parameters of the charger, i.e. speed of charging, power rating, cost, volume and weight, number of phases, voltage levels, ease of charging and availability of charging places, limitations on power electronic components, power factor, harmonic distortion, monitoring equipment, standards, and persons safety. The study should involve battery knowledge, so that the charger could be fully adapted to the battery, giving a long battery life length.
- Suggest and evaluate possible integrated chargers, meaning integration of the charger and the available drive system used for propulsion of the vehicle.
- Prototype building in cooperation with the whole group (including industry). One prototype coordinator from industry administrates the task. The task also incorporates preparations for lab testing.

MASTER THESIS SCOPE

The thesis is part on the sub project *“On Board Integrated Charging”*. The main goal is to *design, simulate and implement a 3-phase boost battery charger with power factor correction*.

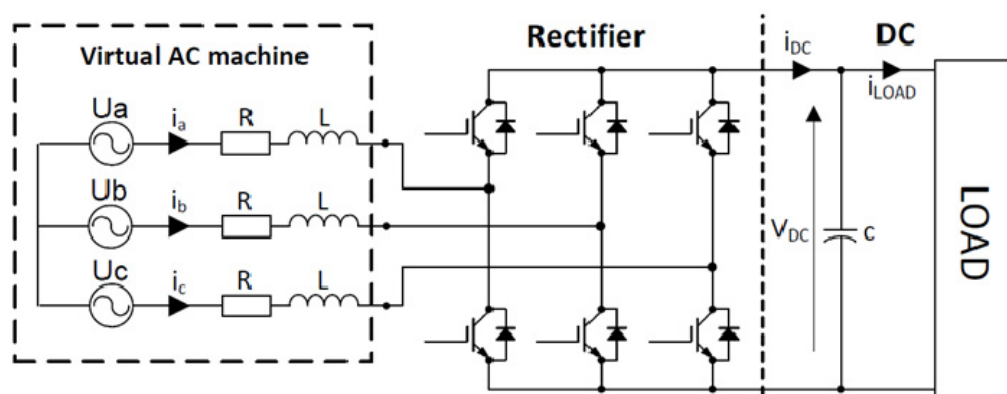


Figure 1.1 : Rectifier schematic with AC machine

The Figure 1.1 represent our system. The first idea was to use an AC motor on the AC-side. Some data are given in Table 1.1.

¹ SHC is composed with three different partners : three universities with Lund Institute of Technology (LTH), Royal Institute of Technology (KTH) and Chalmers University of Technology (CTH), The Swedish Energy Agency (Energimyndigheten) and automotive industry with AB Volvo, Volvo Car Corporation, Saab Automobile AB, GM Powertrain Sweden AB, Scania CV AB, BAE Systems Hägglunds AB.

POWER SOURCE	- 3-phase - 50Hz - PMSM 115V±20% phase voltage
POWER LEVEL	- 15kW
BATTERY VOLTAGE	- 320-400VDC (nominal value 350VDC)
MATERIAL	- Motor (KTH development) - IGBT Rectifier - Battery - dSpace system - Hardware (in development) - Piece of software to develop for implementation (probably C) - Sensors (full access I/V/Speed)

Table 1.1 : Scope data

At the beginning of thesis, a first plan had been established.

- 1) Literature review (how the system work/find literature resources)
- 2) Topology selection (VFOC is preferred method regarding to this specific application)
- 3) System design (inductance value, switching frequency, control design)
- 4) Simulation with Matlab/Simulink
- 5) Addition of PMSM to the model and using the leakage inductance of the machine as energy storage device (Re-design/Re-simulation)
- 6) Implementation
 - a. dSpace system
 - b. Software development
 - c. Hardware test (in development)
- 7) Testing and debugging / Report

Nevertheless, after a couple of weeks we decided to simplify the system to keep a grid connected rectifier and try to implement it in the laboratory to test the controller.

The main goal of the thesis is to develop and test the control algorithm of the converter.

* *
*

We will start this thesis with an overview of three-phase controlled rectifiers (chapter 2), with steady state operation, modeling, limitations. Then, the overview will focus on control strategies, and finally, a Pulse Width Modulation (PWM) will be describe.

Chapter 3 will be the main part of the report with Voltage Oriented Control design and simulation. We will see the current and voltage controller, stability analysis, Phase Locked Loop (PLL), and finally a simulation of grid connected converter.

The last part chapter 4 will give the main guidelines for implementation of the controller using dSpace system.

2 THREE PHASE CONTROLLED RECTIFIERS

2.1 Introduction

In the following part, we will see some topologies for 3-phase rectifiers. But we can start to explain why those topologies appeared. The high harmonic content and a low power factor cause some problems in power distribution system. New standards have been introduced by governments or organizations to limit the harmonic content of the current drawn from the power line by rectifiers. Consequently, new topologies have been deployed for rectification applications [9] .

We can introduced five topologies (Figure 2.1).

The figure a) present a simple solution of Boost converter. The main drawback of this solution is stress on the components and low frequency distortion of the input current.

The topologies b) and c) use PWM rectifier modules with a very low current rating (20-25% level of RMS current comparable with e) topology). Hence they have a low cost potential and provide only the possibility of regenerative braking mode b) or active filtering c).

Figure d) presents a converter called a Vienna rectifier. The main advantage is low switch voltage, but non-typical switches are required.

Figure e) presents the most popular topology. This universal topology has the advantage of using a low-cost three-phase module with a bidirectional energy flow capability, and it can also provide a unity power factor (UPF). However, its disadvantages are a high per-unit current rating, poor immunity to shoot-through faults, and high switching losses [9] .

Topologies are compared in a table (see Table 2.1). A diode rectifier is also included to the table for comparison.

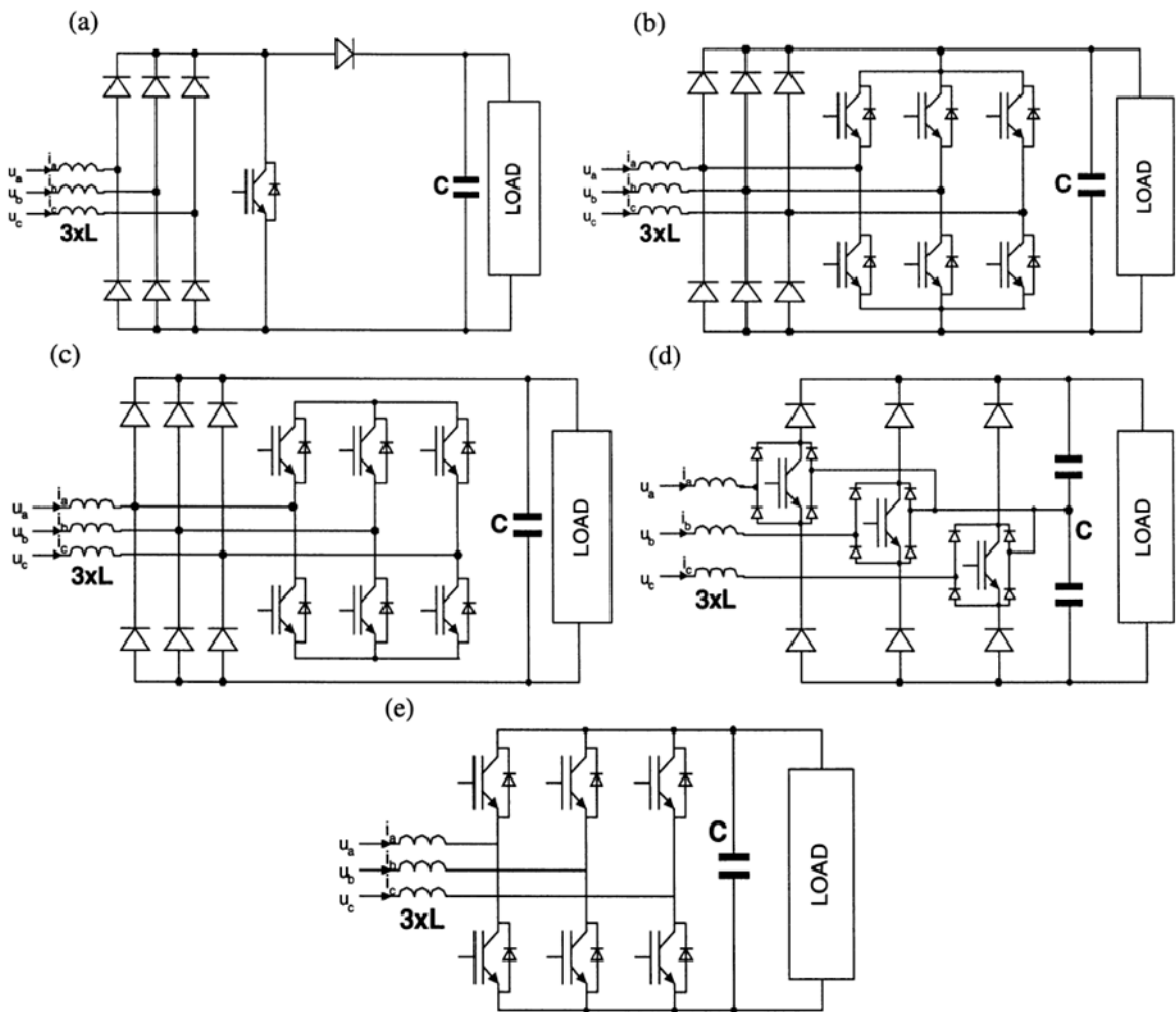


Figure 2.1 : Three-phase rectifier topologies [9] [13]

FEATURE TOPOLOGY	REGULATION OF DC OUTPUT VOLTAGE	LOW HARMONIC DISTORSION OF LINE CURRENT	NEAR SINUSOIDAL CURRENT WAVEFORMS	POWER FACTOR CORRECTION	BIDIRECTIONAL POWER FLOW	REMARKS
Diode rec.	-	-	-	-	-	
Rec. (a)	+	-	-	+	-	
Rec. (b)	-	-	-	-	+	
Rec. (c)	-	+	+	+	-	UPF
Rec. (d)	+	+	+	+	-	UPF
Rec. (e)	+	+	+	+	+	UPF

Table 2.1 : Three-phase rectifier topologies, performance comparison [9] [13]

2.2 Universal bridge topology

2.2.1 Steady state operation

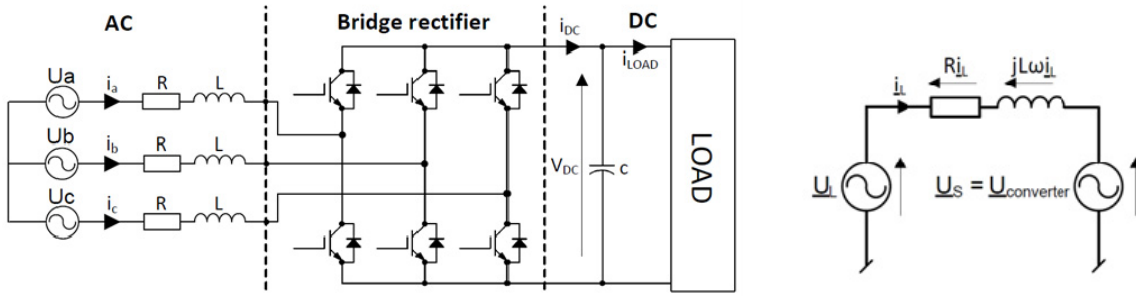


Figure 2.2 : Rectifier schematics [9]

Figure 2.2 shows basic diagram of the three-phase boost converter. u_L is the line voltage and u_s is the bridge converter voltage controllable from de the dc-side. We can draw a general phasor diagram and diagrams for both rectification and regeneration operation at unity power factor (UPF).

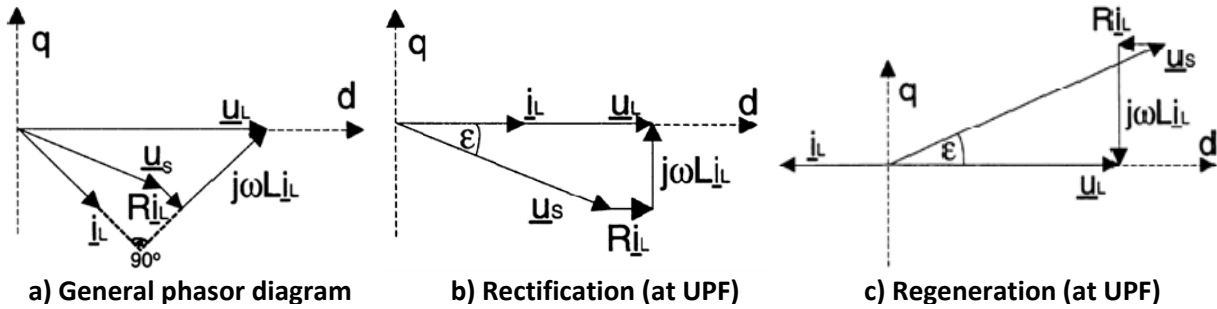


Figure 2.3 : Phasor diagrams [9]

The line current i_L is controlled by the voltage drop across the inductance L interconnecting the two voltage sources (line and converter).

When we control the phase angle ϵ and the amplitude of converter voltage u_s , we control indirectly the phase and amplitude of the line current. In this way, the average value and sign of the dc current is subject to control that is proportional to the active power conducted through the converter. The reactive power can be controlled independently with a shift of the fundamental harmonic current I_L with respect to voltage U_L [9].

Remark : Inductors connected between the line and the rectifier input bring a current source character of the input circuit and provide the boost feature of the converter [9].

2.2.2 Mathematical model

DESCRIPTION OF INPUT VOLTAGE AND CURRENT

The three-phase line voltage and current are

$$\begin{aligned}
 u_a &= E_m \cos(\omega t) \\
 u_b &= E_m \cos\left(\omega t - \frac{2\pi}{3}\right) \\
 u_c &= E_m \cos\left(\omega t - \frac{4\pi}{3}\right)
 \end{aligned} \tag{2.1}$$

$$\begin{aligned}
 i_a &= I_m \cos(\omega t + \varphi) \\
 i_b &= I_m \cos\left(\omega t + \varphi - \frac{2\pi}{3}\right) \\
 i_c &= I_m \cos\left(\omega t + \varphi - \frac{4\pi}{3}\right)
 \end{aligned} \tag{2.2}$$

and since there is no neutral connection, we obtain

$$i_a + i_b + i_c = 0. \tag{2.3}$$

A three-phase system can be described with only two components α and β (real and imaginary respectively). Furthermore, we call a **space vector** the quantity ([4] [12])

$$v^s(t) = v_\alpha(t) + jv_\beta(t) = \frac{2}{3}K \left(v_a(t) + v_b(t)e^{j\frac{2\pi}{3}} + v_c(t)e^{j\frac{4\pi}{3}} \right). \tag{2.4}$$

where K is a scaling constant (amplitude invariant $K = 1$, RMS-invariant $K = 1/\sqrt{2}$, power invariant $K = \sqrt{3/2}$ – Refer to APPENDIX A for details).

RECTIFIER ABC-MODEL [9]

$$\begin{aligned}
 u_{Sab} &= (S_a - S_b) u_{dc} \\
 u_{Sbc} &= (S_b - S_c) u_{dc} \\
 u_{Sca} &= (S_c - S_a) u_{dc}
 \end{aligned} \tag{2.5}$$

with S_i the switching function defined by : $S_i = \begin{cases} 1 & \text{upper switch ON} \\ 0 & \text{bottom switch ON} \end{cases}$ with phase $i = a, b, c$.

$$\begin{aligned}
 u_{Sa} &= f_a \cdot u_{dc} \\
 u_{Sb} &= f_b \cdot u_{dc} \\
 u_{Sc} &= f_c \cdot u_{dc}
 \end{aligned} \tag{2.6}$$

$$\begin{aligned}
 f_a &= S_a - S^* = S_a - \frac{1}{3}(S_a + S_b + S_c) = \frac{2S_a - (S_b + S_c)}{3} \\
 f_b &= \frac{2S_b - (S_a + S_c)}{3} \\
 f_c &= \frac{2S_c - (S_a + S_b)}{3}
 \end{aligned} \tag{2.7}$$

(f_{abc} are 0, $\pm 1/3$ or $\pm 2/3$).

The rectifier is defined by four equations, one for each phase (voltage) and one for the currents (dc-link).

$$\begin{bmatrix} u_a \\ u_b \\ u_c \end{bmatrix} = R \begin{bmatrix} i_a \\ i_b \\ i_c \end{bmatrix} + L \frac{d}{dt} \begin{bmatrix} i_a \\ i_b \\ i_c \end{bmatrix} + \begin{bmatrix} u_{Sa} \\ u_{Sb} \\ u_{Sc} \end{bmatrix} \tag{2.8}$$

$$C \frac{du_{dc}}{dt} = S_a i_a + S_b i_b + S_c i_c - i_{load} \quad (2.9)$$

The combination of the previous equations can be represented as a block diagram.

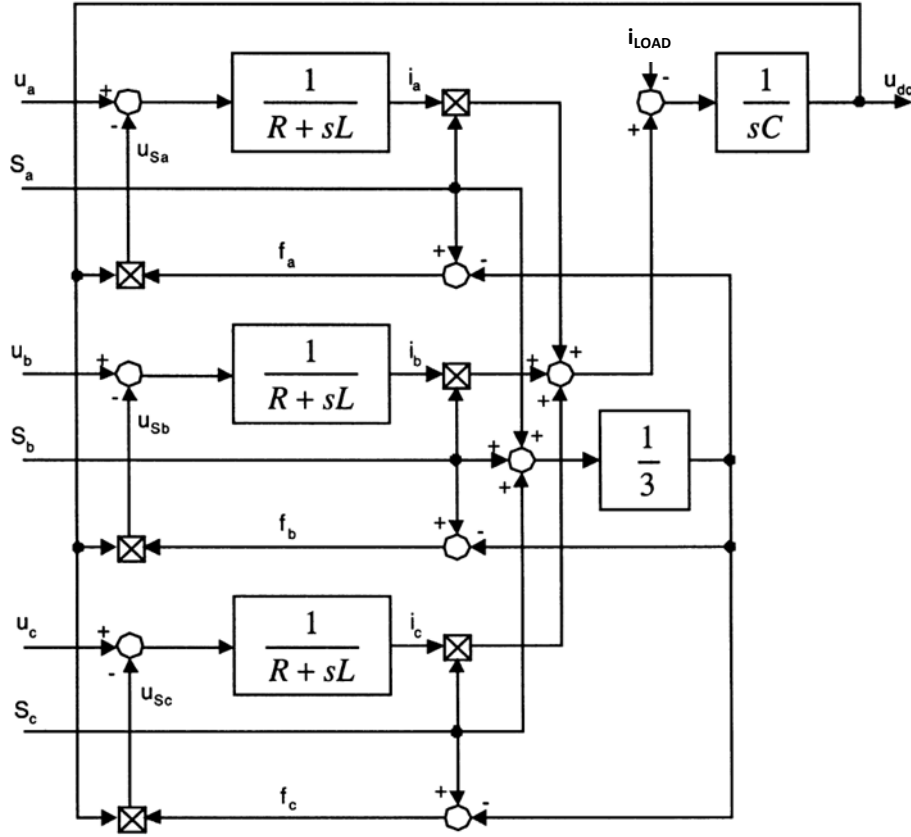


Figure 2.4 : Rectifier model [9]

RECTIFIER $\alpha\beta$ -EQUATIONS

We define the **amplitude invariant** Clarke transformation (see APPENDIX A) with ([4] [12])

$$\begin{bmatrix} \alpha \\ \beta \end{bmatrix} = \begin{bmatrix} \frac{2}{3} & -\frac{1}{3} & -\frac{1}{3} \\ 0 & \frac{1}{\sqrt{3}} & -\frac{1}{\sqrt{3}} \end{bmatrix} \begin{bmatrix} a \\ b \\ c \end{bmatrix} \quad (2.10)$$

$$\begin{bmatrix} a \\ b \\ c \end{bmatrix} = \begin{bmatrix} 1 & 0 \\ -\frac{1}{2} & \frac{\sqrt{3}}{2} \\ -\frac{1}{2} & -\frac{\sqrt{3}}{2} \end{bmatrix} \begin{bmatrix} \alpha \\ \beta \end{bmatrix} \quad (2.11)$$

Then, applying this transformation we can find the voltage equations in $\alpha\beta$ -coordinates

$$\begin{bmatrix} u_\alpha \\ u_\beta \end{bmatrix} = R \begin{bmatrix} i_\alpha \\ i_\beta \end{bmatrix} + L \frac{d}{dt} \begin{bmatrix} i_\alpha \\ i_\beta \end{bmatrix} + \begin{bmatrix} u_{S\alpha} \\ u_{S\beta} \end{bmatrix} \quad (2.12)$$

$$C \frac{du_{dc}}{dt} = \frac{3}{2} (S_\alpha i_\alpha + S_\beta i_\beta) - i_{load}. \quad (2.13)$$

RECTIFIER dq -EQUATIONS

Now, we need to apply the Park transformation (see APPENDIX A and [4] [12]) which is

$$v_{dq} = v^s e^{-j\theta} \quad (2.14)$$

where v^s is a space vector ($v^s = v_\alpha + jv_\beta$). We get

$$u^s = Ri^s + L \frac{di^s}{dt} + u_s^s \quad (2.15)$$

$$\Leftrightarrow u_{dq} e^{j\theta} = Ri_{dq} e^{j\theta} + L \left(e^{j\theta} \left(j\omega i_{dq} + \frac{di_{dq}}{dt} \right) \right) + e^{j\theta} u_{sdq}$$

$$\Leftrightarrow u_{dq} = Ri_{dq} + L \frac{di_{dq}}{dt} + jL\omega i_{dq} + u_{sdq} \quad (2.16)$$

And finally, with separation of Real and Imaginary part we obtain

$$u_d = Ri_d + L \frac{di_d}{dt} - \omega Li_q + u_{sd} \quad (2.17)$$

$$u_q = Ri_q + L \frac{di_q}{dt} + \omega Li_d + u_{sq} \quad (2.18)$$

$$C \frac{du_{dc}}{dt} = \frac{3}{2} (S_d i_d + S_q i_q) - i_{load} \quad (2.19)$$

INSTANTANEOUS POWER [4]

From the well known relation $P = \text{Re}\{\underline{V} \underline{I}^*\}$ for single phase rms-value-scaled phasors \underline{V} and \underline{I} ("*" indicates complex conjugate), we know that instantaneous power for three-phase system will be proportional to

$$\text{Re}\{v^s (i^s)^*\} = \text{Re}\{v^{dq} (i^{dq})^*\} \quad (2.20)$$

Note that the formula is independent of the coordinate system.

From the space vector definition we get (the time argument "(t)" is removed for simplicity)

$$v^s (i^s)^* = \left(\frac{2}{3}K\right)^2 \left(v_a + v_b e^{j\frac{2\pi}{3}} + v_c e^{j\frac{4\pi}{3}} \right) \left(i_a + i_b e^{j\frac{2\pi}{3}} + i_c e^{j\frac{4\pi}{3}} \right)^*$$

$$= \left(\frac{2}{3}K\right)^2 \left[v_a i_a + v_b i_b + v_c i_c + j \frac{1}{\sqrt{3}} (v_a (i_c - i_b) + v_b (i_a - i_c) + v_c (i_b - i_a)) \right]$$

And finally, the Real part gives us the **active power**

$$P = \frac{3}{2K^2} \text{Re}\{v^s (i^s)^*\} = \frac{3}{2K^2} \text{Re}\{v^{dq} (i^{dq})^*\} = v_a i_a + v_b i_b + v_c i_c. \quad (2.21)$$

And with Imaginary part we obtain the **reactive power**

$$Q = \frac{3}{2K^2} \text{Im}\{v^s (i^s)^*\} = \frac{3}{2K^2} \text{Im}\{v^{dq} (i^{dq})^*\}$$

$$= \frac{1}{\sqrt{3}} [v_a (i_c - i_b) + v_b (i_a - i_c) + v_c (i_b - i_a)]. \quad (2.22)$$

For ideal, positive sequence space vectors (voltage is reference)

$$v^s = KE_m e^{j\omega t} \text{ and } i^s = KI_m e^{j\omega t + \varphi}$$

where E_m and I_m are amplitude, the active power is given by

$$P = \frac{3}{2K^2} \text{Re}\{v^s (i^s)^*\} = \frac{3}{2K^2} \text{Re}\{v^{dq} (i^{dq})^*\} = \frac{3}{2} E_m I_m \cos\varphi = 3VI \cos\varphi \quad (2.23)$$

Where V and I are rms-values. This previous relation will be use in the DC-link voltage controller design.

2.2.3 Limitations

MINIMUM DC-LINK VOLTAGE

For proper operation of the rectifier, a minimum dc-link voltage is needed to obtain undistorted current waveforms. To have a full control of the rectifier, its six diodes must be polarized negatively at all value of ac-voltage supply. To keep the diodes blocked, we need to ensure a dc-link voltage higher than the peak dc-voltage generated by the diodes alone. Theoretically for diode rectifier, the maximum dc output voltage is the peak value of line-to-line RMS voltage [9] .

$$V_{DCmin} > \sqrt{2}V_{LL(rms)} = \sqrt{2} \cdot \sqrt{3} \cdot V_{LN(rms)} \quad (2.24)$$

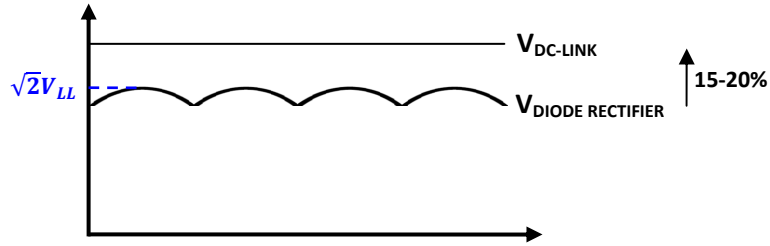


Figure 2.5 : DC-link voltage condition

It will be better to select a DC-link voltage about 15-20% more than $\sqrt{2}V_{LL}$.

IMPORTANT : The previous voltage $V_{LL(rms)}$ correspond to the converter voltage (Us). There is no line impedance taking in account here.

Nevertheless, if there is no line impedance ($R = 0\Omega$, $L=0H$) we can continue to write the equation (2.24) according to the amplitude of supply voltage E_m :

$$V_{DCmin} > \sqrt{2} \cdot \sqrt{3} \cdot V_{LN(rms)} = \sqrt{3} E_m \cdot \quad (2.25)$$

ATTENTION : This is a true definition but doesn't apply in all situation [9] . The DC-link voltage depends on the PWM method. In our case, we will use a sinusoidal PWM. In this case the maximum reference voltage is $V_{dc}/2$ (Figure 2.6 [23]).

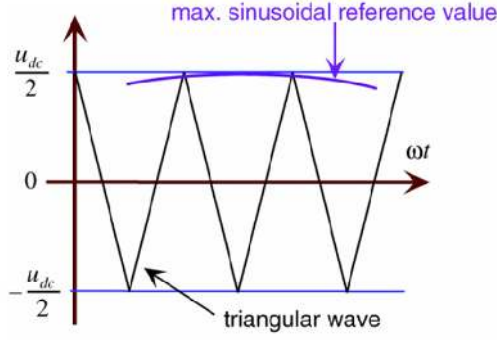


Figure 2.6 : Maximum sinusoidal reference voltage (converter voltage U_s) for sinusoidal PWM [23]

Finally, our minimum DC-link voltage will be

$$V_{LN(peak)} = \frac{V_{DC}}{2} \quad (2.26)$$

$$\frac{V_{LL(rms)}}{\sqrt{3}} \sqrt{2} = \frac{V_{DC}}{2}$$

$$V_{DCmin} > 2 V_{LN(peak)} = \frac{2\sqrt{2}}{\sqrt{3}} V_{LL(rms)} = 1.663 V_{LL(rms)} \quad (2.27)$$

MINIMUM DC-LINK VOLTAGE AND INDUCTANCE

The book [9] (chapter11 p434) defines a minimum DC-link voltage taking in account the line inductance value. The demonstration seems to be valid in our case for amplitude invariant (they assume a maximum converter voltage equal to $\frac{2}{3}V_{dc}$ (i.e. radius of switching hexagon). It will be $\sqrt{\frac{3}{2}}V_{dc}$ for power invariant). They define a DC-link voltage as

$$V_{dc} > \sqrt{3[E_m^2 + (\omega L i_d)^2]}. \quad (2.28)$$

We can observe that R is neglected and if L = 0 (if there is no inductance voltage), we find again the equation (2.25) where $V_{DCmin} > \sqrt{3}E_m$.

From this equation we can get the maximum inductance value as

$$L < \frac{\sqrt{\frac{V_{DC}^2}{3} - E_m^2}}{\omega i_d}. \quad (2.29)$$

A low inductance will give a high current ripple and will make the design more dependent on the line impedance (refer to “3.8 Grid modeling” and “3.9.3 Simulation results”). According to [9] , a high value of inductance will give a low current ripple, but simultaneously reduce the operation range of the rectifier. The voltage drop across the inductance controls the current. This voltage drop is controlled by the voltage of the rectifier but its maximal value is limited by the dc-link voltage. Consequently, a high current (high power) through the inductance requires either a high dc-link voltage or a low inductance (low impedance).

2.3 Control strategies

2.3.1 Introduction

The control of PWM converter can be considered as a dual problem with vector control of an induction motor IM (see figure and table below).

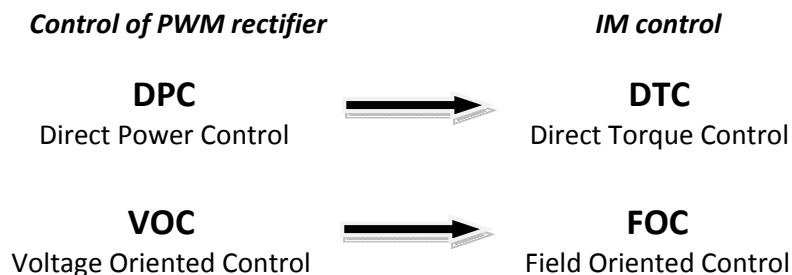


Figure 2.7 : PWM rectifier and IM control duality

Control of PWM rectifier	IM control
Speed control loop of vector drive	dc-link voltage
Reference angle between stator current and rotor flux	Reference angle of line voltage

Table 2.2 : PWM rectifier and IM control duality [9]

We can classify the PWM rectifier method in two categories : **voltage** based and **virtual flux** based control (See following Figure 2.8).

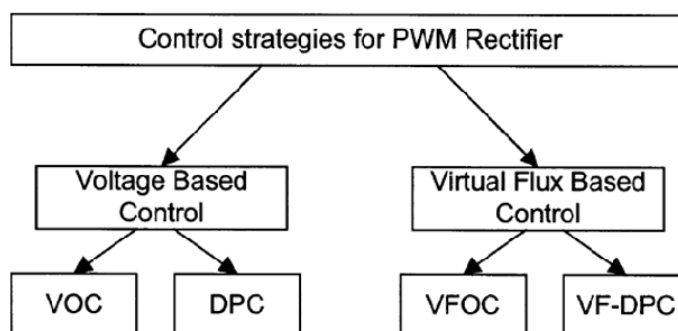


Figure 2.8 : Control strategies [9]

All these control strategies can achieve the same main goals, such as high power factor and near sinusoidal input current waveforms.

The Voltage Oriented Control (VOC) guarantees high dynamic and static performance via an internal current control loop. But the quality depends mainly on the current control strategy.

The Direct Power Control (DPC) is based on the instantaneous active and reactive power control loop. There are no internal current control loop and no PWM modulator block. The switching state are determined with a switching table based on the instantaneous errors between the commanded and estimated values of active and reactive power.

The Virtual Flux Based Control (VF-) correspond to a direct analogy of IM control.

2.3.2 Direct Power Control and Virtual Flux Direct Power Control

The DPC method is similar to Direct Torque Control (DTC) for induction motor. Instead of torque and stator flux the instantaneous active and reactive powers are controlled. The following figure shows the scheme of the DPC method.

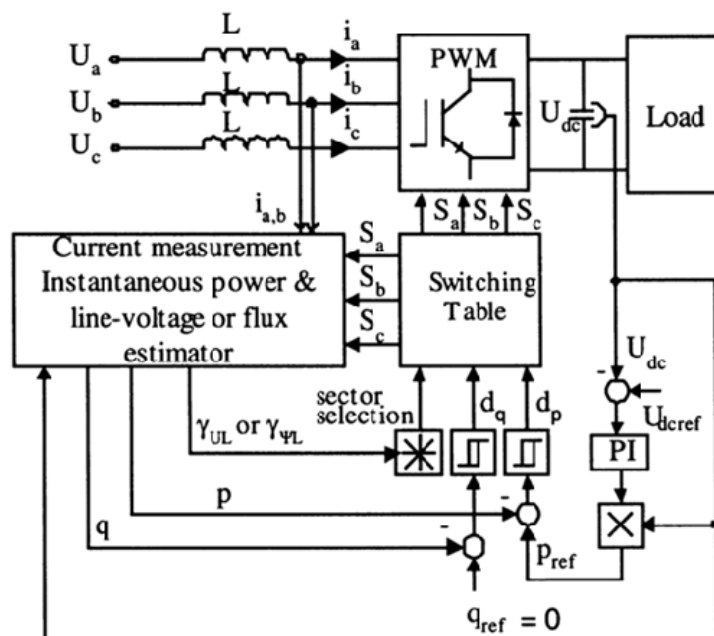


Figure 2.9 : Block scheme (DPC, VF-DPC)[9]

The power estimation of DPC is based on the line voltage. An important disadvantages of the method is the need of current differentiation to estimate this power. Other relevant points can be found ([9]) :

- Need high sample frequency because the estimated value are changing all the time.
- Need high inductance value because the switching frequency is not constant.
- A non-constant switching frequency means trouble to design an input filter.
- Calculation of power and voltage should be avoid during switching (errors).

The virtual flux method is an improvement of Voltage Oriented Control (VOC). The virtual flux is an integration of line voltage u_L .

For the VF-DPC, we can summaries the following characteristics.

- No line voltage sensors required. Furthermore, a voltage sensor-less line power estimation is much less noisy due to natural low-pass behavior of the integrator.
- Simple and noise robust power estimation algorithm, easy to implement in a DSP.
- Lower sampling frequency (as conventional DPC).
- Sinusoidal line currents (low THD).
- No separate PWM voltage modulation block.
- No current regulation loops.
- Coordinate transformation and PI controllers not required.
- High dynamic, decoupled active and reactive power control.
- Power and voltage estimation gives the possibility to obtain instantaneous variables with all harmonic components, which has an influence for improvement of total power factor and efficiency.
- Easier calculations for p and q than voltage based method, no differentiation of line current.

The typical disadvantages of VF-DPC are :

- Variable switching frequency.

- Solution requires a fast microprocessor and A/D converters.

2.3.3 Voltage and Virtual Flux Oriented Control

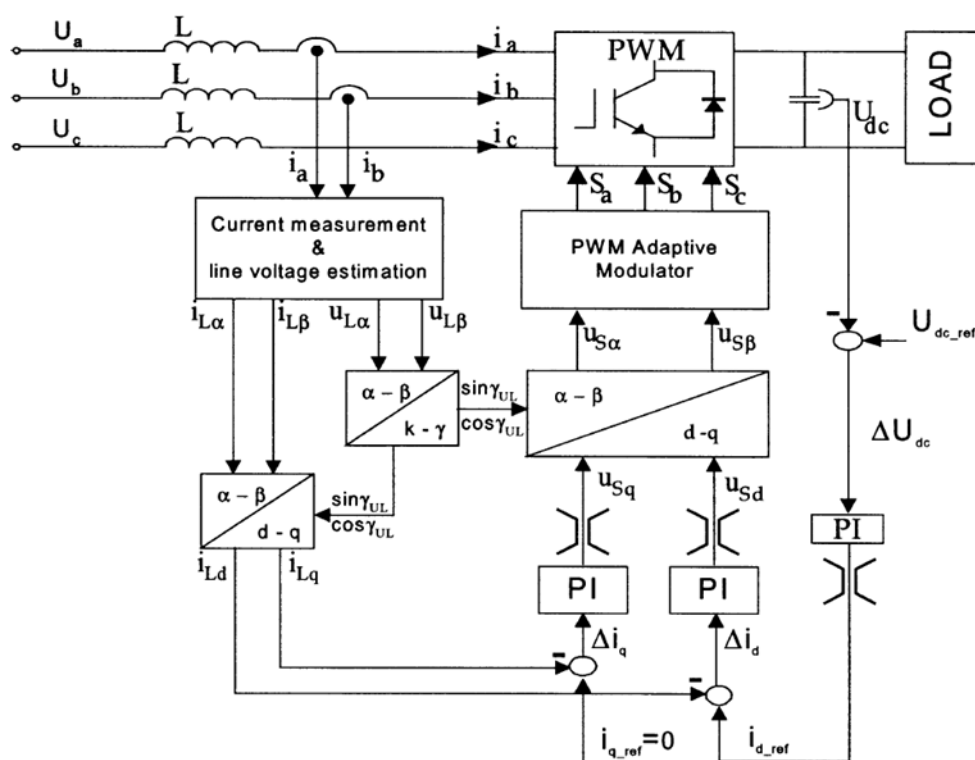


Figure 2.10 : VOC block scheme [9]

The Voltage Oriented Control (VOC) and Virtual Flux Oriented Control (VFOC) are close to Field Oriented Control for induction motor. The method is based on the transformation between stationary coordinates $\alpha\beta$ and synchronous rotating coordinates dq . This strategy guarantees :

- Fast transient response
- High static performance via internal current control loop.

Consequently, the performance depends on the quality of the current control loop.

We can find several strategies that can be applied for current control. A widely used scheme for high performance current control is the dq synchronous controller, where the regulated current are DC quantities. This eliminates steady-state errors.

VOC and VFOC provide some **advantages** compared to DPC.

- Low sampling frequency for good performance (cheaper A/D converters and microcontroller)
- Fixed switching frequency (easier design of input filter)

Furthermore, VFOC provides improved rectifier control under non-ideal line voltage condition (because ac voltage sensorless operation is much less noisy thanks to the natural low-pass behavior of the integrator used in the flux estimator).

Both methods also have some **disadvantages** :

- Coupling occurs between active and reactive components and some decoupling solution is required.
- Coordinate transformation and PI controllers are required.

2.3.4 Comparison and discussion

The following table summarizes the main characteristics of the different control strategies.

TECHNIQUE	ADVANTAGES	DISADVANTAGES
VOC	<ul style="list-style-type: none"> ▪ Fixed switching Freq. (easier design input filter) ▪ Advanced PWM strategies can be used ▪ Cheap A/D converters 	<ul style="list-style-type: none"> ▪ Coordinate transformation and decoupling between active and reactive components is required ▪ Complex algorithm ▪ Input power factor lower than for DPC
DPC	<ul style="list-style-type: none"> ▪ No separate PWM block ▪ No current regulation loop ▪ No coordinate transformation ▪ Good dynamics ▪ Simple algorithm ▪ Decoupled active and reactive power control ▪ Instantaneous variables with all harmonics components estimated (improve power factor and efficiency) 	<ul style="list-style-type: none"> ▪ High inductance and sample frequency needed ▪ Power and voltage estimation should be avoid at the moment of switching ▪ Variable switching frequency ▪ Fast microprocessor and A/D converters required
VFOC	<ul style="list-style-type: none"> ▪ Fixed switching Freq. (easier design input filter) ▪ Advanced PWM strategies can be used ▪ Cheap A/D converters 	<ul style="list-style-type: none"> ▪ Coordinate transformation and decoupling between active and reactive components is required ▪ Complex algorithm ▪ Input power factor lower than for VF-DPC
VF-DPC	<ul style="list-style-type: none"> ▪ Simple and noise resistant power estimation algorithm, easy to implement in a DSP ▪ Lower sampling frequency than for DPC ▪ Low THD of line currents with distorted or unbalanced supply ▪ No separate PWM block ▪ No current regulation loop ▪ No coordinate transformation ▪ Good dynamics ▪ Simple algorithm ▪ Decoupled active and reactive power control 	<ul style="list-style-type: none"> ▪ Variable switching frequency ▪ Fast microprocessor and A/D converters required

Table 2.3 : Control strategies comparison [9]

VOC vs. VFOC

One of the only advantages of VFOC against VOC is that VFOC provides improved rectifier control under non-ideal line voltage condition (because ac voltage sensorless operation is much less noisy thanks to the natural low-pass behavior of the integrator used in the flux estimator).

Switching Frequency

A FIXED switching frequency is required in our project mainly because it means : easier design (input filter for eg.) and the sample frequency can be lower. Only VOC or VFOC can provide this feature.

Power factor

DPC has better power factor than VOC but has variable switching frequency. DPC also means complicated calculations for p and q (need differentiation of line current, risk of instability).

A good power factor can be achieved with VF-DPC and the method has lots of advantages but as we want a fixed switching frequency, VOC or VFOC should be chosen.

If the switching frequency can be variable, the VF-DPC strategy is obviously the best solution (but the cost can become a problem. The method need fast microprocessors and A/D converters).

2.4 Pulse Width Modulation

The Pulse Width Modulation used in our system, a sinusoidal PWM will be used.

2.4.1 Sinusoidal PWM

Sinusoidal modulation is based on a triangular carrier signal. The idea is to compare three sinusoidal reference voltages U_{a^*} , U_{b^*} and U_{c^*} to this triangular wave. By comparison, the logical signals S_a , S_b and S_c , which define switching instants of power transistor, are generated. Operation with constant carrier signal concentrate voltage harmonics around switching frequency and multiple of switching frequency.

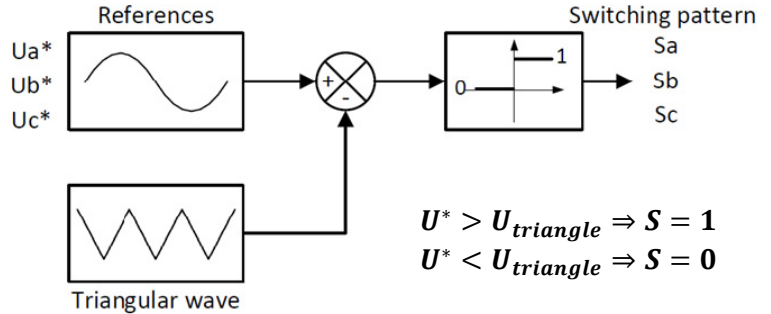


Figure 2.11 : Sinusoidal PWM

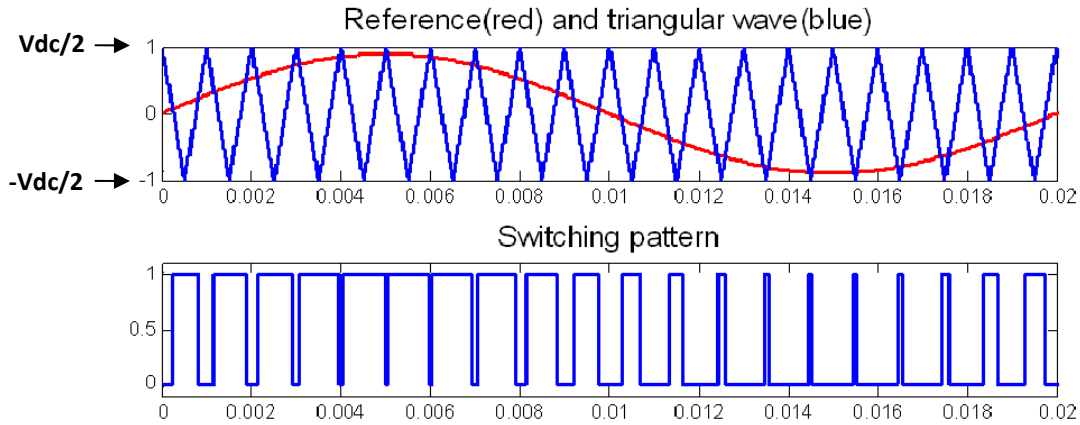


Figure 2.12 : Sinusoidal PWM basic waveforms

➤ Maximum sinusoidal reference voltage

Using a sinusoidal PWM, the maximum reference value is $V_{dc}/2$.

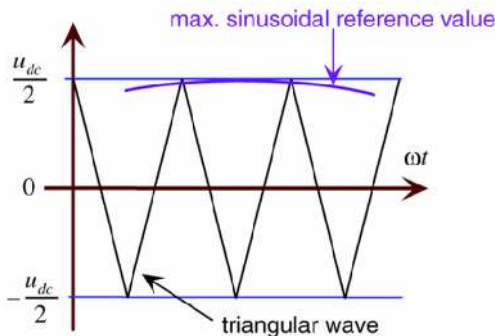


Figure 2.13 : Maximum sinusoidal reference voltage (sinusoidal PWM) [23]

➤ Maximum slope

The slope of the triangular wave should be higher than the slope of the reference voltage. We can write

$$\frac{dU_{triangle}}{dt} > \frac{dU_{reference}}{dt} \tag{2.30}$$

2.4.2 Digital implementation

➤ Synchronous sampling [4]

In a digital current control system, the current is sampled with interval T_s . To avoid electromagnetic interference (EMI) due to ON/OFF switchings of the valves, it is useful to synchronize the sampling with converter switching. Current sampling is taken in between switchings. This coincides with the positive and negative peak values of the triangular waveform.

Using synchronous sampling, approximately the mean value of the current is obtained. Thus, not only EMI is avoided, but also the current ripple is reduced. This method can be effective enough to avoid low-pass filtering before sampling.

We will select the sample frequency as :

$$F_S = 2 F_{triangle\ wave} = 2 F_{SW} \tag{2.31}$$

(F_{SW} is the switching frequency, $F_{triangle\ wave} = F_{SW}$)

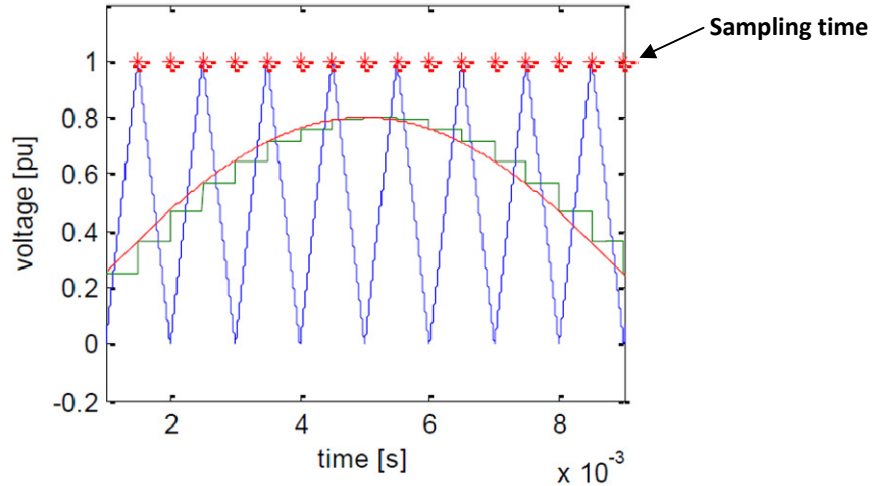


Figure 2.14 : Asymmetric PWM – Synchronous sampling illustration [23]

Two samples can be acquired over each switching period. According to [4] a fast sampling enables higher bandwidth of the current controller, then it's possible to reduce the sampling rate for example to the switching rate : $F_S = F_{SW}$ (or less).

2.4.3 Dead time effect

When we speak about implementation of converter, we need to inject deadtime (delay) in PWM signals to avoid short circuit in DC-link (i.e. both transistor of one leg are conducting). The system becomes safer but, the performance are affected.

This is temporary a loss of control. For example in an inverter, the output voltage waveform deviates from that for which it is originally intended. Since this is repeated over and over for every switching operation, its detrimental effect may become significant in PWM inverters that operate in high switching frequency. This is known as the deadtime effect. During the delay time, both transistors of the leg cease to conduct. Another consequence of the deadtime effect is the appearance of undesirable harmonics ([31] [32]).

We can find several strategies for deadtime injection. An example is given below.

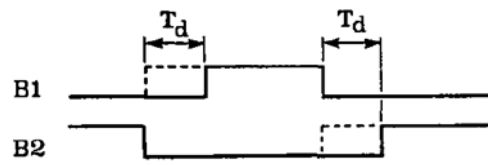


Figure 2.15 : One leg with transistors B1 and B2 – On/Off states, deadtime T_d [32]

3 VOLTAGE ORIENTED CONTROL – SIMULATION

3.1 Introduction – References chosen

As we explain in the previous section, Voltage Oriented Control (VOC) or Virtual Flux Oriented Control (VFOC) should be chosen. We decided to start with a VOC.

Before going further in the design and simulation of the controller, we need to precise some important references chosen in this report.

3-PHASE SYSTEM DEFINITION

$$\begin{aligned} u_a &= E_m \cos(\omega t) \\ u_b &= E_m \cos\left(\omega t - \frac{2\pi}{3}\right) \\ u_c &= E_m \cos\left(\omega t - \frac{4\pi}{3}\right) \end{aligned}$$

COORDINATE TRANSFORMATION

$$\begin{bmatrix} \alpha \\ \beta \end{bmatrix} = \begin{bmatrix} \frac{2}{3} & -\frac{1}{3} & -\frac{1}{3} \\ 0 & \frac{1}{\sqrt{3}} & -\frac{1}{\sqrt{3}} \end{bmatrix} \begin{bmatrix} a \\ b \\ c \end{bmatrix} \text{ and } \begin{bmatrix} a \\ b \\ c \end{bmatrix} = \begin{bmatrix} 1 & 0 \\ -\frac{1}{2} & \frac{\sqrt{3}}{2} \\ -\frac{1}{2} & -\frac{\sqrt{3}}{2} \end{bmatrix} \begin{bmatrix} \alpha \\ \beta \end{bmatrix} \quad (2.10)(2.11)$$

$$\begin{bmatrix} d \\ q \end{bmatrix} = \begin{bmatrix} \cos\theta & \sin\theta \\ -\sin\theta & \cos\theta \end{bmatrix} \begin{bmatrix} \alpha \\ \beta \end{bmatrix} \text{ and } \begin{bmatrix} \alpha \\ \beta \end{bmatrix} = \begin{bmatrix} \cos\theta & -\sin\theta \\ \sin\theta & \cos\theta \end{bmatrix} \begin{bmatrix} d \\ q \end{bmatrix}. \quad (3.1) (3.2)$$

You can refer to APPENDIX A for details. We only use **AMPLITUDE INVARIANT** in this thesis. Indeed, after transformation from ABC-to-dq coordinates, the d-components is equal to E_m , and the q-component equal to zero.

POWER, CURRENT DIRECTION

We chose a reference as shown in the following schematic, the current is flowing from the grid to the rectifier.

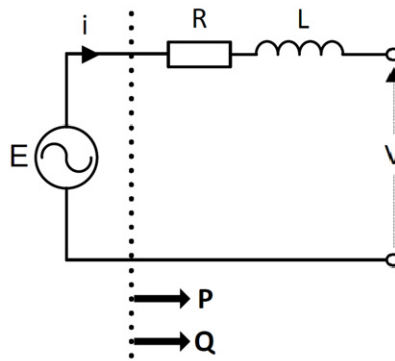


Figure 3.1 Reference for I, P, Q

3.2 System block diagram

The voltage oriented control scheme is shown Figure 3.2.

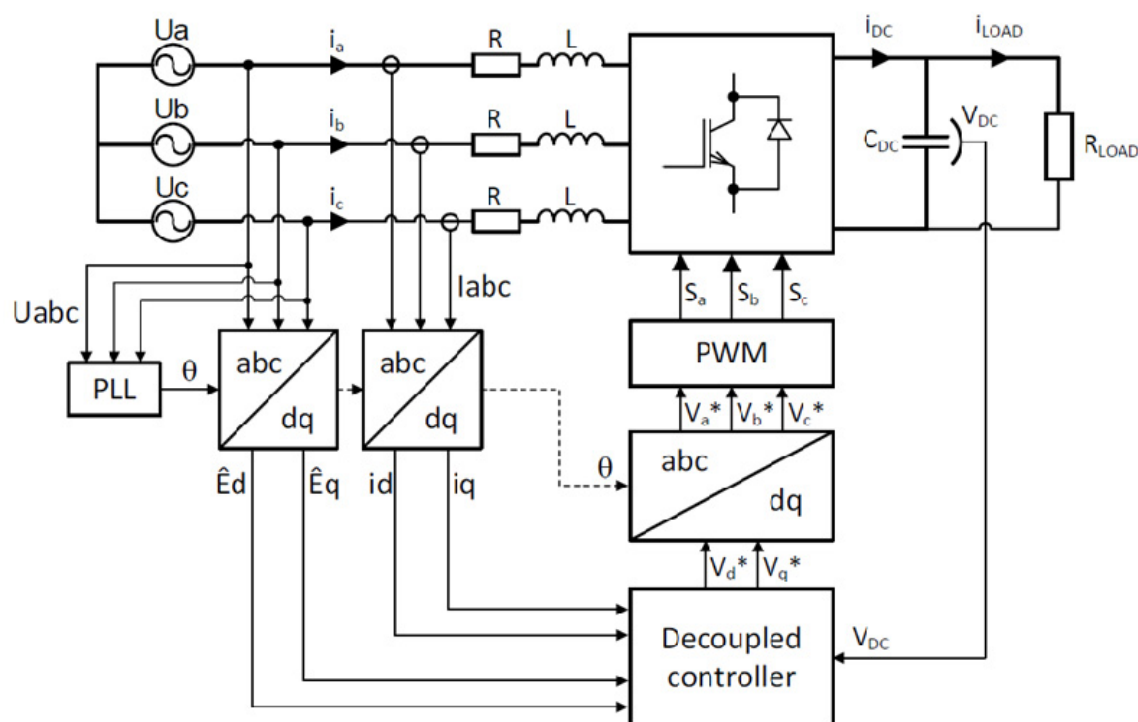


Figure 3.2 : System block diagram

First of all, the line voltage U_{abc} need to feed the PLL (Phase Locked Loop, see “3.7 Phase Locked Loop (PLL)”) and the voltage angle calculated is used for three-phase to dq -coordinate transformation of line current and voltage.

Secondly, the dq -coordinate values and the DC-link voltage value are used in a decoupled controller which will be described in the section “3.4 Current controller” and “3.5 DC-link voltage controller”.

Finally, the reference voltages created by the controller are sent to the PWM block (Pulse Width Modulation) to create the switching patterns S_{abc} ($S = 1$ means upper switch ON, lower switch OFF ; $S = 0$ means upper switch OFF, lower switch ON).

Remark : The reference voltage from the controller correspond to the converter voltage U_s (see design of the current controller in section “3.4 Current controller”).

The system will be simulated in Matlab/Simulink. According to the previous figure, we will have four main parts in the model : the PLL, a decoupled controller composed by a current and voltage controller, a PWM block, and a rectifier model (with grid impedance R and L included).

3.3 PWM Simulation

A description of the sinusoidal PWM implemented here is available in section “2.4 Pulse Width Modulation”.

3.3.1 Simulink implementation of PWM

⇒ PWM block using switch

The amplitude of triangular wave should be $V_{dc}/2$. But V_{dc} is not constant in our case. We should first normalized the reference value by $V_{dc}/2$ and compare this value with a triangular wave with an amplitude of 1. The following figure show the Simulink block diagram.

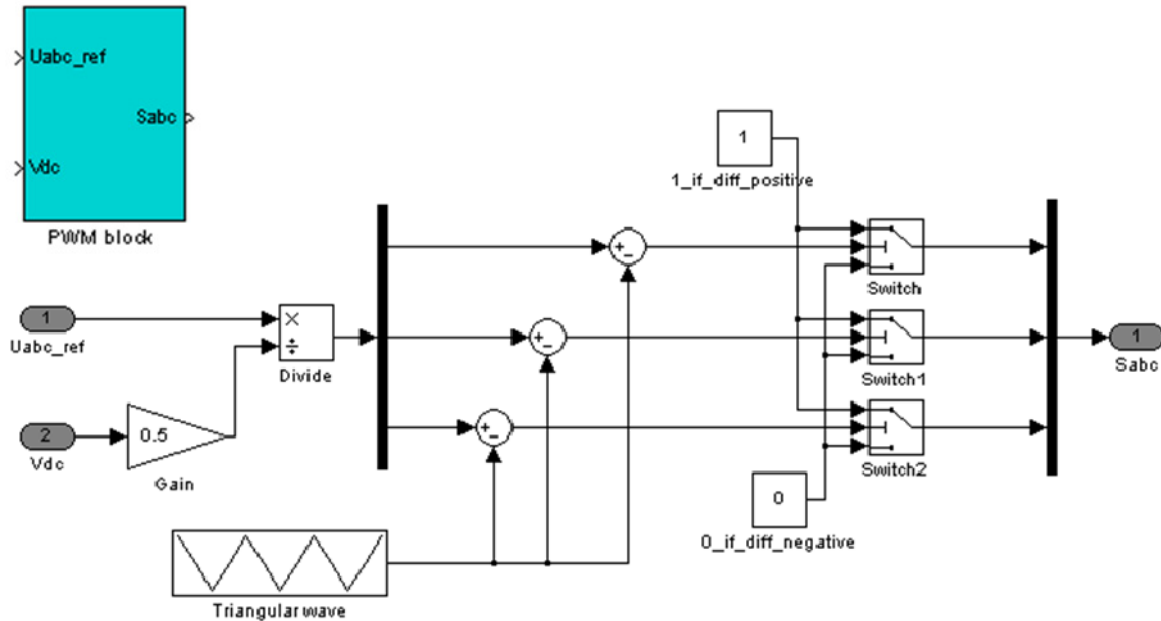


Figure 3.3 : Simulink PWM block

⇒ PWM block without switch

We can also use a PWM block without switching to create the switching pattern. The reference voltage is normalized by $V_{dc}/2$ to obtain a signal within a range $[-1 ; +1]$, then divide by 2 and translate to get signal in the range $[0 ; +1]$ like the switching function S_{abc} . This simple model can be useful in Simulink to reduce the simulation time if needed. In a complete simulation with controller, the behavior of the system is similar using Figure 3.3 or Figure 3.4.

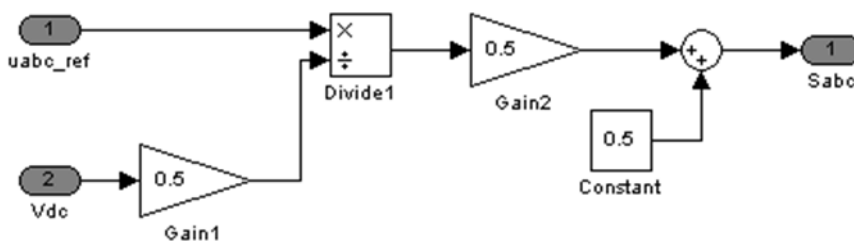


Figure 3.4 : Simulink PWM block without triangular wave

➤ **Synchronization verification**

We have to check which carrier wave we should have (at t=0, triangle amplitude is 1 or 0?). We need to be sure that we sample every triangular wave peak (we need to check if at t=0, Matlab take a sample or not).

We can verify it by sampling the triangular wave, using a “sample and hold” block. The signals before and after sampling are plotted below. As we can see, we sample on each triangle peak (blue point).

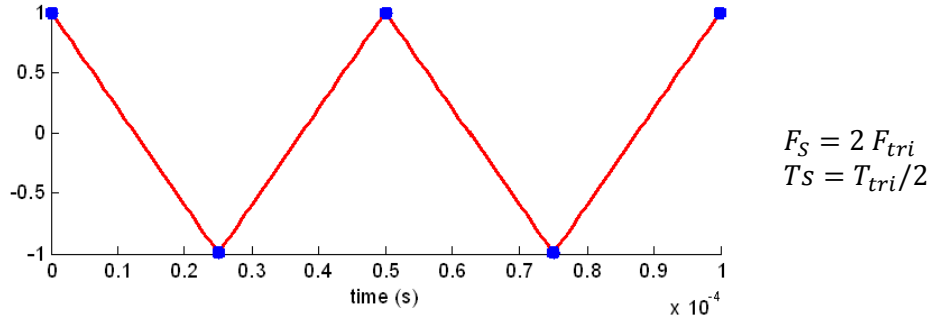


Figure 3.5 : Synchronization verification

3.4 Current controller

This section is mainly based on the reference [4] and [14] . We are giving a summary for controller design based on Internal Model Control (IMC) with synchronous PI control (decoupled controller).

To make the following more understandable, a first schematic for decoupled controller is given Figure 3.6 with the current controller and the dc-link voltage controller (describe in section “3.5 DC-link voltage controller”).

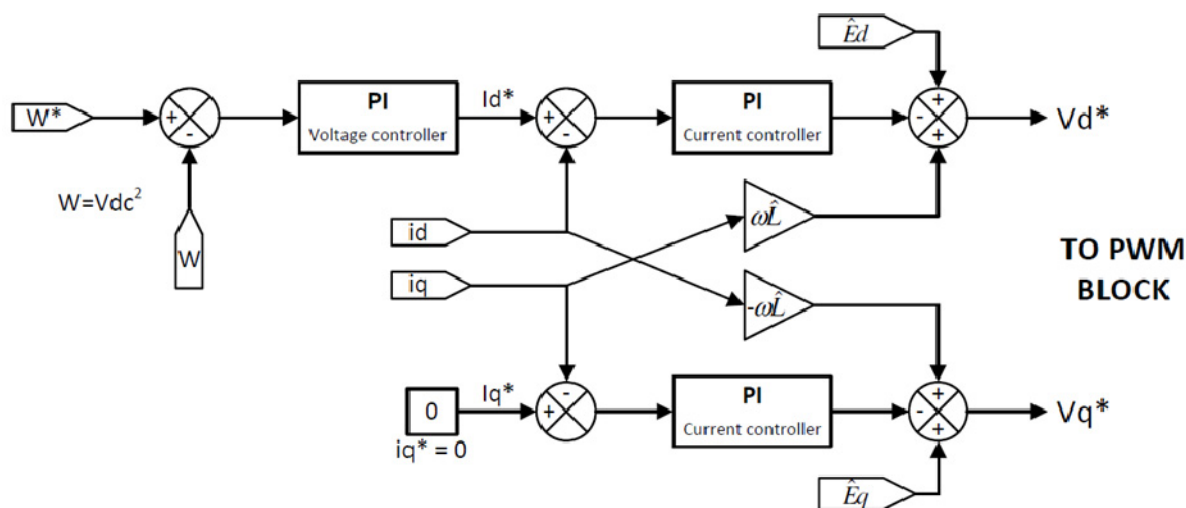


Figure 3.6 : Decoupled controller (current and dc-link voltage controller)

3.4.1 Internal Model Control

Internal Model Control (IMC) is a method for controller design, for which the resulting controller becomes directly parameterized in terms of the plant model parameters and the desired closed-loop bandwidth.

For example, the controller transfer function will be

$$F(s) = \frac{\alpha^n}{(s + \alpha)^n - \alpha^n} \hat{G}^{-1}(s) \tag{3.3}$$

that is, a low pass filter with bandwidth α , \hat{G} is an estimation of the plant (process), and n the order or G .

A brief tutorial is available in [14] , Chapter 6, page 83. This method is used for the following controller design.

3.4.2 Synchronous PI control

PI controllers are inherently incapable of giving zero steady state control error for a sinusoidal reference. The integral action removes the error only if the reference value is constant in steady state.

Using Clarke and Park transformations, the current measurements are transformed to DC-quantities, then, a simple PI controller can give good results (but not always optimal performances).

Main qualities for dq-frame current controller are then :

- fast dynamic response,

- good accuracy current tracking,
- less sensitive to parameter variations.

(Sources :[4] [9]).

3.4.3 Design of the synchronous PI controller

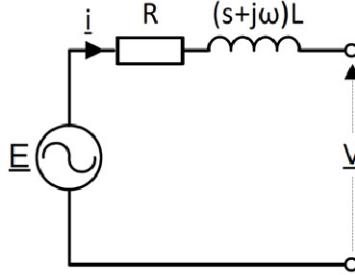


Figure 3.7 : Synchronous coordinates schematic (see APPENDIX A-A.5)

⇒ Synchronous coordinates equation (notation, $\underline{x} = x_{dq} = x_d + jx_q$)

$$L \frac{di}{dt} = \underline{E} - (R + j\omega L)\underline{i} - \underline{v} \quad (3.4)$$

$$(R + sL + j\omega L)\underline{i} = \underline{E} - \underline{v} \Rightarrow \underline{i} = \frac{\underline{E} - \underline{v}}{R + sL + j\omega L}$$

And the system transfer function $\underline{G}(s)$ is

$$\underline{G}(s) = \frac{\underline{i}}{\underline{v}} = -\frac{1}{R + sL + j\omega L}. \quad (3.5)$$

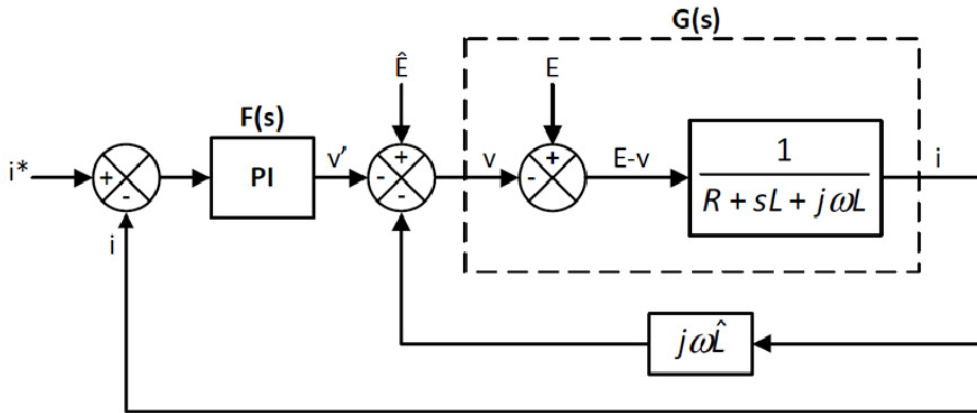


Figure 3.8 : Current control with inner decoupling loop

⇒ Cross coupling cancellation

The first step in the controller design is to cancel the cross coupling initiated by the term $j\omega L\underline{i}$ (since multiplication by j maps the d axis on q axis and vice versa). This easily possible if we have an accurate estimation of L which is \hat{L} .

According to [9] , a PI current controller has no satisfactory tracing performance for the coupled system described by equations (2.17)(2.18). For high performance and accuracy current tracking we need to cancel this cross-coupling. We select v as

$$\underline{v} = -\underline{v}' + \underline{\hat{E}} - j\omega\hat{L}\underline{i} \quad (3.6)$$

with \hat{E} the estimated value of E . Then, if $\hat{L} = L$ and $\hat{E} = E$ we get

$$\underline{\dot{i}} = \frac{\underline{v}'}{R + sL} \Rightarrow \underline{G}'(s) = \frac{\underline{\dot{i}}}{\underline{v}'} = \frac{1}{R + sL} \quad (3.7)$$

with $\underline{G}'(s)$ the decoupled system transfer function from \underline{v}' to $\underline{\dot{i}}$.

➤ Controller transfer function $F(s)$

As the complex transfer function is a first order (representing two non-interacting first order system in the d and q directions), a PI controller is enough :

$$F(s) = k_p + \frac{k_i}{s} \quad (3.8)$$

Based on IMC method of [14] , we can write

$$F(s) = \frac{\alpha_i}{s} \hat{G}'^{-1}(s) = \frac{\alpha_i}{s} (\hat{R} + s\hat{L}) = \alpha_i \hat{L} + \frac{\alpha_i \hat{R}}{s} \quad (3.9)$$

with α_i (rad/s) the current controller bandwidth where the pole of $G'(s)$ is placed, and $\hat{G}'(s)$ the estimation of $G'(s)$. Finally, we obtain the PI coefficients :

$$\boxed{k_p = \alpha_i \hat{L} \text{ and } k_i = \alpha_i \hat{R} .} \quad (3.10) \quad (3.11)$$

For this inner current control loop, the bandwidth α_i should be selected smaller than a decade below the sampling frequency (F_s [Hz]) [14]).

$$\boxed{\alpha_i < 2\pi \frac{F_s}{10}} \quad (3.12)$$

➤ Decoupled current control design

In order to establish the decoupled current control diagram, we have to continue with equation (3.6). We define \underline{l} , complex integrator state variable as :

$$\frac{d\underline{l}}{dt} = \underline{\varepsilon} \quad (3.13)$$

$$\begin{aligned} \underline{v} &= -\underline{v}' + \hat{\underline{E}} - j\omega \hat{L} \underline{\dot{i}} \\ \Leftrightarrow \underline{v} &= \hat{\underline{E}} - k_p \underline{\varepsilon} - k_i \underline{l} - j\omega \hat{L} \underline{\dot{i}} \\ \Leftrightarrow \underline{v} &= (\hat{\underline{E}}d + j\hat{\underline{E}}q) - k_p(\varepsilon d + j\varepsilon q) - k_i(l_d + jl_q) - j\omega \hat{L}(id + jiq) \end{aligned}$$

Then, we can write the real and imaginary part to get our reference voltage and draw our current controller block diagram :

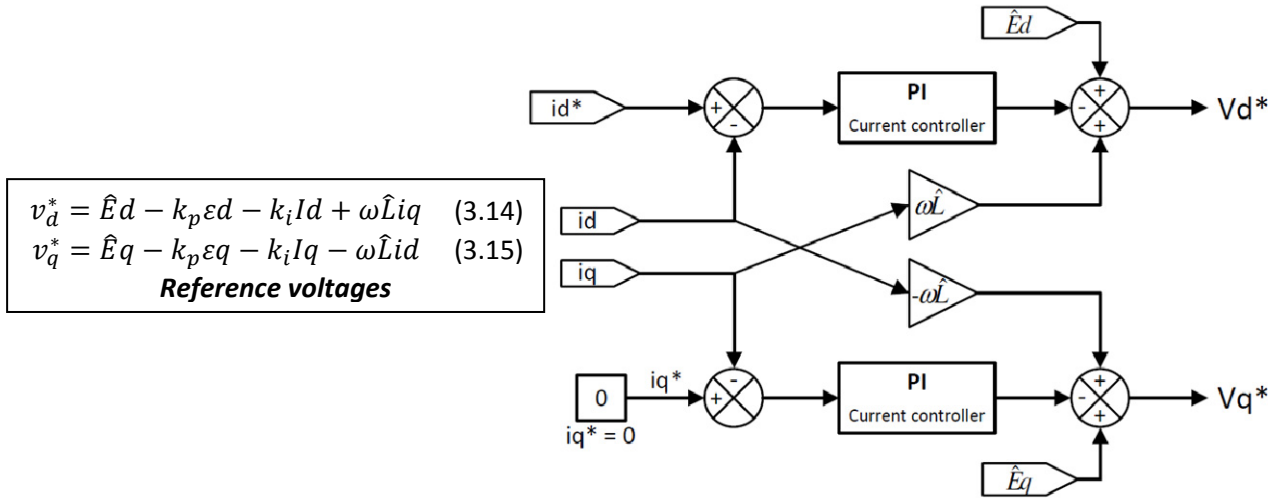


Figure 3.9 : Current controller block diagram

Comments : In our system, the line current i_L is split into a q-component i_{Lq} and a d-component i_{Ld} . i_{Ld} determines the active power flow whereas i_{Lq} the reactive power. The **unit power factor** (UPF) condition is met when the line current vector i_L is aligned with line voltage u_L . In this case, we have to set i_{Lq} to zero in our controller ($i_q^* = 0$).

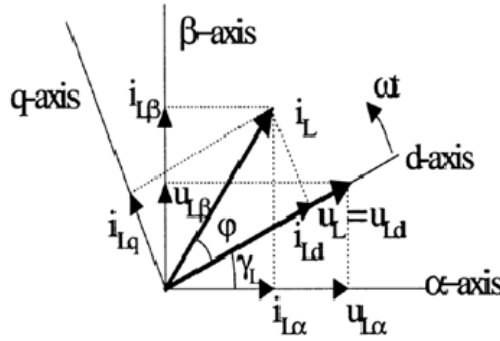


Figure 3.10 : Vector diagram of VOC – Line current and voltage [9]

Furthermore, we can write down the equation for power and see that the reactive power is set to zero. From the power equations established in section “2.2.2 Mathematical model” we can write

$$P = \frac{3}{2} \text{Re}\{v^{dq} (i^{dq})^*\} = \frac{3}{2} (v_d i_d + v_q i_q) = \frac{3}{2} (E_d i_d + E_q i_q) \quad (3.16)$$

$$Q = \frac{3}{2} \text{Im}\{v^{dq} (i^{dq})^*\} = \frac{3}{2} (v_q i_d - v_d i_q) = \frac{3}{2} (E_q i_d - E_d i_q) \quad (3.17)$$

Now if we set the reference i_q to zero and we know that the line voltage vector is aligned with the d-axis, so $E_q = 0 \text{ V}$. Finally, we get

$$P = \frac{3}{2} E_d i_d \quad (3.18)$$

$$Q = 0$$

3.4.4 Active damping, voltage saturation, anti-windup

ACTIVE DAMPING

As it's fully explained in [4] (section 1.4–p24), the current control error ε could be decrease be increasing R. Therefore, we can add a inner feedback loop which add Ra (just using signal, there is no energy transfer or more losses). This method improve disturbance rejection capability because

the dynamics are speeded up from L/R to $L/(R+Ra)$. Active damping is also used when R and L value are not estimated precisely.

This active damping is not implemented in this thesis.

REFERENCE VOLTAGE SATURATION

We have treated the current control loop as an ideal and linear system. In practice, this is not correct because the reference voltage is limited to an upper and lower value. For large step of the d-current, the controller might demand a large voltage vector (outside the switching hexagon that defines the switching possibilities). This exceeds the realizable voltage modulus of a PWM converter ([4] [14]).

The saturation is applied on the modulus of the complex value of the reference voltage $\underline{v} = vd + jvq$, that is, $|\underline{v}| = \sqrt{vd^2 + vq^2}$.

The saturation value depends on the DC-link voltage. The maximum value of reference voltage is $V_{max} = V_{dc}/2$.

The simplest method to create the saturation $[V_{dc}/2 ; -V_{dc}/2]$ in Simulink is to normalized the modulus of reference voltage by $V_{dc}/2$ before the saturation block. Then, the saturation block is the set to $[1 ; -1]$ (it means a saturation between $V_{dc}/2$ and $-V_{dc}/2$). Finally, we multiply back the output of the saturation block by $V_{dc}/2$.

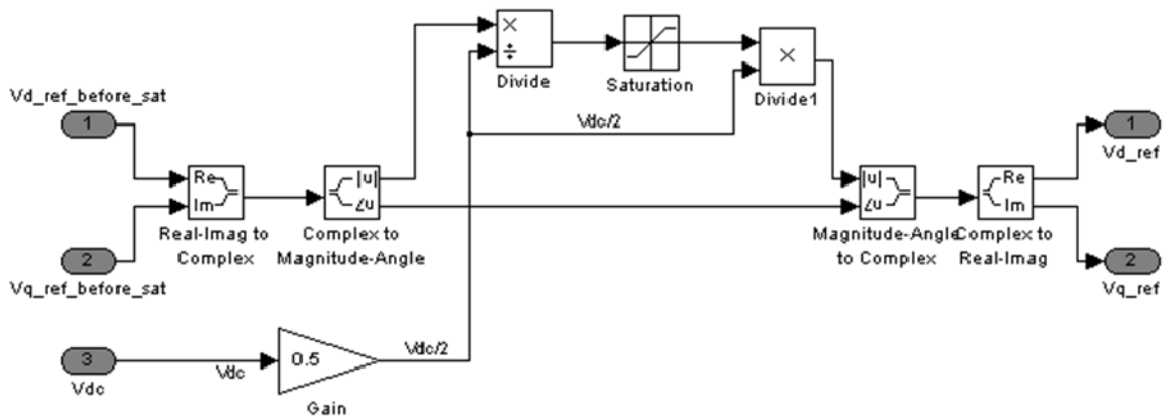


Figure 3.11 : Reference voltage saturation – Simulink implementation

INTEGRATOR ANTI-WINDUP

Principle

As we said in the previous section, for large step of the d-current, the controller might demand a too large voltage vector (outside the switching hexagon). This exceeds the realizable voltage modulus of a PWM converter ([14]).

We call v the reference voltage. The PI controller is :

$$\frac{dI(t)}{dt} = \varepsilon$$

$$v(t) = k_p \varepsilon(t) + k_i I(t)$$

Once v become limited (\bar{v}), the integrator part of the PI controller can introduce a phenomenon called *integrator windup*. An integrator windup generally manifest itself by an overshoot (to the step response). In order to avoid windup, the integrator part I should not be updated with too large error ε . We should feed the integrator with another error $\bar{\varepsilon}$, so that $v = \bar{v}$.

$$\bar{v}(t) = k_p \bar{\varepsilon}(t) + k_i I(t)$$

Then, writing the difference $\bar{v} - v$ we can obtain

$$\bar{\varepsilon} = \varepsilon + \frac{\bar{v} - v}{k_p}$$

The following controller results :

$$\begin{aligned} \frac{dI(t)}{dt} &= \bar{\varepsilon} \\ v(t) &= k_p \varepsilon(t) + k_i I(t) \\ \bar{v} &= [v]_{min}^{max} \end{aligned}$$

(source : [4] [14])

In our case...

For the decoupled controller, the following equation have been found :

$$v_{dq}^* = \hat{E}_{dq} - k_p \varepsilon_{dq} - k_i I_{dq} - j\omega \hat{L}i_d + \omega \hat{L}i_q$$

Now we call \bar{v} the value of v_{dq}^* after saturation, we can write :

$$\bar{v} = \hat{E}_{dq} - k_p \bar{\varepsilon}_{dq} - k_i I_{dq} - j\omega \hat{L}i_d + \omega \hat{L}i_q$$

By writing the difference $v_{dq}^* - \bar{v}$, we can find $\bar{\varepsilon}_{dq}$:

$$\bar{\varepsilon}_{dq} = \varepsilon_{dq} + \frac{v_{dq}^* - \bar{v}}{k_p} \tag{3.19}$$

The PI current controller will be created as follow.

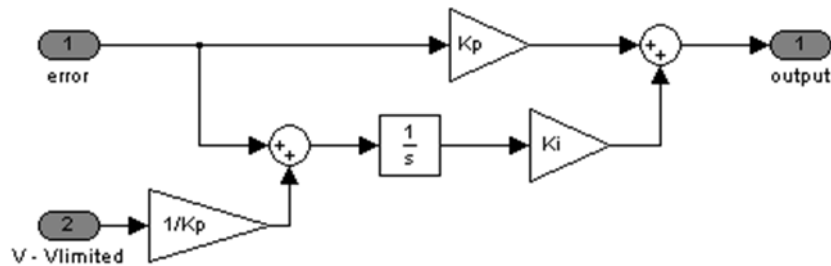


Figure 3.12 : PI controller with anti-windup

3.4.5 Current controller simulation

BLOCK DIAGRAM

The simulation have been done following the following equations (equation (2.8) of section "2.2.2 Mathematical model") :

$$\begin{bmatrix} u_a \\ u_b \\ u_c \end{bmatrix} = R \begin{bmatrix} i_a \\ i_b \\ i_c \end{bmatrix} + L \frac{d}{dt} \begin{bmatrix} i_a \\ i_b \\ i_c \end{bmatrix} + \begin{bmatrix} u_{Sa} \\ u_{Sb} \\ u_{Sc} \end{bmatrix}$$

For each phase we know that the current is equal to

$$i = \frac{u - u_S}{R + sL}$$

Also, we can draw the following diagram block (Figure 3.13).

- I_d^* will be chosen ;

- $U_a U_b U_c$ are line voltage ;
- $E_d E_q$ are the dq-transformation of $U_a U_b U_c$.

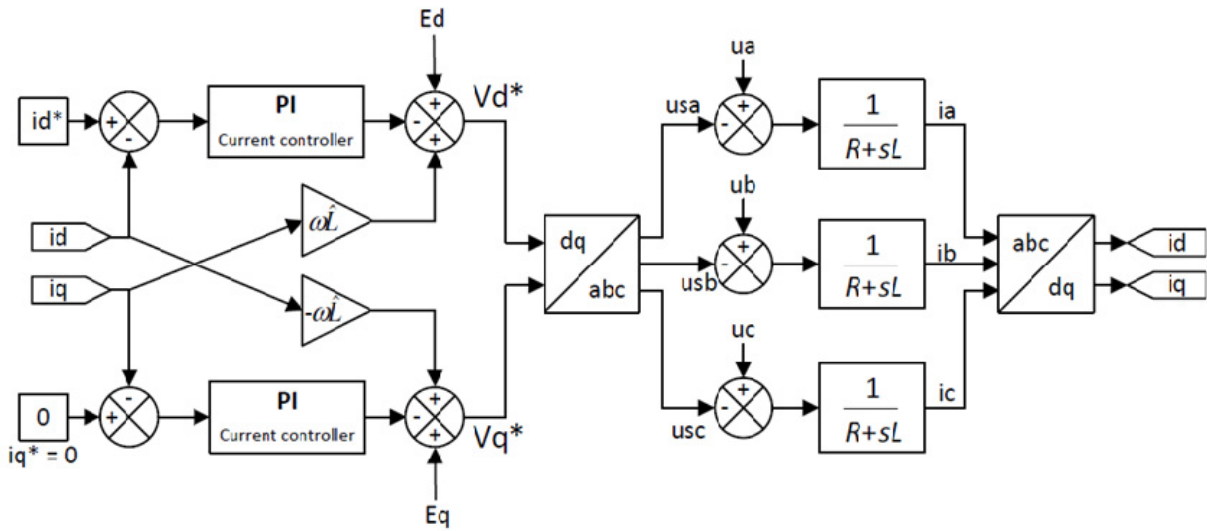


Figure 3.13 : Block diagram for current control tests

Remark : The tests can also be simulated in dq but we’ve decided to stay in ABC-frame to model the rectifier and the grid impedance to be as close as possible to the real system.

SIMULATION

The system have been simulated in continuous and discrete (only the continuous simulation is shown here). No saturation or anti-windup are present in this simulation. They will be added later.

Parameters	Value
R (Ω)	0.1
L (H)	5e-3
ω (rad/s)	$2\pi 50$
E_m (V), ph-to-gnd amplitude (=Ed)	$115\sqrt{2}$
I_d^* (A)	3
I_d^* step (A) at 0.025s	3
I_q^* (A)	0
Fsw (kHz), switching frequency	20
$\alpha_i = 2\pi F_{SW}/10$ (rad/s)	1.26e4
PI controller, Kpi	62.8
PI controller, Kii	1.26e3

Table 3.1 : Current controller simulation parameters

- The bandwidth of the current controller have been selected at : $\frac{F_{SW}}{10} = 2 \text{ kHz}$ (we chose to take a decade smaller than the switching frequency).
- \hat{L} is selected equal to L .
- The Simulink block diagram is available in APPENDIX B-B.1, Figure 0.7. We also advice to read the simulation of coordinate transformation in APPENDIX A-A.4 before.

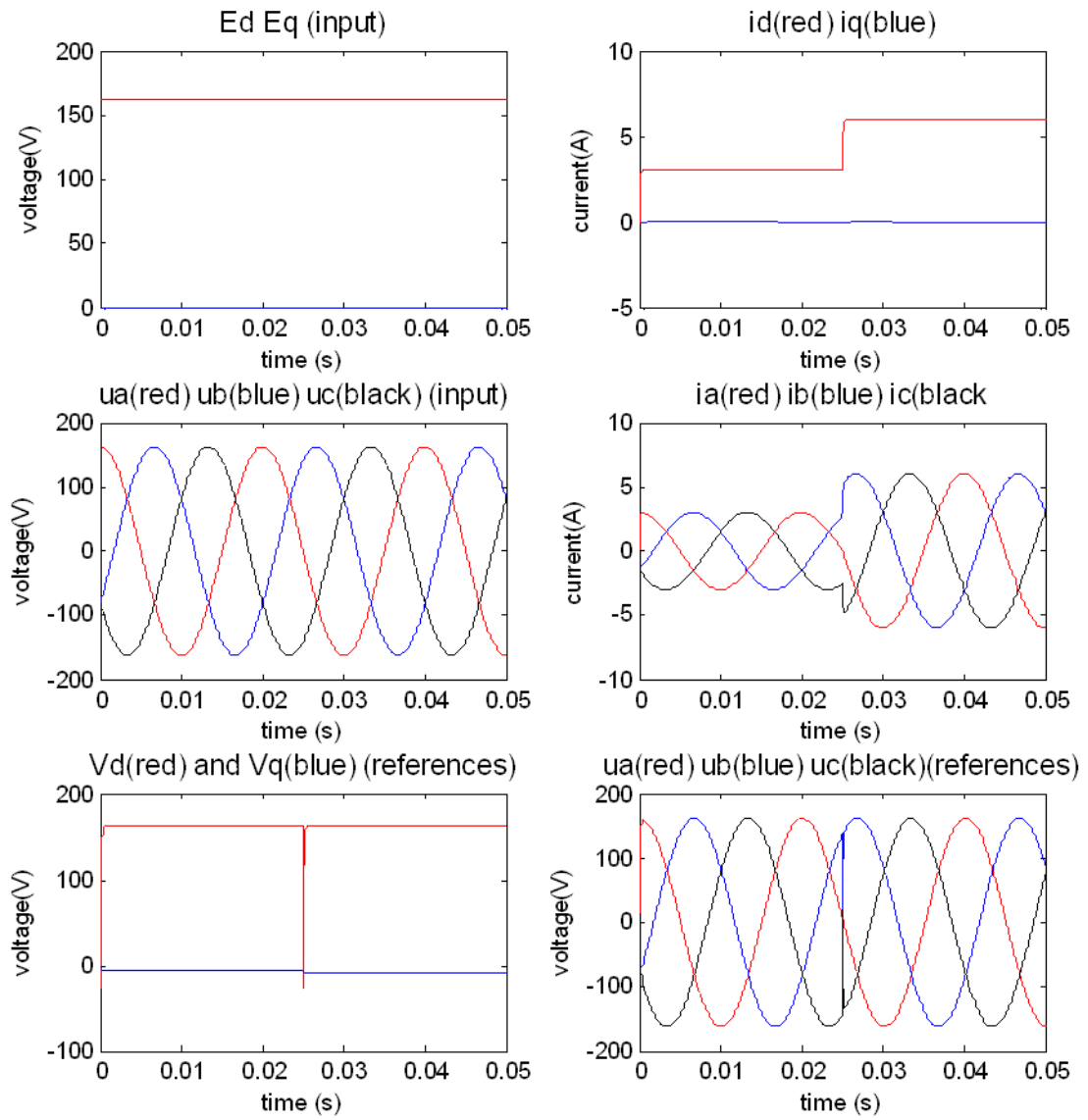


Figure 3.14 : Current control simulation

Remark : The value of i_q is zero when a zoom is done (even if a q-current is visible in the previous figure).

3.5 DC-link voltage controller

3.5.1 DC-link model and linearization

DC-LINK MODEL

The DC-link voltage is modeled as a pure capacitor. This capacitor is an energy storage where the stored electrical energy in Joule is

$$E_c = \frac{1}{2} C \cdot v_{dc}^2 \quad (3.20)$$

The time derivative of this stored energy should be equal to the sum of instantaneous grid power and load power [14].

$$\frac{1}{2} C \frac{dv_{dc}^2}{dt} = P_g - P_{load} \quad (3.21)$$

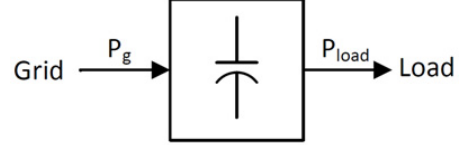


Figure 3.15 : Energy transfer

As we can see, the previous equation is not linear with respect to V_{dc} .

LINEARIZATION

The design of the voltage controller is facilitated thanks a feedback linearization. The feedback linearization transforms the nonlinear dc-voltage dynamics to a equivalent linear system, on which traditional linear controller design can be applied.

We now choose a new state variable W .

$$W = v_{dc}^2 \quad (3.22)$$

Then, equation (3.21) becomes

$$\frac{1}{2} C \frac{dW}{dt} = P_g - P_{load} \quad (3.23)$$

which is linear with respect to W . The physical interpretation is that the energy is chosen to represent the dc-link voltage dynamics instead of the voltage itself. Other type of linearization can be found [14].

3.5.2 Design of voltage controller

System transfer function

Following [14] and the Internal Model Control method, we can write

$$\begin{aligned} \frac{1}{2} C \frac{dW}{dt} &= P_g - P_{load} \\ P_g &= \frac{3}{2} E_g id \end{aligned} \quad (3.18)$$

$$P_{load} = \frac{v_{dc}^2}{R_{load}} = \frac{W}{R_{load}} \quad (3.24)$$

where id is the d-current, and the grid voltage $E_g = E_d$. The coefficient $\frac{3}{2}$ comes from the amplitude invariant transformation (see section "2.2.2 Mathematical model" about power calculation).

$$\frac{1}{2} C \frac{dW}{dt} = \frac{3}{2} E_g id - P_{load} \quad (3.25)$$

$$\begin{aligned} \Leftrightarrow \frac{L}{2}CsW &= \frac{3}{2}E_g id - P_{load} \\ \Leftrightarrow CsW &= 3E_g id - 2P_{load} \\ \Leftrightarrow W &= \frac{3E_g}{sC} id - \frac{2}{sC}P_{load} \end{aligned}$$

Then, the system transfer function $G(s)$ is

$$G(s) = \frac{W}{id} = \frac{3E_g}{sC} \quad (3.26)$$

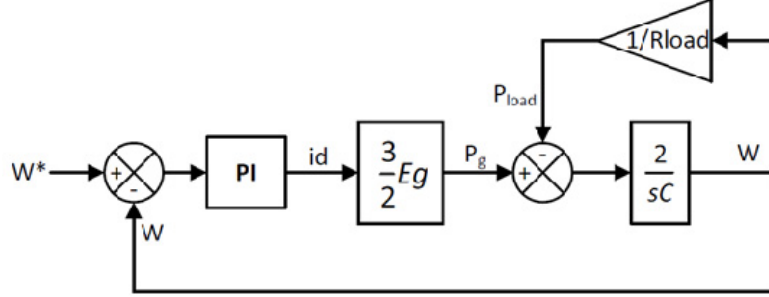


Figure 3.16 : Voltage control loop

➔ Controller transfer function

$$F(s) = \frac{\alpha_v}{s} \hat{G}^{-1}(s) = \frac{\alpha_v \hat{C}}{3\hat{E}_g} \quad (3.27)$$

where $\hat{G}(s)$ is the estimation of $G(s)$ and α_v (rad/s) is the bandwidth of the voltage controller. Then, $F(s)$ give us a proportional coefficient Kp_v :

$$Kp_v = \frac{\alpha_v \hat{C}}{3\hat{E}_g} = \frac{\alpha_v \hat{C}}{3\hat{E}_m} \quad (3.28)$$

with $\hat{E}_g = \hat{E}_d = \hat{E}_m$ (E_m is the amplitude of the three-phase input voltage in the model section "2.2.2 Mathematical model")

We will choose α_v at least a decade smaller than the current control bandwidth.

$$\alpha_v < \frac{\alpha_i}{10} \quad (3.29)$$

As we can see there is no integrator part in the controller. In our controller, we will add a small integrator part with gain Ki_v (for example $Ki_v = 0.01$).

3.5.3 Voltage saturation, anti-windup, active damping

SATURATION, ANTI-WINDUP

Exactly as the current controller, we have to add a saturation (on current id^*) and an anti-windup is highly recommended (useful is the saturation limit is reached).

In this case we can write :

$$id^* = k_p \varepsilon + k_i I$$

with $I = \frac{\varepsilon}{p}$. If we do the same calculation than the current controller case, we can find :

$$\bar{\varepsilon} = \varepsilon + \frac{\bar{id} - id^*}{k_p} \quad (3.30)$$

Then, the PI voltage controller scheme will be as below.

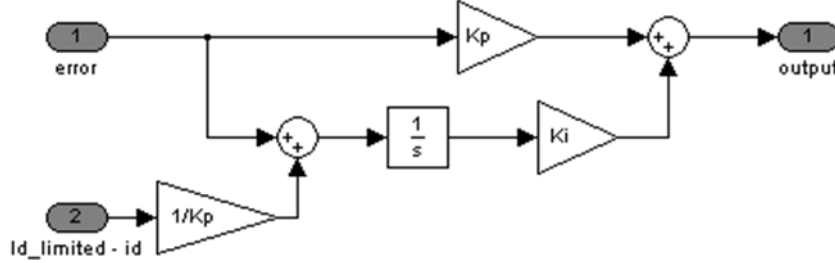


Figure 3.17 : PI controller with anti-windup

ACTIVE DAMPING

Previously, we found a system transfer function $G(s)$ (equation (3.26)) as

$$G(s) = \frac{W}{id} = \frac{3E_g}{sC}$$

which has a pole at the origin. [14] advice to add an active damping in this case, to place the pole at $-\alpha_v$, with α_v the bandwidth of the voltage controller.

System transfer function

Based on [14] , we can find the following equations and block diagram (Figure 3.18). We can start again with equation (3.25):

$$\frac{1}{2}C \frac{dW}{dt} = \frac{3}{2}E_g id - P_{load} \quad (3.25)$$

We chose to define id with

$$id = id' - GaW \quad (3.31)$$

where Ga is the active conductance that provides active damping. Then, by substituting equation (3.31) into (3.25), the system model becomes

$$\frac{1}{2}C \frac{dW}{dt} = \frac{3}{2}E_g id' - \frac{3}{2}E_g GaW - P_{load} \quad (3.32)$$

The system transfer function becomes

$$G'(s) = \frac{W}{id'} = \frac{3E_g}{sC + 3E_g Ga} \quad (3.33)$$

As we can see, we still have a first order system but the pole can be chosen with Ga . Placing the pole at $-\alpha_v$ we can find Ga as

$$sC + 3E_g Ga = 0 \Leftrightarrow (-\alpha_v)C + 3E_g Ga = 0$$

$$\boxed{Ga = \frac{\alpha_v C}{3E_g}} \quad (3.34)$$

➔ **Controller transfer function**

Following the previous IMC method, we obtain

$$F(s) = \frac{\alpha_v}{s} \widehat{G}^{-1}(s) = \frac{\alpha_v \widehat{C}}{3\widehat{E}_g} + \frac{\alpha_v G a}{s} \quad (3.35)$$

$Kp_v = \frac{\alpha_v \widehat{C}}{3\widehat{E}_g} = \frac{\alpha_v \widehat{C}}{3\widehat{E}_m}$	$Ki_v = \alpha_v G a = \frac{\alpha_v^2 C}{3\widehat{E}_m}$
(3.28)	(3.36)

with $\widehat{E}_g = \widehat{E}_d = \widehat{E}_m$.

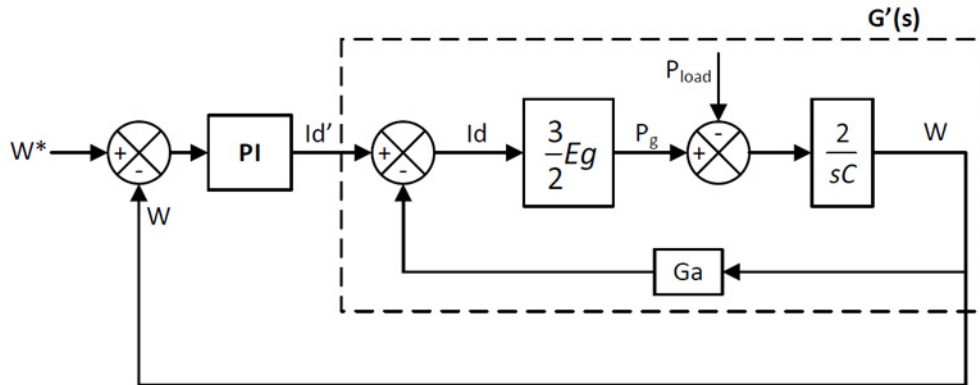


Figure 3.18 : Voltage control loop with active damping

3.5.4 Voltage controller simulation

The system represented in Figure 3.19 is first simulated without saturation, then with saturation, and finally, an anti-windup is added. The simulation parameters and Simulink scheme are presented below.

Parameters	Value
C (μF)	2200
ω (rad/s)	2π50
Em (V), ph-to-gnd amplitude (=Ed)	115√2
Fsw (kHz), switching frequency	20
α _v = 2π F _{SW} /100 (rad/s)	1.26e3
PI controller, K _p v	0.0057
PI controller, K _i v	0.01
Vdc reference (V)	400
Rload (Ω)	500

Table 3.2 : Voltage controller simulation

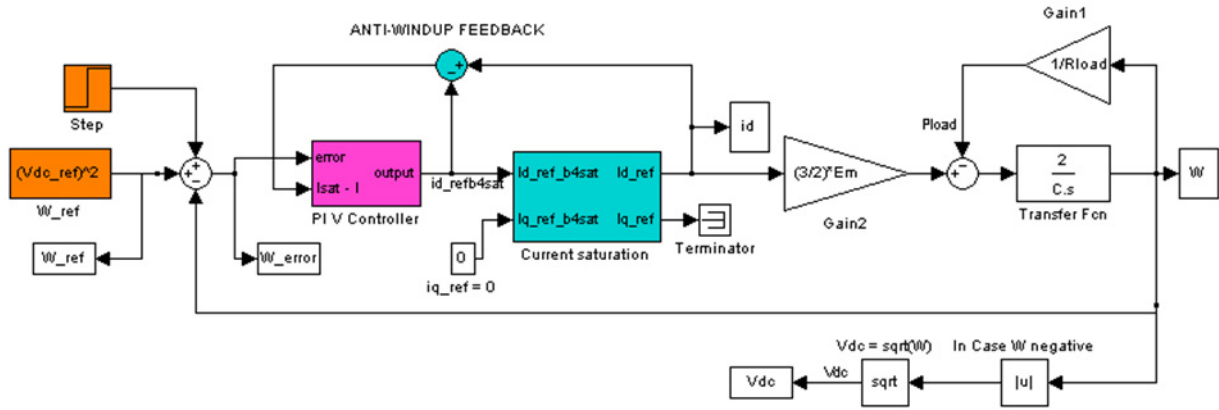


Figure 3.19 : Voltage controller – Simulink block scheme

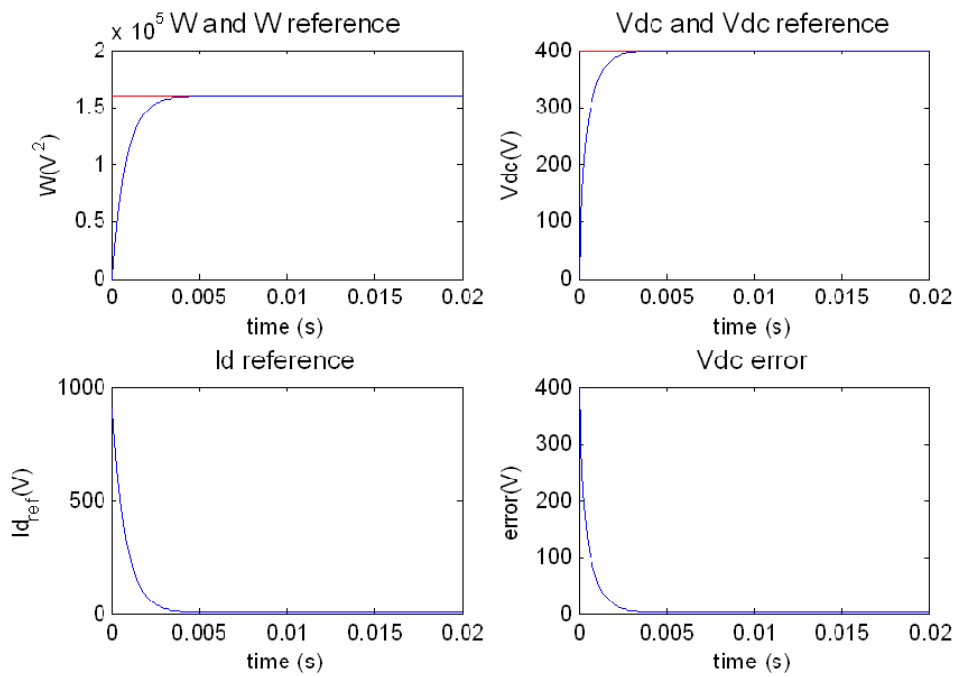


Figure 3.20 : Voltage control – Without saturation

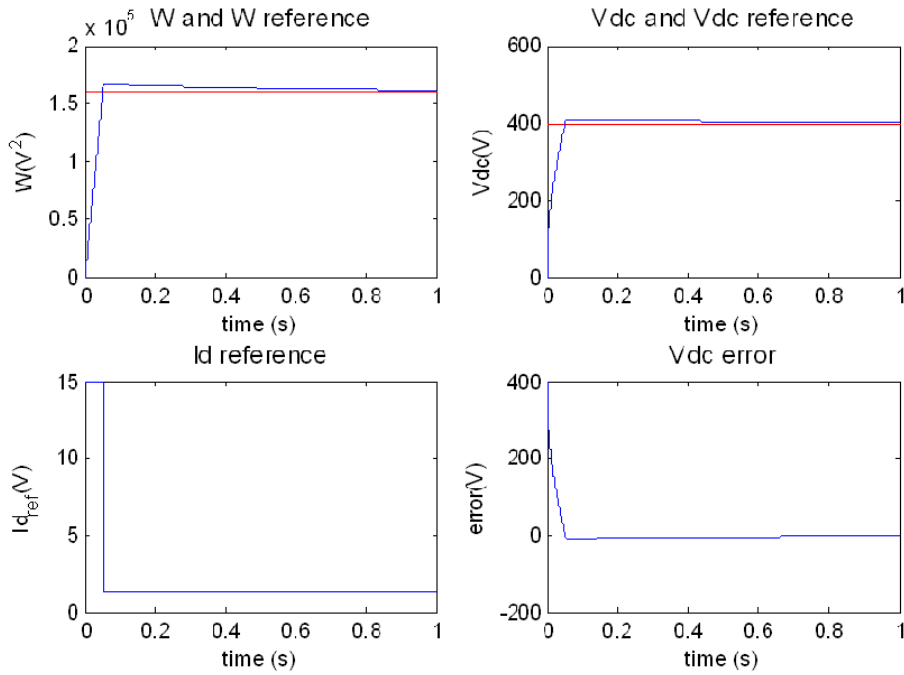


Figure 3.21 : Voltage control – With saturation15A

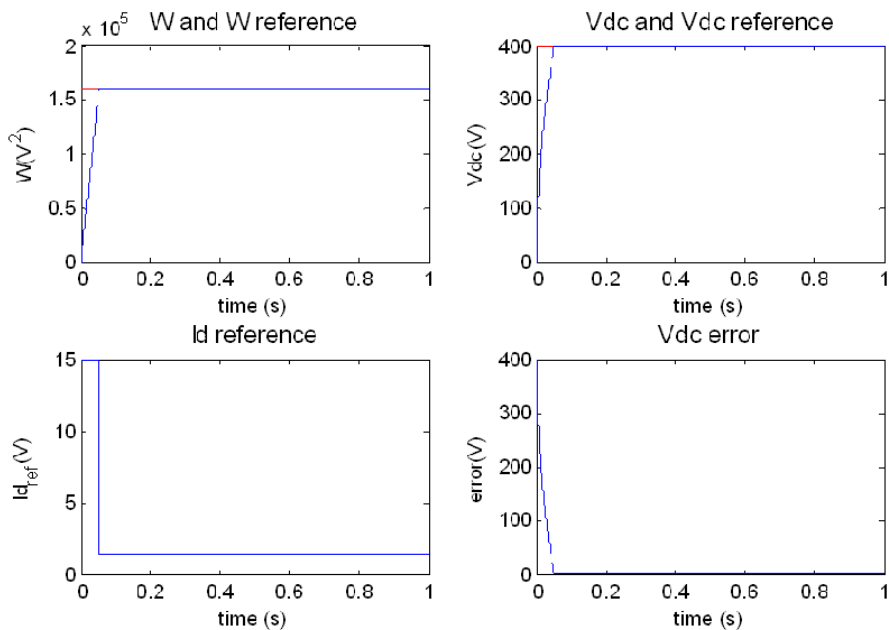


Figure 3.22 : Voltage control – With saturation15A and anti-windup

➡ **Without saturation (Figure 3.20)**

We can see a fast response, a small error close to zero (0.0001V at 3second). But, we observe a very high current about 800A. We need to add the saturation here.

➡ **With saturation (Figure 3.21)**

The error has been increased lightly (Error 0.06V with Rload = 500Ω, Error 0.1V with Rload = 50Ω). We observe that the error depends on the saturation upper and lower value and depends also on the load.

As the current is now limited the response is much slower. Finally, we also observe the so called integrator windup due to the saturation.

➔ **With saturation and anti-windup (Figure 3.22)**

We now include the back calculation anti-windup and as we can see, the overshoot disappeared. The error is also reduce.

➔ **With saturation, anti-windup and active damping (APPENDIX B-B.2, Figure 0.8, Table 0.1)**

In this simulation, the active damping doesn't influence the system.

3.5.5 Simulation with current controller

The whole system can now be simulated. The rectifier is modeled according to the following Simulink scheme (Figure 3.23 and Figure 3.24) and data (Table 3.3)

PARAMETERS	VALUE
R (Ω)	0.1
L (H)	5e-3
C (μ F)	2200
ω (rad/s)	$2\pi 50$
Em (V), ph-to-gnd amplitude (=Ed)	$115\sqrt{2}$
Fsw (kHz), switching frequency	20
Rload (Ω)	500
Vdc reference (V)	400
$\alpha_i = 2\pi F_{SW}/10$ (rad/s)	1.26e4
$\alpha_v = 2\pi F_{SW}/100$ (rad/s)	1.26e3
V controller, Kpv	0.0057
V controller, Kiv	0.01
I controller, Kpi	62.8
I controller, Kii	1.26e3
I saturation (A)	± 15
Vdc step at 0.03 (V)	50

Table 3.3 : *Current and voltage controller simulation parameters*

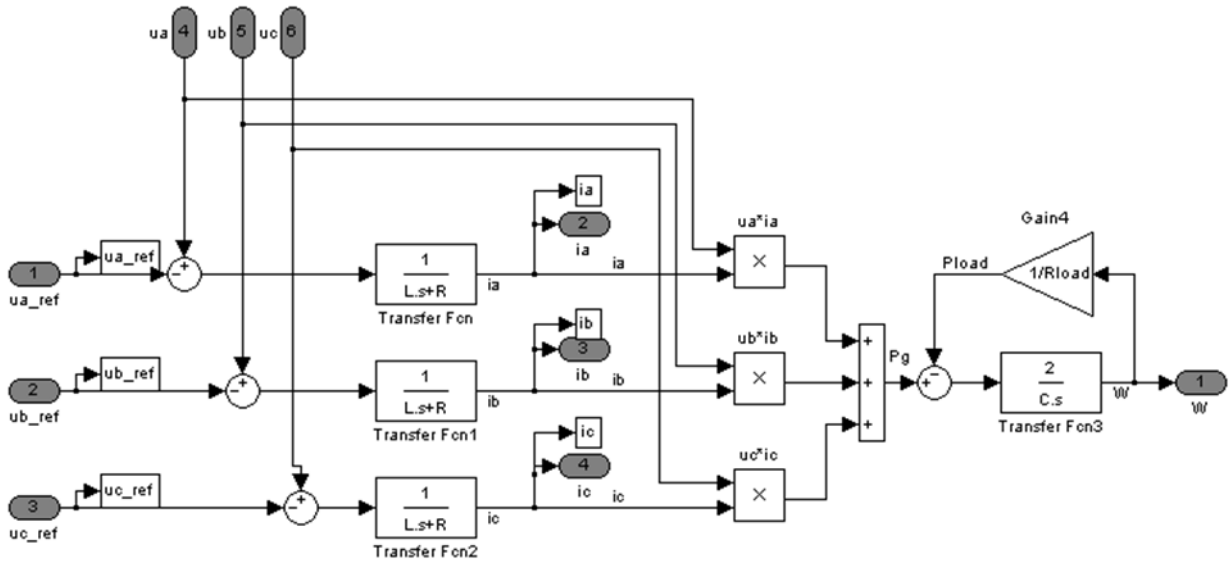


Figure 3.23 : Simulink block scheme – Grid impedance and dc-link model

In the previous figure, the signals $uabc_ref$ come from the controller (after dq-to-abc transformation).

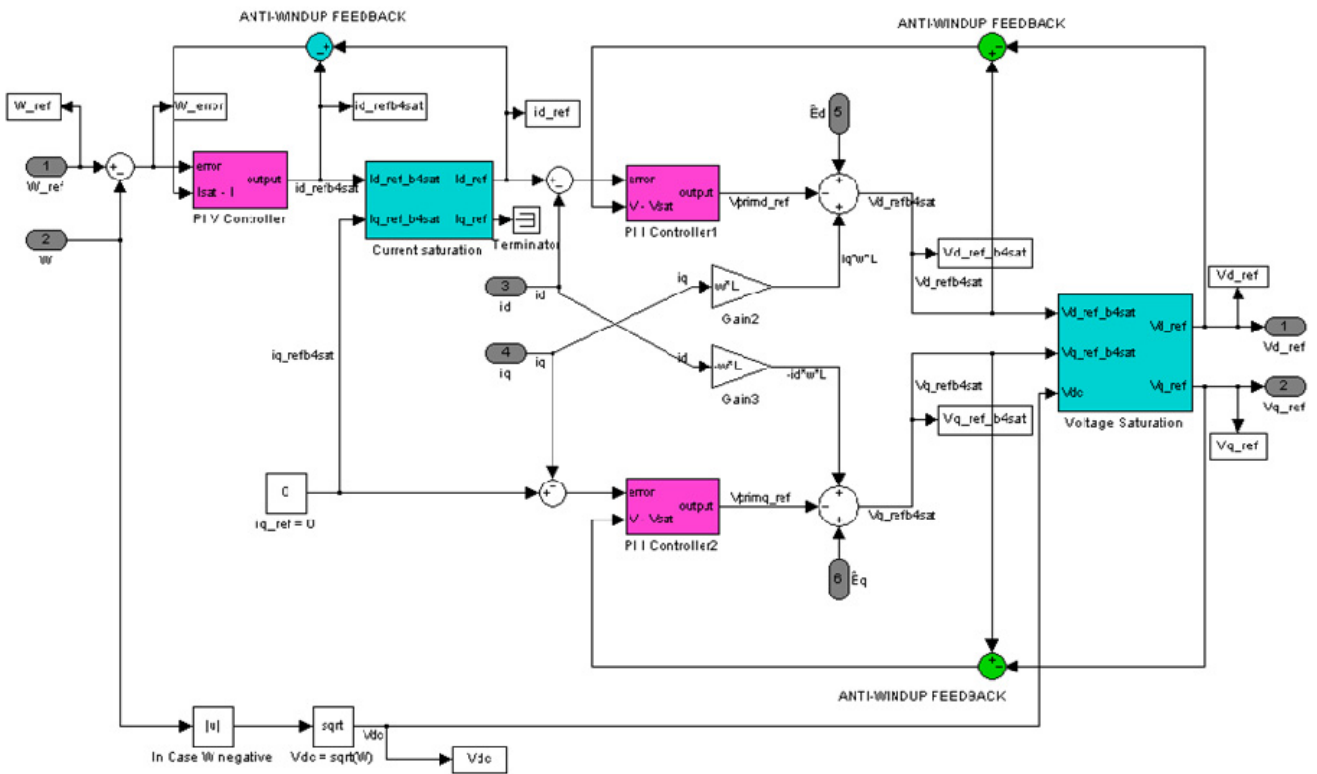


Figure 3.24 : Simulink block scheme – Controller

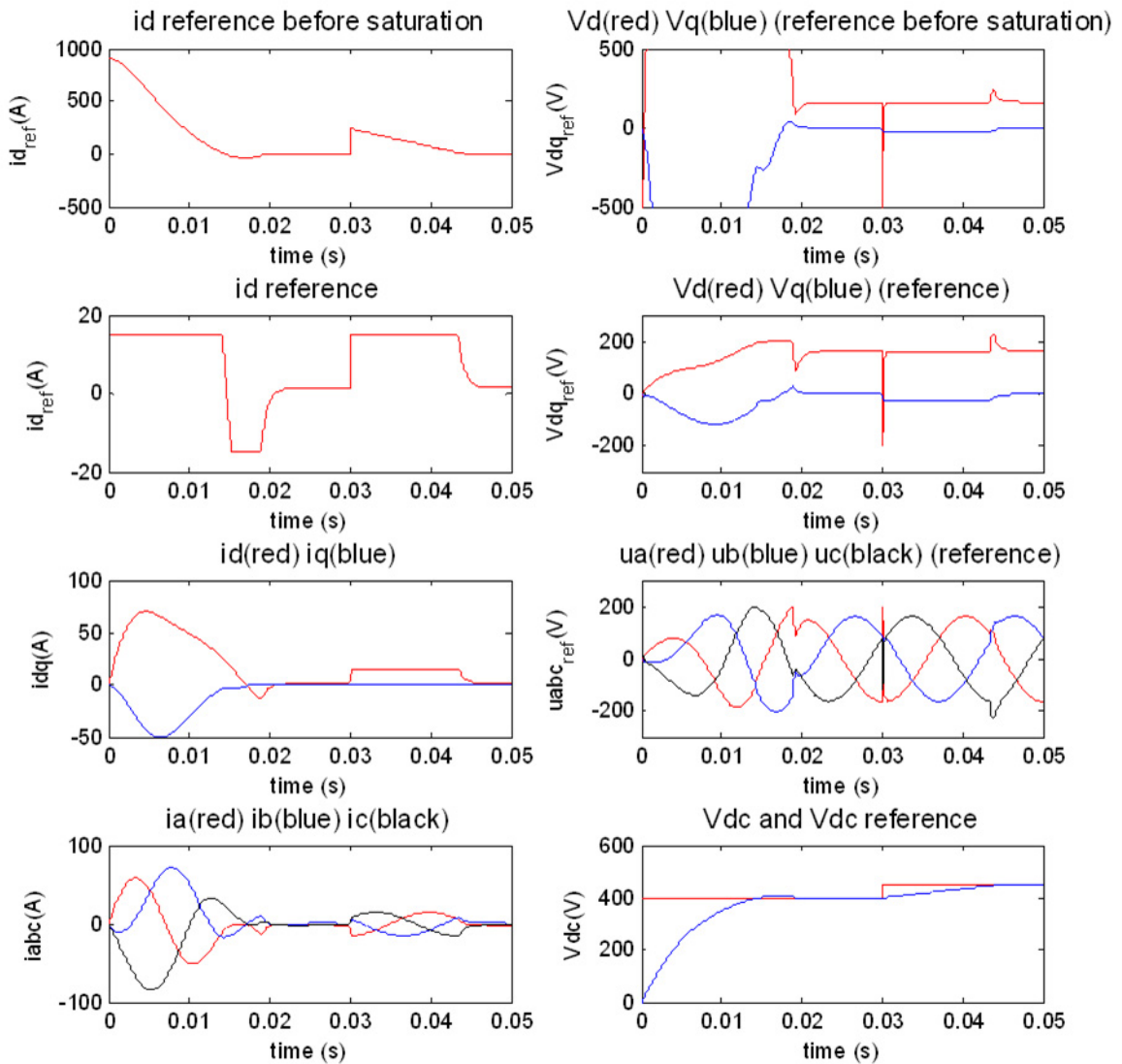


Figure 3.25 : Controller simulation results

In the Figure 3.25, we observe a very high current when the system start (i_d reaches 70A), and we can see also a small overshoot on V_{dc} . This is due to the capacitor charging. Now we apply a small step on V_{dc} reference (50V), and we can see that the d-current reaches the saturation limit (15A) when V_{dc} is increasing towards the reference value (450V). Finally, when V_{dc} reaches the reference value (without overshoot), the current is stabilize around 1.3A (steady state value).

DISCRETE SIMULATION

All the previous design and simulation have also been implemented in discrete time since the controller will be discrete in reality. You can find a discrete simulation of the controller (same scheme as Figure 3.24) in APPENDIX D.

3.5.6 Controller improvements

FILTERS

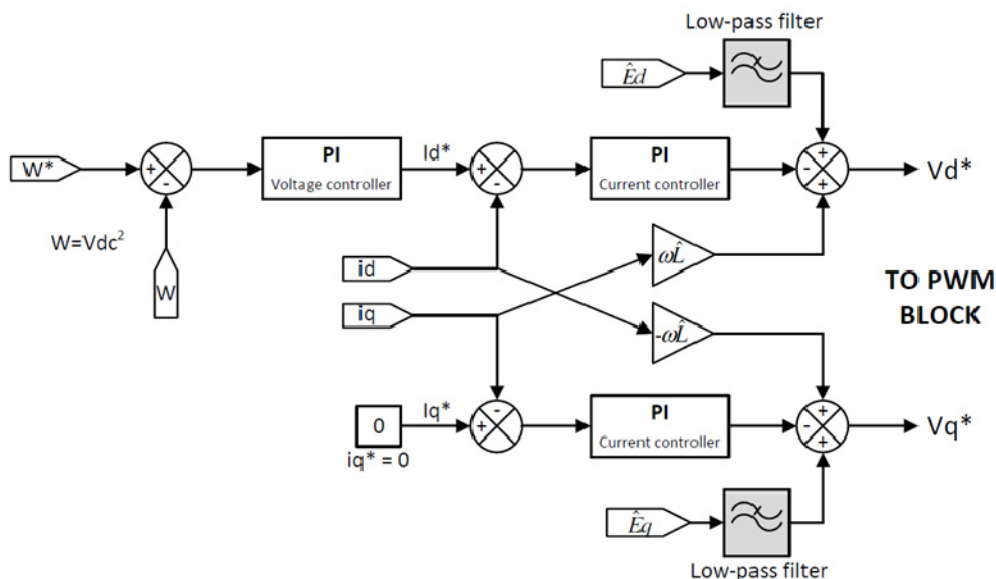


Figure 3.26 : Decoupled controller with filter

$\hat{E}dq$ represent the line voltage (grid, or V_{PCC}) and Vdq the converter voltage. We received a piece of advice regarding the feed-forward term $\hat{E}dq$ in the controller Figure 3.26. This feed-forward could turn the system unstable if some high frequency oscillations appear on $\hat{E}dq$.

To remove any high frequency oscillations, we decided to add a filter for each feed-forward. We chose a first order discrete filter with a bandwidth a decade lower than the current control bandwidth :

$$\alpha_{filter} = \frac{\alpha_i}{10} \tag{3.37}$$

If the grid is stiff enough, the bandwidth of the filter can be equal to the current controller bandwidth.

INTEGRATORS

We can see in the previous scheme that two integrator are in cascade, an integrator in the voltage controller and one in the current controller. The current controller integrator can probably be removed (then, the anti-windup also).

LOAD COMPENSATION

In the papers [11] , a load compensation has been proposed to minimized the influence of rapid changes of the converter load. The feed-forward information (see schematic on Figure 3.27) about the actual converter load has also contributed to improve the transient response of the DC-link voltage. This compensation is not implemented in this report.

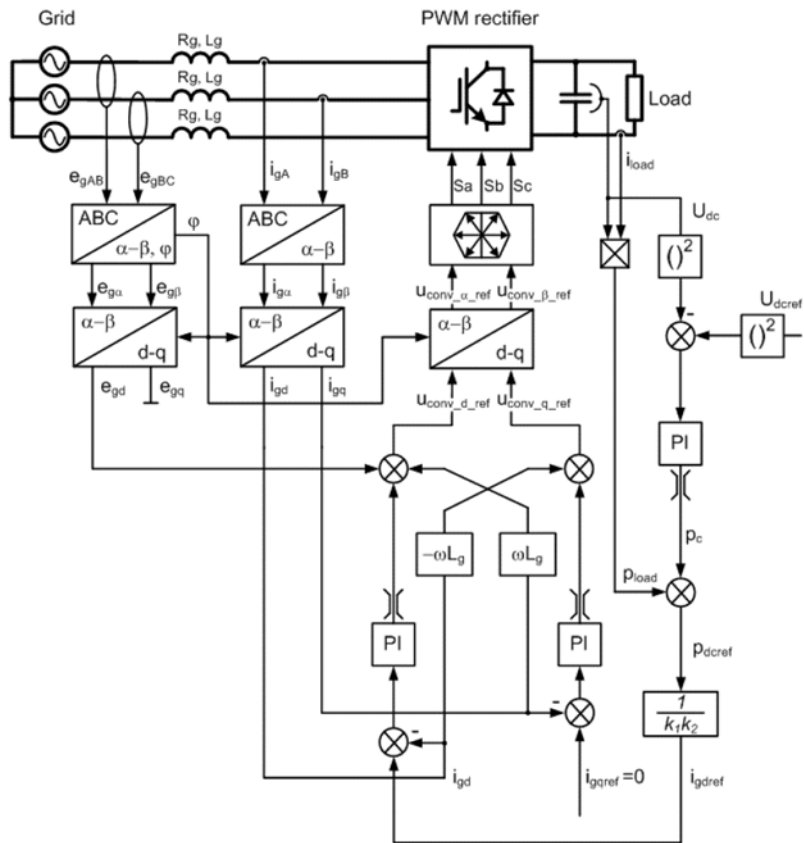


Figure 3.27 : Improvement proposed in [11]

3.6 Stability analysis

We decided to do a small stability analysis with the current controller only, voltage controller, then both voltage and current controller together. Furthermore, the analysis is done for three different voltage controller. First, only a proportional controller is taking in account (Kp_v). In a second time, the integration part is added ($Ki_v = 0.01$). And finally, the active damping coefficient Ga is added.

3.6.1 Current controller

If the cross coupling cancellation is ideal, that is, $\hat{L} = L$, we saw in section “3.4.3 Design of the synchronous PI controller” (and see Figure 3.8) that the system transfer function becomes

$$G'(s) = \frac{1}{R + sL} \quad (3.7)$$

If we see \hat{E} as a disturbance that we neglect, we obtain the following diagram

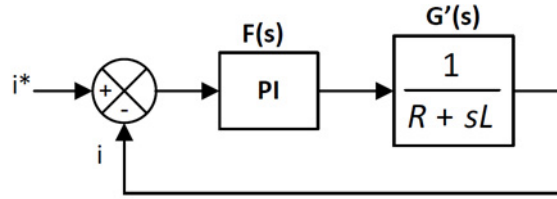


Figure 3.28 : stability analysis of current control

Now, following the IMC, we saw that the controller is calculated with

$$F(s) = \frac{\alpha_i}{s} \hat{G}'^{-1}(s) = \frac{\alpha_i}{s} (\hat{R} + s\hat{L})$$

The open- and closed-loop transfer function are noted respectively $L_i(s)$ and $S_i(s)$

$$L_i(s) = F(s)G'(s) \quad (3.38)$$

$$S_i(s) = \frac{L_i(s)}{1 + L_i(s)} \quad (3.39)$$

Furthermore, if $\hat{L} = L$ and $\hat{R} = R$, we can obtain the open- and closed-loop transfer function

$$L_i(s) = \frac{\alpha_i}{s} \quad (3.40)$$

$$S_i(s) = \frac{s}{s + \alpha_i} \quad (3.41)$$

$S_i(s)$ is a first order system, low pass filter, with a cut-off frequency α_i rad/s.

There is only one pole for $S_i(s)$ and it's located at $-\alpha_i$ (negative Real part of the Imaginary domain means stability).

3.6.2 Voltage controller

PROPORTIONAL CONTROL ONLY

We consider again the Figure 3.16 without load disturbance P_{load} and we obtain the following diagram. The system transfer function is (equation (3.26))

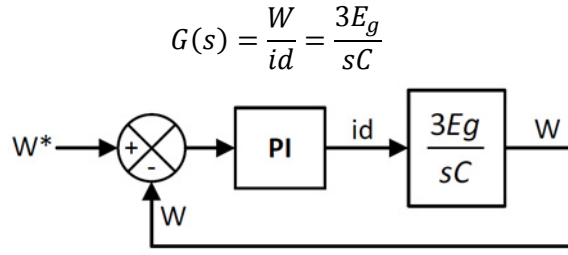


Figure 3.29 : stability analysis of voltage controller

The open- and closed-loop transfer function are noted respectively $L_v(s)$ and $S_v(s)$.

$$L_v(s) = \frac{\alpha_v}{s} \quad (3.42)$$

$$S_v(s) = \frac{s}{s + \alpha_v} \quad (3.43)$$

As the previous case, if $\hat{C} = C$ and $\hat{E}g = Eg$, $S_v(s)$ is a first order system, low pass filter, with a cut-off frequency α_v rad/s.

There is only one pole for $S_v(s)$ and it's located at $-\alpha_v$ (negative Real part of the Imaginary domain means stability).

PROPORTIONAL AND INTEGRAL CONTROL

As we explain during the voltage controller design, we decided to add a small integration constant.

The open- and closed-loop transfer function are noted respectively $L_v(s)$ and $S_v(s)$.

$$L_v(s) = F(s)G(s) = \left(Kp_v + \frac{Ki_v}{s}\right) \left(\frac{3E_g}{sC}\right) = \left(\frac{\alpha_v \hat{C}}{3\hat{E}g} + \frac{Ki_v}{s}\right) \left(\frac{3E_g}{sC}\right) = \frac{\alpha_v Cs + 3E_g Ki_v}{Cs^2} \quad (3.44)$$

$$S_v(s) = \frac{L_v(s)}{1 + L_v(s)} = \frac{\alpha_v Cs + 3E_g Ki_v}{Cs^2 + \alpha_v Cs + 3E_g Ki_v} \quad (3.45)$$

WITH ACTIVE DAMPING GA

In this case, we consider the following diagram.

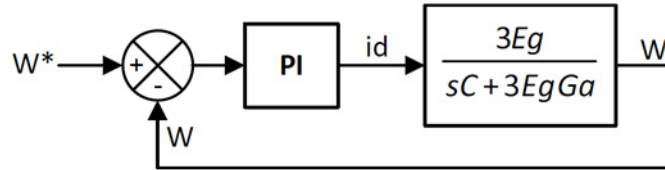


Figure 3.30 : stability analysis of voltage controller with active damping

$$L_v(s) = F(s)G(s) = \left(Kp_v + \frac{Ki_v}{s}\right) \left(\frac{3E_g}{sC + 3E_g Ga}\right) = \frac{\alpha_v Cs + \alpha_v^2 C}{Cs^2 + 3E_g Ga s} \quad (3.46)$$

$$S_v(s) = \frac{L_v(s)}{1 + L_v(s)} = \frac{\alpha_v Cs + \alpha_v^2 C}{Cs^2 + (3E_g Ga + \alpha_v C)s + \alpha_v^2 C} \quad (3.47)$$

3.6.3 Complete controller

To study the complete controller, we consider the following diagram.

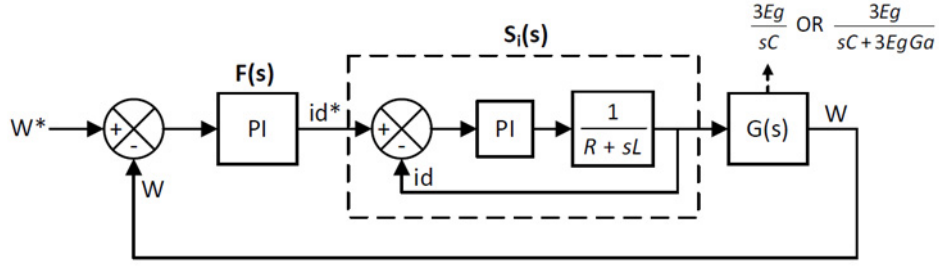


Figure 3.31 : stability analysis of controller

We can now write the open- and closed-loop transfer function $L_{vi}(s)$ and $S_{vi}(s)$:

$$L_{vi}(s) = F(s)S_i(s)G(s) = L_v(s)S_i(s) \quad (3.48)$$

$$S_{vi}(s) = \frac{L_{vi}(s)}{1 + L_{vi}(s)} \quad (3.49)$$

The following table sum-up the different transfer functions of the controller.

	P CONTROL	PI CONTROL	PI AND ACTIVE DAMPING GA
$S_i(s)$		$\frac{\alpha_i}{s + \alpha_i}$	
$L_v(s)$	$\frac{\alpha_v}{s}$	$\frac{\alpha_v Cs + 3E_g Ki_v}{Cs^2}$	$\frac{\alpha_v Cs + \alpha_v^2 C}{Cs^2 + 3E_g Ga s}$
$S_v(s)$	$\frac{\alpha_v}{s + \alpha_v}$	$\frac{\alpha_v Cs + 3E_g Ki_v}{Cs^2 + \alpha_v Cs + 3E_g Ki_v}$	$\frac{\alpha_v Cs + \alpha_v^2 C}{Cs^2 + (3E_g Ga + \alpha_v C)s + \alpha_v^2 C}$
$L_{vi}(s)$	$\frac{\alpha_v \alpha_i}{s^2 + \alpha_i s}$	$\frac{\alpha_v \alpha_i C s + 3E_g Ki_v \alpha_i}{Cs^3 + \alpha_i Cs^2}$	$\frac{\alpha_v \alpha_i C s + \alpha_v^2 \alpha_i C}{Cs^3 + (3E_g Ga + \alpha_i C)s^2 + \alpha_i 3E_g Ga s}$
$S_{vi}(s)$	$\frac{\alpha_v \alpha_i}{s^2 + \alpha_i s + \alpha_v \alpha_i}$	$\frac{\alpha_v \alpha_i C s + 3E_g Ki_v \alpha_i}{Cs^3 + \alpha_i Cs^2 + \alpha_v \alpha_i C s + 3E_g Ki_v \alpha_i}$	$\frac{\alpha_v \alpha_i C s + \alpha_v^2 \alpha_i C}{Cs^3 + (3E_g Ga + \alpha_i C)s^2 + (\alpha_i 3E_g Ga + \alpha_v \alpha_i C)s + \alpha_v^2 \alpha_i C}$

Table 3.4 : Transfer functions

3.6.4 Nyquist and Bode diagram

We can now plot the Nyquist and bode diagram for the complete controller. The Nyquist diagram should be plot for the open-loop transfer function $L_{vi}(s)$. Bode plot are given for the closed-loop transfer function $S_{vi}(s)$.

The following table shows the data used for Matlab script.

PARAMETERS	VALUE
R (Ω)	0.05
L (H)	3e-3
C (μF)	2200
ω (rad/s)	2 π 50
Em (V), ph-to-gnd amplitude (=Ed)	115 $\sqrt{2}$
Fsw (kHz), switching frequency	10
Rload (Ω)	500
$\alpha_i = 2\pi F_{SW}/10$ (rad/s)	6.283e+003

$\alpha_v = 2\pi F_{SW}/100$ (rad/s)	628.3
V controller, Kpv	0.0028
V controller, Kiv	Given later
I controller, Kpi	18.8496
I controller, Kii	314.1593
Ga	Given later

Table 3.5 : Calculation data

PROPORTIONAL CONTROL ONLY

PARAM.	VALUE
Kpv	0.0028
Kiv	0
Kpi	18.8496
Kii	314.1593
Ga	0
Pole1	-5575.1
Pole2	-708.1

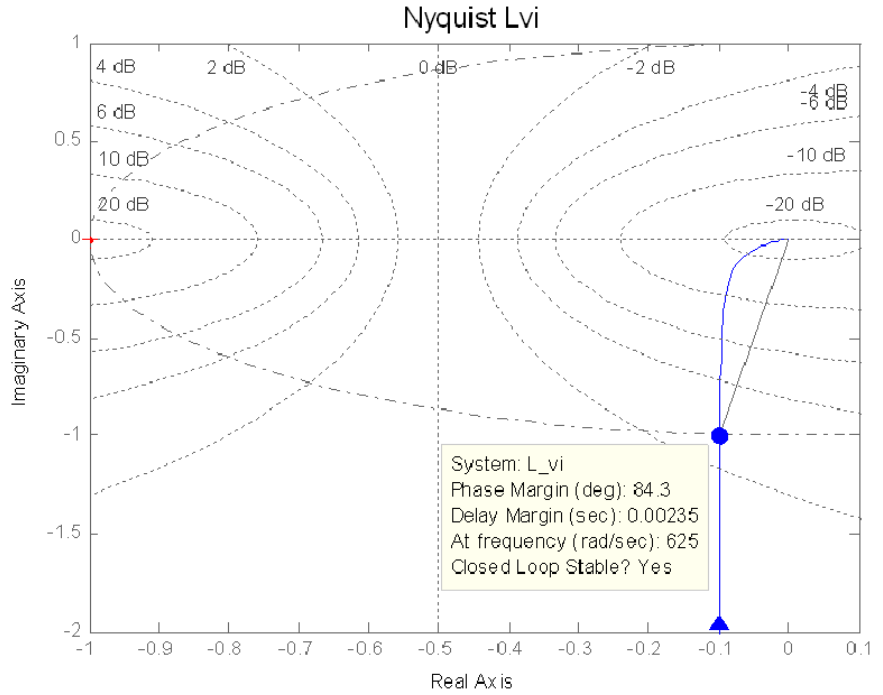


Figure 3.32 : P control – Nyquist plot of open-loop $L_{vi}(s)$

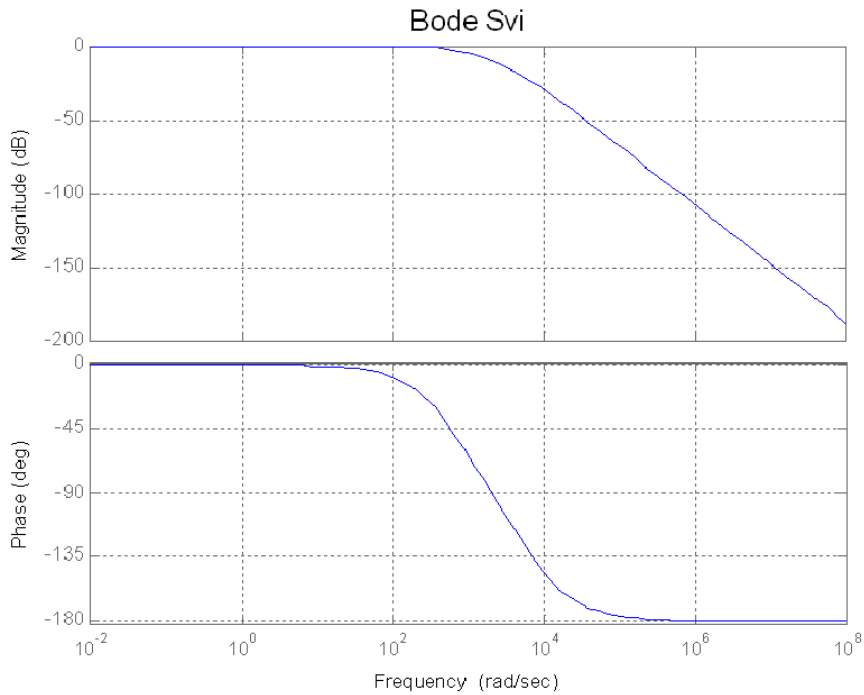


Figure 3.33 : P control – Bode plot of closed-loop $S_{vi}(s)$

PROPORTIONAL AND INTEGRAL CONTROL

PARAM.	VALUE
Kpv	0.0028
Kiv	0.01
Kpi	18.8496
Kii	314.1593
Ga	0
Pole1	-5575.6
Pole2	-704.1
Pole3	-3.5

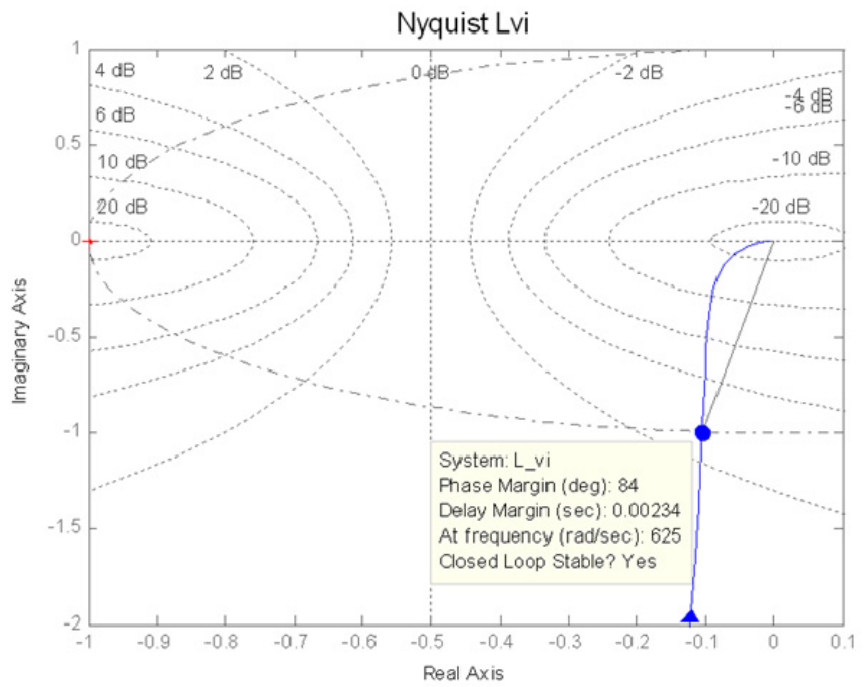


Figure 3.34 : PI control – Nyquist plot of open-loop $L_{vi}(s)$

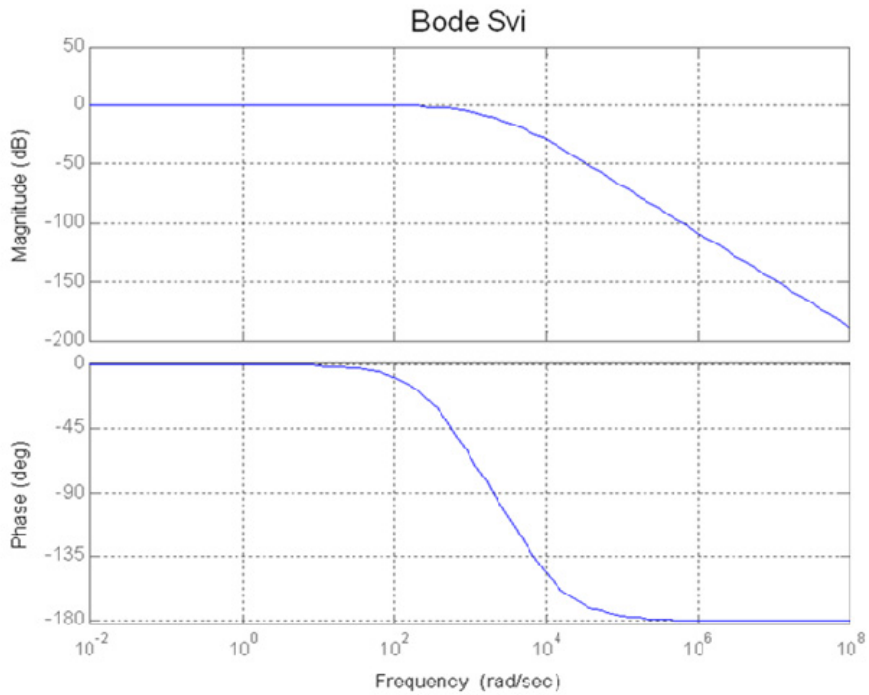


Figure 3.35 : PI control – Bode plot of closed-loop $S_{vi}(s)$

WITH ACTIVE DAMPING GA

PARAM.	VALUE
Kpv	0.0028
Kiv	1.7801
Kpi	18.8496
Kii	314.1593
Ga	0.0028
Pole1	-5575.1
Pole2	-708.1
Pole3	-628.3

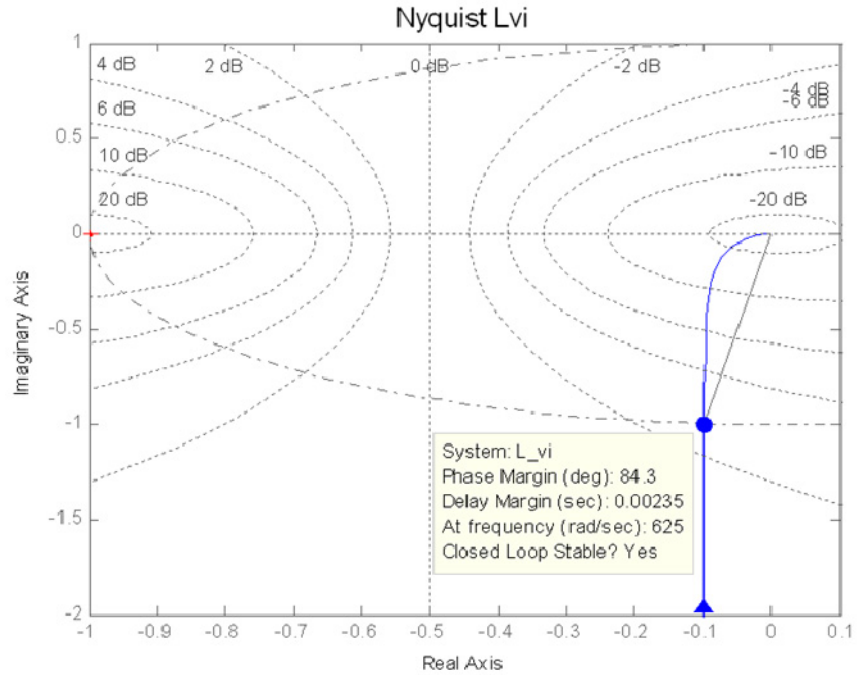


Figure 3.36 : PI Ga control – Nyquist plot of open-loop $L_{vi}(s)$

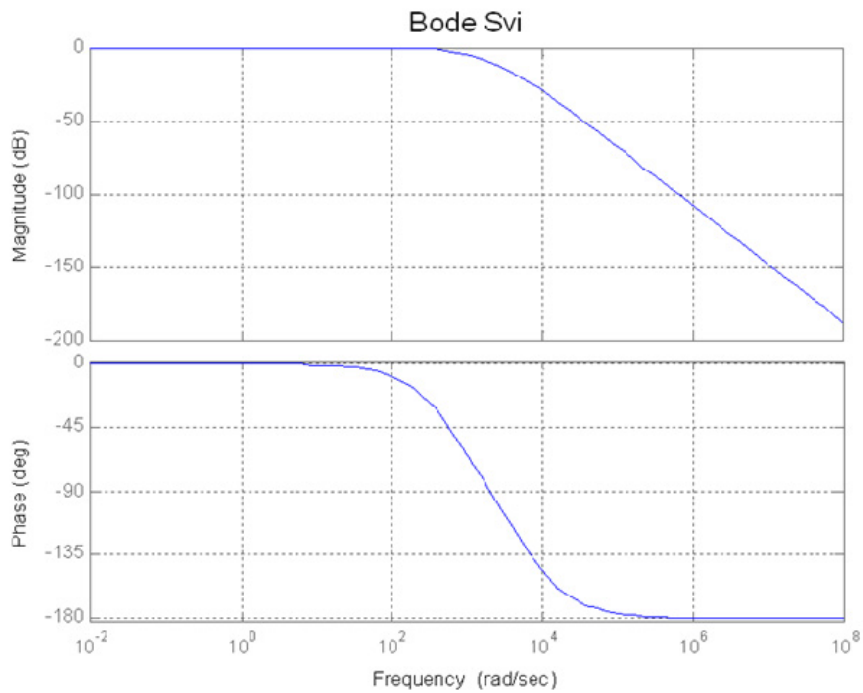


Figure 3.37 : PI Ga control – Bode plot of closed-loop $S_{vi}(s)$

3.6.5 Conclusion

All the previous Nyquist plot show stability, the blue curve is far enough from the point “-1”. The phase margins are about 84deg (a good phase margin is higher than 60deg). The Gain margin

are also good in our cases (infinite). Nevertheless, we feel that the delay margin is really too small compared to the system time constant.

ATTENTION, this analysis is probably too simplistic. We assumed that the converter and grid parameters are perfectly known and it's not correct in reality. The cross coupling cannot be perfectly cancelled and the estimated values are not exactly equal to the real values, that is : $\hat{C} \neq C$, $\hat{E}g \neq Eg$, $\hat{L} \neq L$, $\hat{R} \neq R$.

Another important point is that the analysis have been done in continuous time and should be also done in discrete time in order to be close to the real system (discrete controller).

More Nyquist and Bode graph are plotted in APPENDIX E.

3.7 Phase Locked Loop (PLL)

The PLL is an important and critical part of the system. Its aim is to give the voltage angle of the three-phase system ($U_a U_b U_c$ Figure 2.4). This angle is then used for all the dq-transformations in the model.

3.7.1 Design

The PLL was design according ([4] [14]).

$$\dot{\omega} = \gamma_1 \varepsilon \tag{3.50}$$

$$\dot{\theta} = \omega + \gamma_2 \varepsilon \tag{3.51}$$

where γ_1 and γ_2 are gain parameters and ε the error signal (γ_1 is the Ki, and γ_2 is the Kp of a PI controller). The main difference is that in our case, with d-oriented control, the error signal is selected as:

$$\varepsilon = \hat{E}_q \text{ instead of } \varepsilon = -\hat{E}_d \text{ (chosen for flux oriented control).}$$

Following the analysis of the thesis (or compendium), we can find the following PI parameters and the following scheme.

$$\gamma_1 = \frac{\rho^2}{\hat{E}_g}, \quad \gamma_2 = \frac{2\rho}{\hat{E}_g}, \quad \hat{E}_g = \sqrt{\hat{E}_d^2 + \hat{E}_q^2} \tag{3.52} \tag{3.53} \tag{3.54}$$

where ρ can be seen as the bandwidth of the PLL (rad/s), and \hat{E}_g is the estimated “grid” voltage modulus.

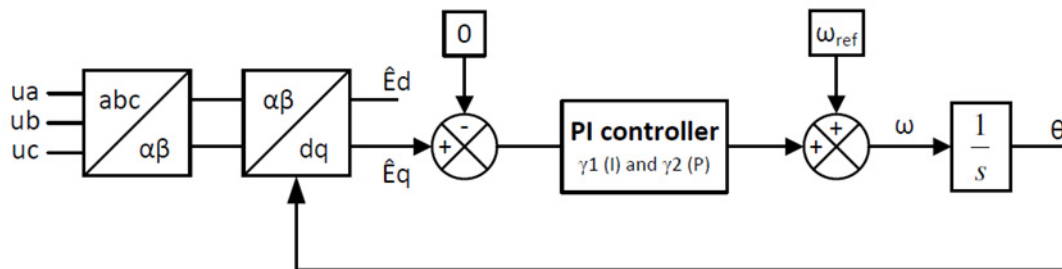


Figure 3.38 : PLL scheme

Comments :

- The PI coefficients can be fixed or calculated in Simulink according to the estimated value (or measured value) $\hat{E}_g = \sqrt{\hat{E}_d^2 + \hat{E}_q^2}$.
- The reference value ($\omega_{ref} = 2 \cdot \pi \cdot 50 \text{ rad/s}$) can be also included as a initial condition in the PI controller integrator.
- The first selection of the PLL bandwidth is about 20Hz. It will be adjust later.

3.7.2 Simulations

The model was implemented in continuous first, then in discrete using the following scheme for a discrete integrator :

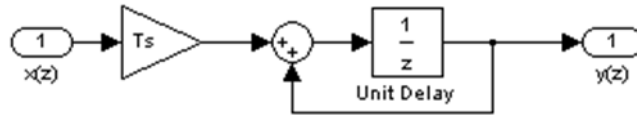


Figure 3.39 : Discrete integrator (APPENDIX C. Digital simulation)

The sample frequency is chosen as : $F_S = 2.F_{SW} = 2.F_{triangular\ wave}$ (F_{sw} is the switching frequency, 20kHz).

Simulation1 : Balanced 3-phase system

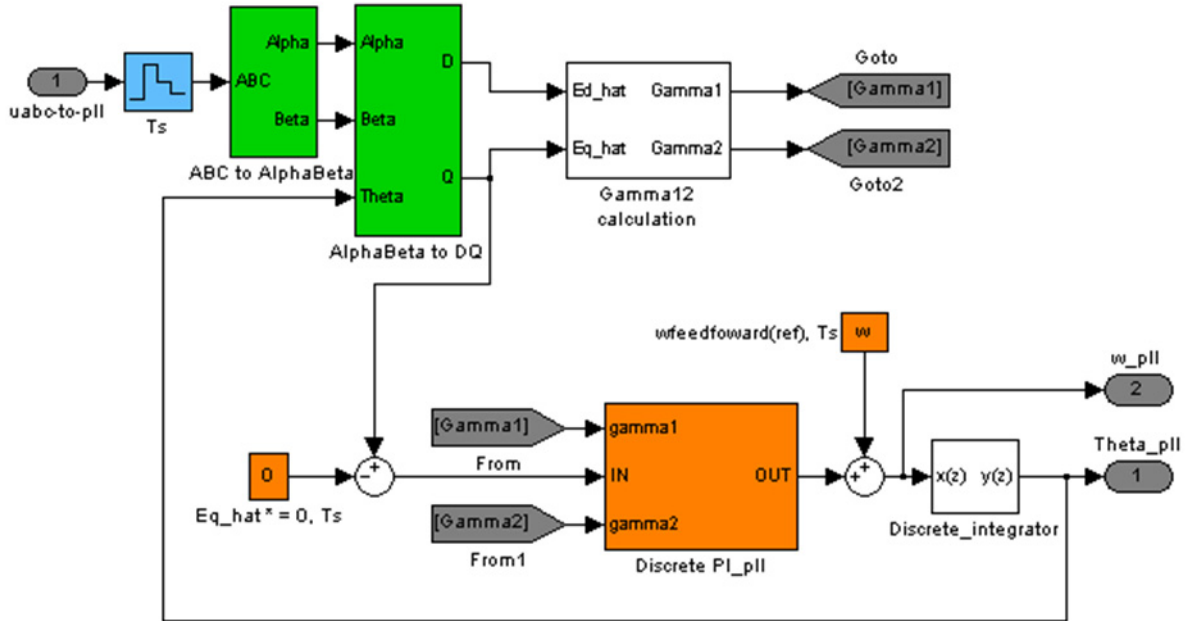


Figure 3.40 : Simulation-Block Scheme

The results show that the original angle and the angle from the pll are equal (angular frequency is also the same, 314.1593rad/s).

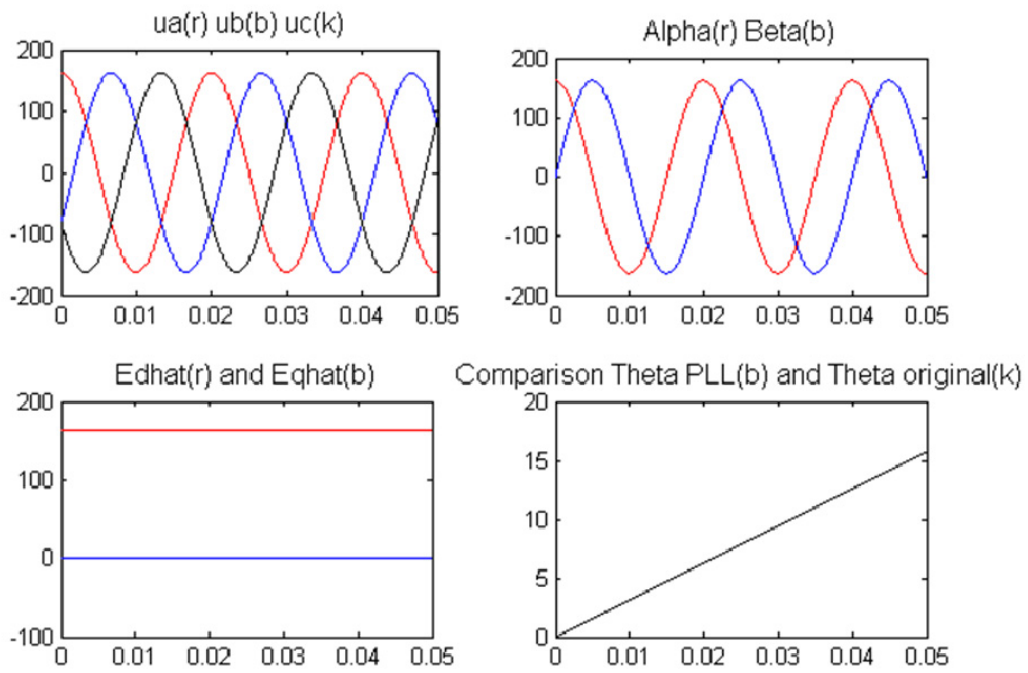


Figure 3.41 : *Simulation-Balanced 3-phase system*

Simulation2 : Unbalanced 3-phase system

Now we create a voltage dip on phase C at 0.025s (30% dip, 70% of the voltage left).

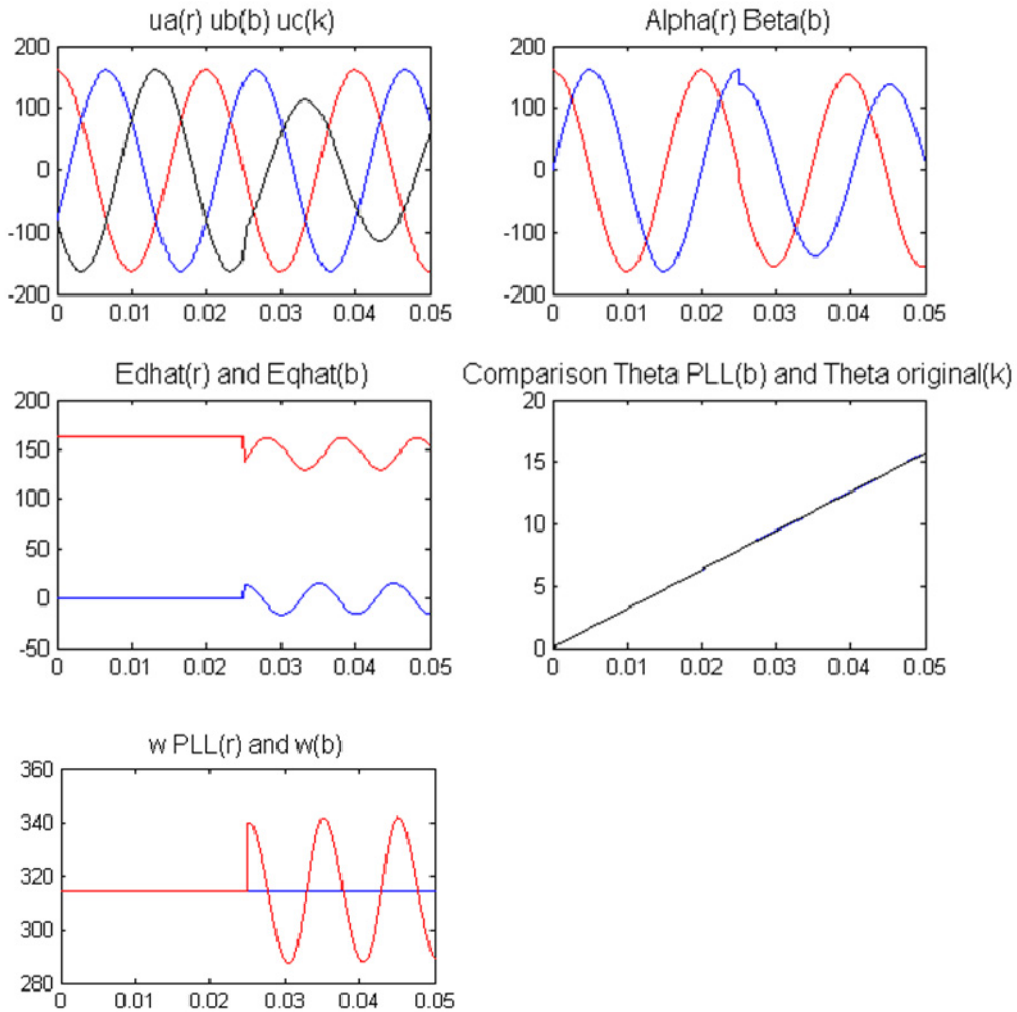


Figure 3.42 : Simulation-Unbalanced 3-phase system

Now an oscillation is produced and we can see a small oscillation on theta_pll too.

Simulation3 : Balanced 3-phase system, noise

We comeback to a balanced grid and we add noise to the 3-phase voltages (random noise for A, square wave for B, sawtooth wave for C, at different frequencies). We can see on the simulation below that the angles are similar (a small error about 0.03deg can be seen with a zoom).

Noise phase A	Noise phase B	Noise phase C
Random wave form	square wave	sawtooth wave
At different frequencies : 100, 150, 200, 250, 1000, 5000, 10000Hz		

Table 3.6 : Noise parameters

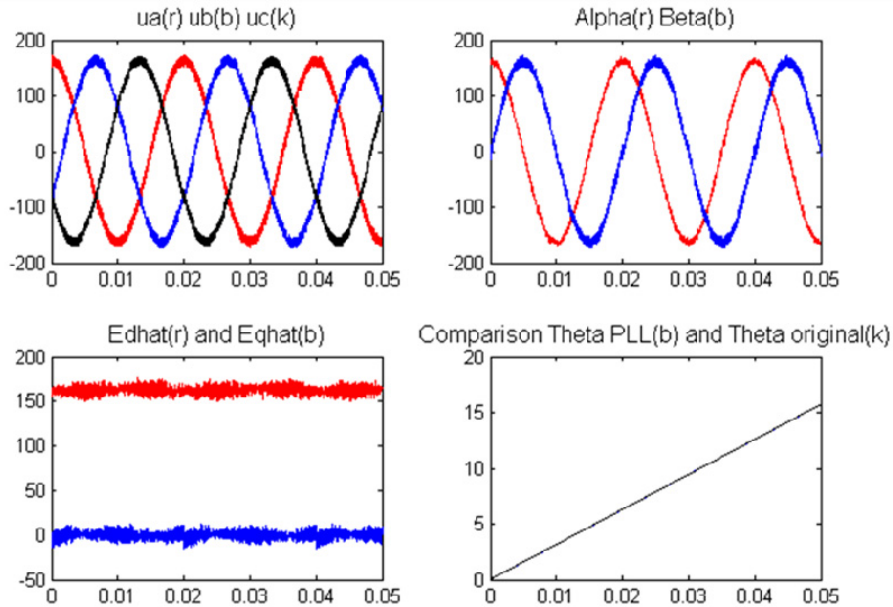


Figure 3.43 : Simulation-Balanced 3-phase system, noise

Remark and conclusion

We saw that the coefficients γ_1 and γ_2 can be calculated in Simulink according to \hat{E}_g . Nevertheless, this can create a simulation issue at beginning of the simulation. We assume that for a first implementation and a stiff grid, fixed coefficients can be easily used. Another solution could be to start with fixed coefficients then switch to variable values.

To remove the oscillations on theta, we advice to reduce the PLL bandwidth to 5Hz.

3.7.3 Improvements and conclusion

As indicated in some papers (for example, see [30] in the case of amplitude distortion, frequency distortion, phase distortion, harmonics, phase loss, random noise, the conventional PLL presented here is not enough. For example, they use a controlled moving average algorithm to extract ω and a phase locker.

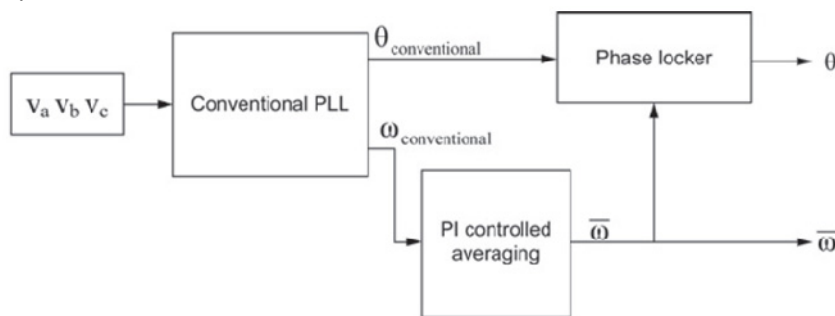


Figure 3.44 : PLL proposed by [30]

3.8 Grid modeling

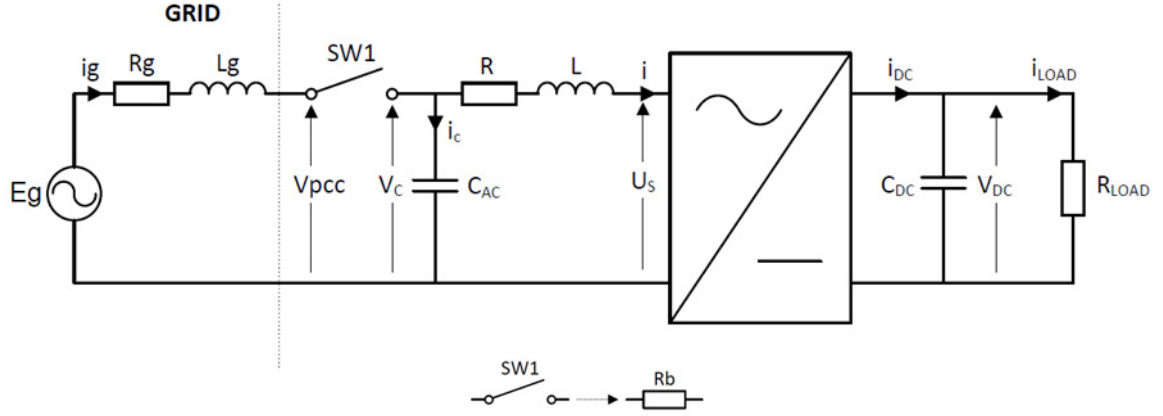


Figure 3.45 : Grid connected converter

The aim of this part is to modify the model introduced in section “2.2.2 Mathematical model” (Figure 2.4) to simulate a grid connected converter. We are going to add the grid voltage and impedance E_g , R_g and L_g . A switch will be modeled with a resistor R_b (high value for an open switch, very small value for a switch closed). We can write four equations as below.

First equation : i_g

$$\begin{aligned} e_g - v_c &= (R_g + R_b)i_g + L_g \frac{di_g}{dt} \\ \Leftrightarrow i_g &= \frac{1}{sL_g} [e_g - v_c - (R_g + R_b)i_g] \end{aligned} \quad (3.55)$$

Second equation : i

$$\begin{aligned} v_c - u_s &= Ri + L \frac{di}{dt} \\ \Leftrightarrow i &= \frac{1}{sL} [v_c - u_s - Ri] \end{aligned} \quad (3.56)$$

Third equation : V_c

$$\begin{aligned} i_g &= i_c + i = C_{ac} \frac{dv_c}{dt} + i \\ \Leftrightarrow v_c &= (i_g - i) \frac{1}{sC_{ac}} \end{aligned} \quad (3.57)$$

Fourth equation : V_{PCC}

$$v_{pcc} = i_g R_b + v_c \quad (3.58)$$

With these four equations, we can establish the scheme Figure 3.47 to replace the simple grid model of Figure 3.46 (establish in section “2.2.2 Mathematical model” Figure 2.4).

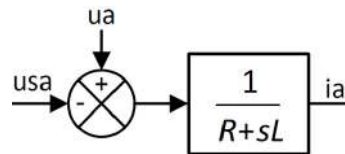


Figure 3.46 : Simple grid model (phase A)

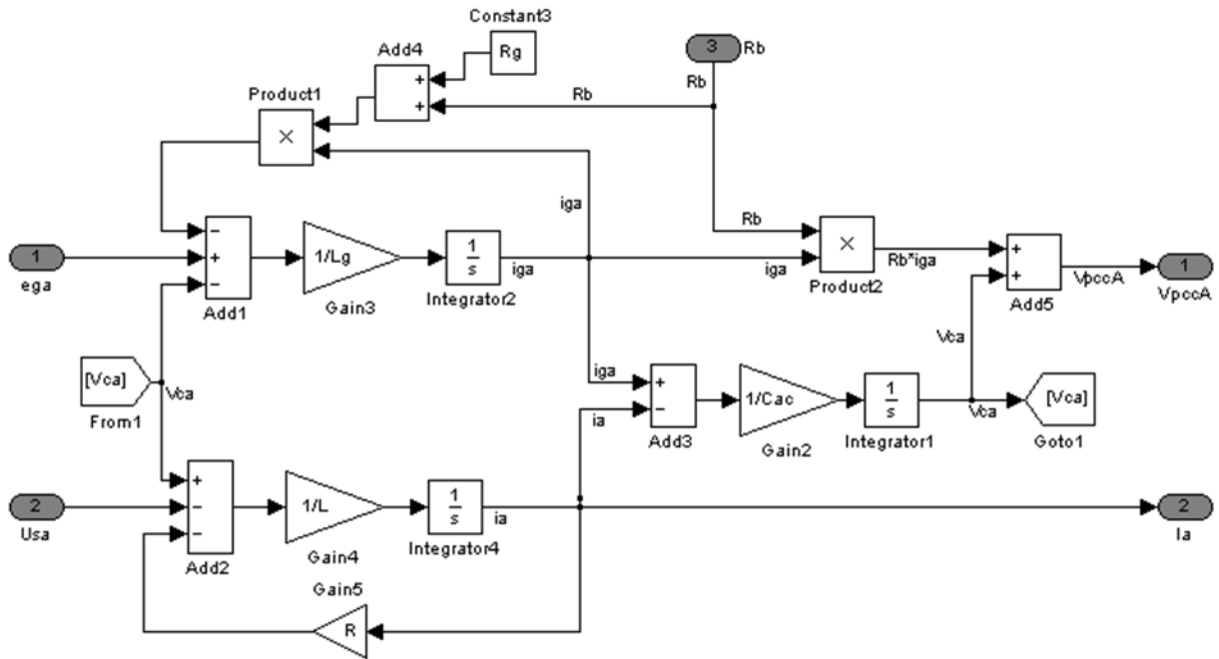


Figure 3.47 : Simulink – New grid model (phase A)

We can also write more simple equations for a model without C_{ac} .

$$\begin{aligned}
 e_g - u_s &= (R_g + R_b + R)i + (L + L_g) \frac{di}{dt} = R_{tot}i + L_{tot} \frac{di}{dt} \\
 v_{pcc} &= e_g - R_g i - L_g \frac{di}{dt}
 \end{aligned} \tag{3.59}$$

Then if we inject di/dt of the first equation in the second :

$$v_{pcc} = e_g - R_g i - \frac{L_g}{L_{tot}} (e_g - u_s - R_{tot} i) \quad \left| \quad \text{If } \frac{L_g}{L_{tot}} \ll 1 \Rightarrow v_{pcc} \approx e_g - R_g i \right.$$

(3.60)
(3.61)

We can remark that if L_g is too big compare to L_{tot} , the voltage V_{pcc} will be highly dependent on the current I and will vary. In the other hand, if L_g is very small compare to L_{tot} , the last term of the equation can be removed and V_{PCC} is more stable.

3.9 Grid connected converter simulation

This section shows the simulations results of the complete system built with (Figure 3.49) :

- **A DISCRETE block**
 - Sampling system (sample and hold block)
 - PLL
 - Decoupled controller
- **PWM block (sinusoidal PWM)**

An asymmetric PWM is used here, as we saw in the section “2.4.1 Sinusoidal PWM”, we have $F_{Sampling} = 2 F_{triangle\ wave} = 2 F_{Switching}$.
- **Grid and rectifier model**

We are now using the model presented in the previous part “3.8 Grid modeling” with small unknown grid impedance $R_g L_g$ and a switch (beaker) SW_1 . We also add a second switch in the output as we can see in Figure 3.48.

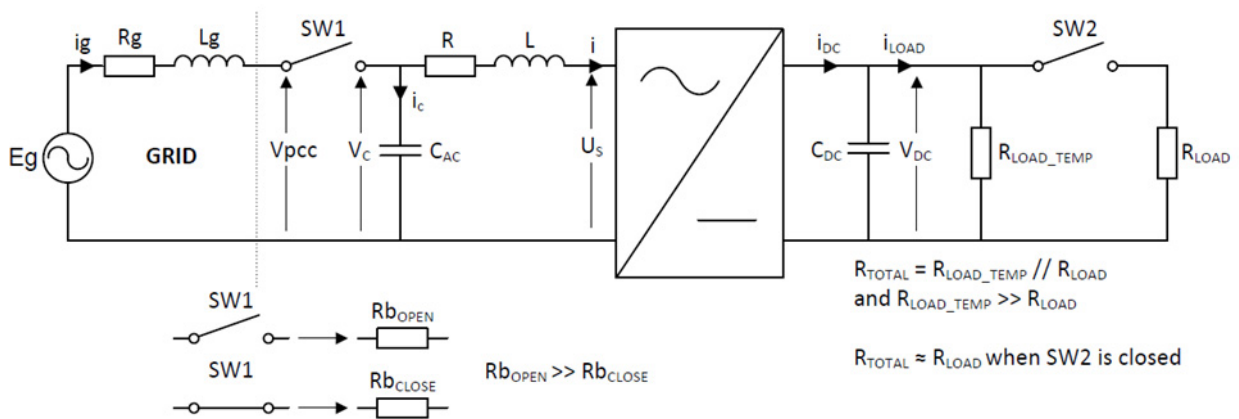


Figure 3.48 : Single phase schematic

3.9.1 Simulation steps, Simulink block diagram

SIMULATION STEPS

The simulation is composed by three steps. In the step I : SW1 and SW2 are open, step II : SW1 closed and SW2 open, step III : SW1 and SW2 closed.

↳ Step I : Synchronization

- SW1 and SW2 are open.
- The voltage V_{PCC} is sent to the PLL and the voltage angle θ is calculated.
- All IGBTs are OFF (the rectifier becomes a simple three-phase diode rectifier). No current is flowing into the rectifier.
- The controller is in **standby mode**. All discrete integrators are disabled. All integrators should be disabled when all IGBTs are OFF. Otherwise, the integrator part of the controller will try to set the error to zero but since there are no switches activated, the error cannot be set to zero. The integrator value will increase.
- DC-link link capacitor is charged to the reference value V_{DCref} (in the simulation, this action is done by setting the Initial Condition to V_{DCref} into the integrator of the DC-link model). **ATTENTION**, the value V_{DCref} should respect the condition explain in “2.2.3 Limitations” : $V_{DCmin} > 2 V_{PCC(LN,peak)}$ where $V_{PCC(LN,peak)}$ is the Line-to-Neutral amplitude of V_{PCC} .

- The load is now R_{LOAD_TEMP} . This resistor is set to a high value to avoid the discharge of C_{DC} .

↳ **Step II : Closing SW1**

- The AC-side capacitor (filter) is charged (small transient).
- All IGBTs are OFF and the controller is in standby mode (no integration).
- As $V_{DC} > 2 V_{PCC(LN,peak)}$, there is no current flowing into the rectifier.

↳ **Step III : Closing SW2 and START**

- SW2 is closed. R_{LOAD_TEMP} can now be neglected since $R_{LOAD_TEMP} \gg R_{LOAD}$.
- The controller is fully activated and the IGBTs can be turned ON.

SIMULINK BLOCK DIAGRAM

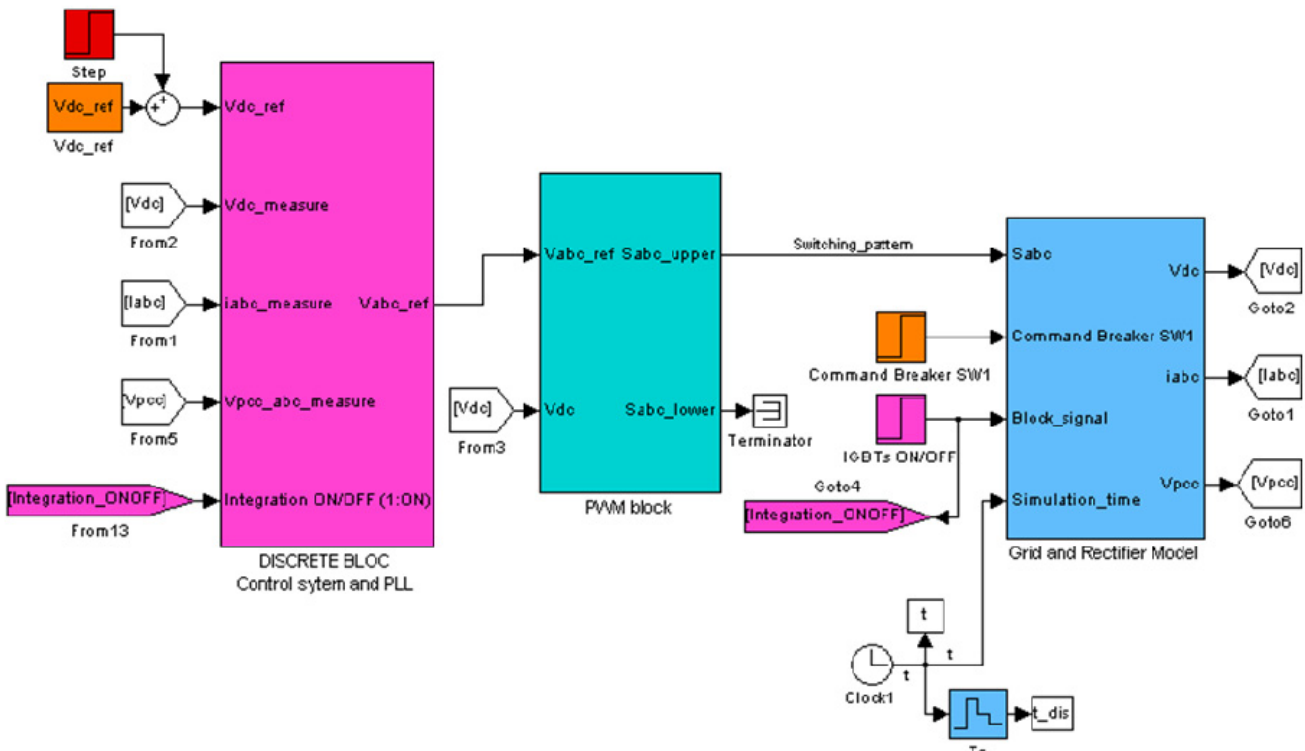


Figure 3.49 : Top level Simulink model

The Figure 3.49 shows the top level block diagram of Simulink. You can find the details of different block in APPENDIX F.

Before presenting the simulation results, we have to precise two important points, that are, how the IGBT OFF-state and how the disabled integrators are modeled in Simulink.

↳ **IGBT OFF-state**

When the IGBTs are OFF in our simulation, no current is flowing into the rectifier (DC-link voltage is high enough and the body diode of the IGBTs are blocked). Consequently, we decided to force the current to zero with the Figure 0.39 in APPENDIX F.

↳ **Disabled integrators**

The integrators are disabled by forcing the value to zero (another solution could be to set K_i to zero). You can see the Simulink block in APPENDIX F, Figure 0.35.

3.9.2 Verification

In this sub-section, we verify that the equation presented in the second Chapter (“2.2.3 Limitations”).

↳ **Grid voltage**

$$\begin{aligned}
 U_{RMS} &= 400 \text{ V (Line-to-Line)} \\
 \Rightarrow V_{RMS} &= \frac{400}{\sqrt{3}} = 230.9 \text{ V (Phase-to-Ground)} \\
 \Rightarrow E_g &= \sqrt{2} \cdot 230.9 = 326.6 \text{ V (Phase-to-Ground amplitude)}
 \end{aligned}$$

↳ **Minimum DC-link voltage**

The minimum DC-link voltage is found with the equation (2.27) of section “2.2.3 Limitations”.

$$\begin{aligned}
 V_{DCmin} &> 2 V_{LN(peak)} = 2 E_g \\
 \Rightarrow V_{DCmin} &> 2 \times 326.6 \\
 \Rightarrow V_{DCmin} &> 653.2 \text{ V.}
 \end{aligned}$$

This minimum value have been verify in our simulation. In the Simulink simulation, we found a minimum DC-link voltage around 660V.

Finally, for our simulation we will select

$$V_{DCref} = 700 \text{ V.}$$

This value is probably a bit low for an experiment. In reality, it will be better to select 15% or 20% more (about 750V or 790V. Refer to “2.2.3 Limitations”).

↳ **Inductance value**

The equation (2.29) of section “2.2.3 Limitations” applied in our system becomes :

$$L < \frac{\sqrt{\frac{V_{DC}^2}{3} - E_g^2}}{\omega id}.$$

As we saw during the voltage controller design, section “3.5.2 Design of voltage controller” equation (3.18), the d-current is calculated by

$$id = \frac{2}{3E_g} P_g$$

Then, in steady-state we can write the equality of power

$$P_g = P_{load} = \frac{v_{dc}^2}{R_{load}} \quad (3.62)$$

Finally, the current becomes

$$\begin{aligned}
 id &= \frac{2}{3E_g} \frac{v_{dc}^2}{R_{load}} \quad (3.63) \\
 \Rightarrow id &= \frac{2}{3} \frac{700^2}{326.6 \times 150} = 6.668 \approx 6.7 \text{ A}
 \end{aligned}$$

This value is totally verified in the following simulation. We can now calculate the inductance.

$$\begin{aligned}
 L &< \frac{\sqrt{\frac{V_{DC}^2}{3} - E_g^2}}{\omega id} \\
 \Rightarrow L &< \frac{\sqrt{\frac{700^2}{3} - 326.6^2}}{2\pi 50 \times 6.7} \\
 \Rightarrow L &< 0.1131 \text{ H}
 \end{aligned}$$

We think that this value too high according to results read in some papers. **We decided to select the inductance around 3mH (it could be 5mH or 10mH).**

3.9.3 Simulation results

SIMULATION 1 AND 2

The following Table 3.7 present a summary of the simulation parameters. All the parameters for this “Simulation1” are presented in APPENDIX F, Table 0.3.

The simulation is performed with **approximation** :

- ➔ We assume that the V_{PCC} voltage is equal to the grid voltage E_g (Figure 3.48). That is only true if the grid impedance is small enough compared to impedance RL.
- ➔ We assume that we know exactly the converter parameters, that is :

$$\hat{R} = R ; \hat{L} = L ; \hat{C} = C$$

GRID AND CONVERTER	VALUE	TIME	VALUE
Grid U_{RMS} (V), line-to-line RMS	400	STEP II: SW1 closing at ... (s)	0.005
R_g (Ω), grid resistance	1e-3	STEP III: IGBTs ON at ... (s)	0.01
L_g (H), grid inductance	1e-5	V_{DCref} step at ... (s)	0.025
R (Ω)	0.05		
L (H)	3e-3		
C (F)	2200e-6		
V_{DCref} (V)	700		
V_{DCref} STEP (V)	30		
R_{LOAD} (Ω)	150		
PWM	VALUE	CONTROLLER	VALUE
Triangular freq. F_c (kHz)	10	Kp_i , current controller	37.6991
Mode	Asymmetric	Ki_i , current controller	628.3185
		Kp_v , voltage controller	0.0028
		Ki_v , voltage controller	0.01
		Sample freq. $F_s = 2F_c$ (kHz)	20

Table 3.7 : Summary of simulation1 parameters

The basic waveforms are plotted in Figure 3.50. All voltages are phase-to-ground voltages. For this simulation1, we selected a small grid impedance and we observe a voltage V_{PCC} without distortions, and we can say that V_{PCC} and the grid voltage e_g are equal (stiff grid). We will see the influence of the grid impedance in the simulation3.

On the current plot (i_{abc}), when the breaker SW1 is closing at time 0.005s, no current is flowing into the rectifier. Then, at time 0.01s, we activate the IGBTs, we close SW2 and the system is starting. We observe a small ripple on the current due to the switching. This ripple increases if the switching frequency decreases or if the line inductance decreases.

Finally, at time 0.025s, the step on V_{DCref} is starting. The current is reaching the saturation limit of $\pm 15A$ and the DC-link voltage is increasing linearly from 700V (initial condition) to 730V. Another Simulation have been done with a bigger step of 100V on V_{DCref} with saturation limit in the current controller about $\pm 50A$ (see APPENDIX F, Figure 0.27).

Furthermore, we observe a small overshoot on the DC-link voltage V_{DC} . This overshoot may increase if the switching frequency decrease. On Simulation2 Figure 3.51a., we plot the DC-link voltage for a switching frequency selected at 3kHz. We observe oscillations. These oscillations can be remove by adjusting the PI controller coefficients. The calculation for the PI coefficients depends on the bandwidth α_i and α_v selected as followow :

$$\alpha_i = 2\pi F_s/10 \text{ and } \alpha_v = 2\pi F_s/100.$$

Nevertheless, when we select a switching frequency 3kHz, we modify the bandwidth ($F_S = 2F_{SW}$) and we modify the PI controllers. For example, if we select the bandwidth with $\alpha_i = 3 \times 2\pi F_S/10$ and $\alpha_v = 3 \times 2\pi F_S/100$, the oscillations are highly reduced (Figure 3.51b.).

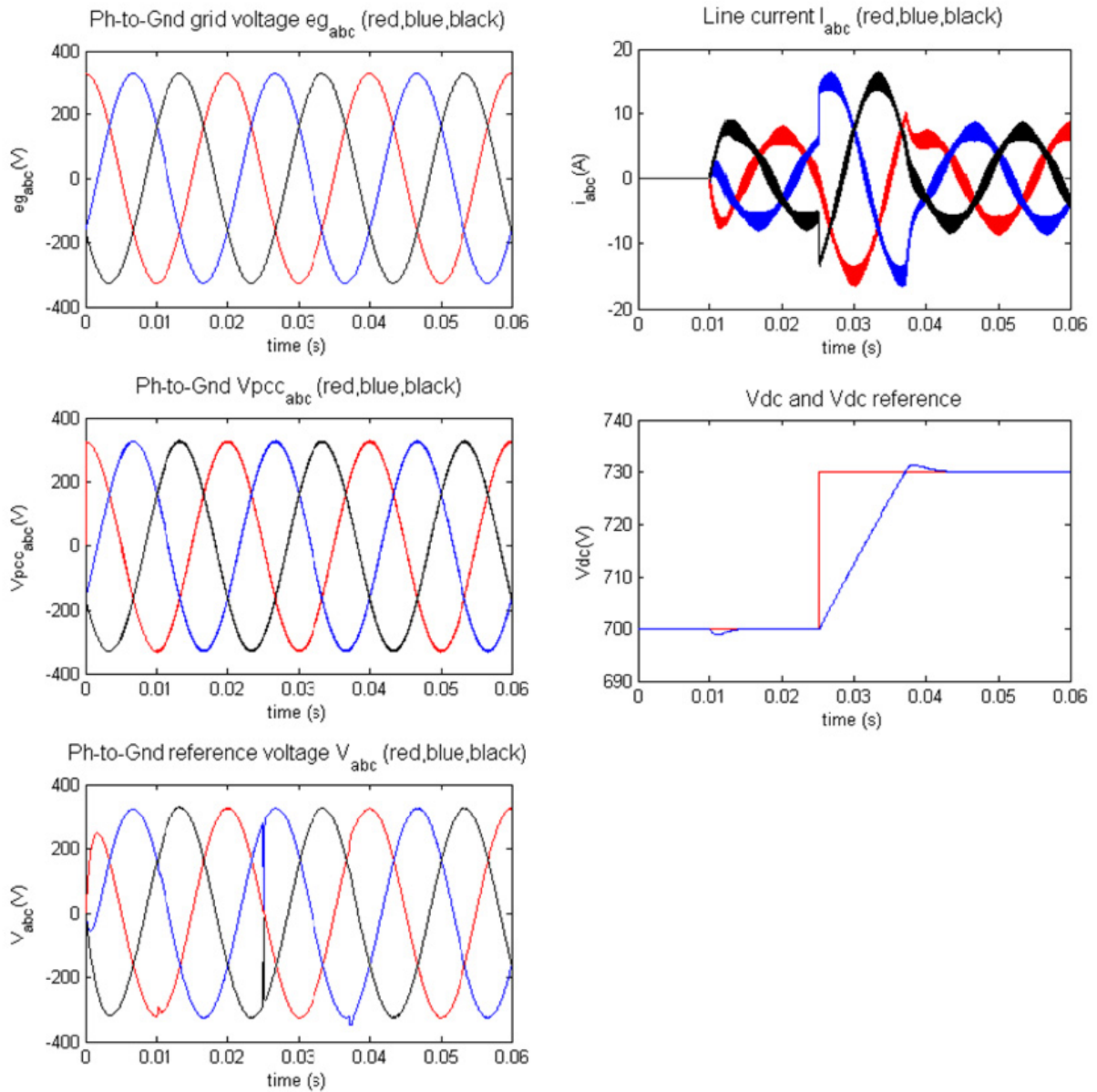


Figure 3.50 : Simulation1 results

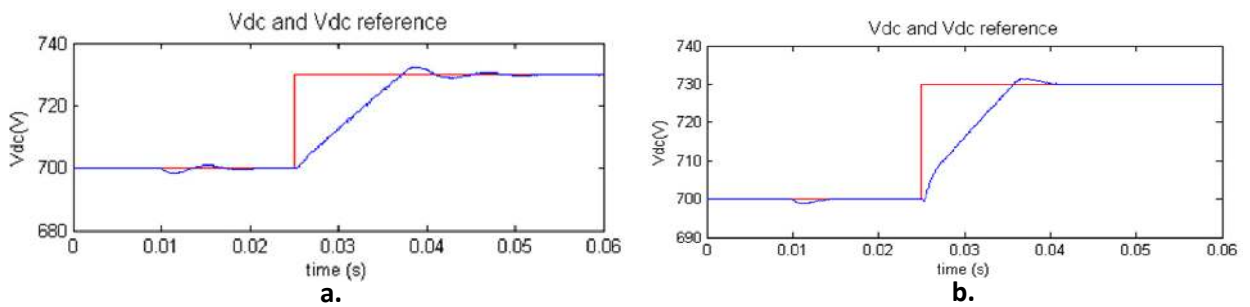


Figure 3.51 : Simulation2 with switching frequency 3kHz

a. V_{DC} voltage

b. V_{DC} with bandwidth $3 \times 2\pi F_S/xxx$

SIMULATION3 – INFLUENCE OF THE GRID IMPEDANCE

The simulation3 have been done to show the influence of the grid impedance on the system. We multiplied by 10 both R_g and L_g .

GRID MODIFICATION	VALUE
R_g (Ω), grid resistance	1e-2
L_g (H), grid inductance	1e-4

Table 3.8 : *Simulation3 – New grid impedance parameters*

As we explain in section “3.8 Grid modeling”, if L_g is too big compare to the total inductance value L_{tot} , the voltage V_{PCC} will be highly dependent on the current and will vary. The Figure 3.52a. shows the effect of the grid impedance, the voltage is distorted. Despite that, the system is still working well even if this voltage is used by the PLL to calculate the voltage angle. Figure 3.52b. shows the voltage angle under simulation3 condition, there is no visible distortion.

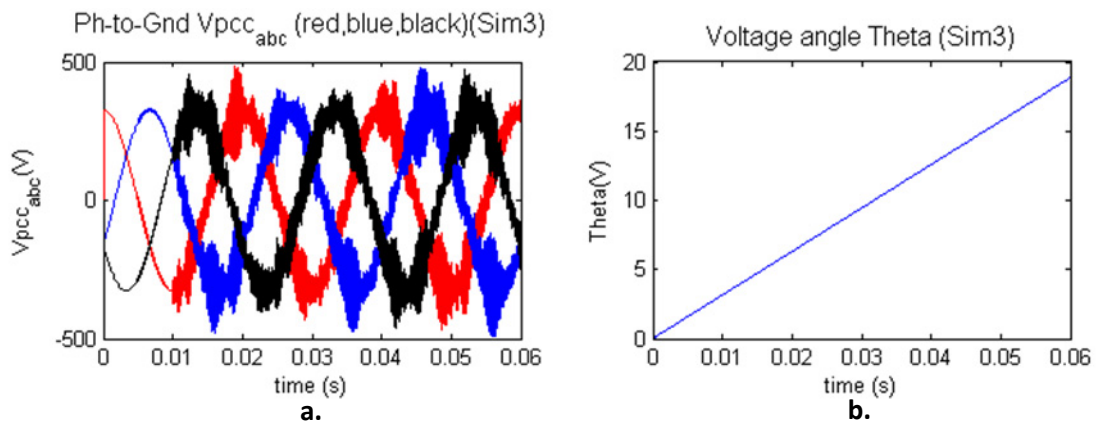


Figure 3.52 : *Simulation3 with new grid parameters*

- a. V_{PCC} voltage
- b. Voltage angle Theta

SIMULATION4 – TEST WITH ACTIVE DAMPING GA

The results of simulation4 is plotted in APPENDIX F, Figure 0.28. The simulation parameters are the same as simulation1 with the following modification on controller parameter. We also re-write the equation to find them (equation XXX section “3.5.3 Voltage saturation, anti-windup, active damping”).

PARAMETER MODIFICATION	VALUE
Kp_v , voltage controller	0.0028
G_a active conductance	0.0028
Ki_v , voltage controller	3.5457

Table 3.9 : *Simulation4*

$$Ga = \frac{\alpha_v C}{3E_g}$$

$$Kp_v = \frac{\alpha_v \hat{C}}{3\hat{E}_g}$$

$$Ki_v = \alpha_v Ga$$

We can see on Figure 0.28 that the controller doesn’t work properly anymore, some oscillation appear on DC-link voltage and the current is completely distorted.

We observed that the simulation becomes stable again by reducing the controller parameters values. The Figure 0.29 shows a simulation with the following modified parameters :

PARAMETER MODIFICATION	VALUE
Kp_v , voltage controller	0.0028
G_a active conductance	2.8216e-005
Ki_v , voltage controller	0.0355

Table 3.10 : Simulation4 – modified parameters

$$Ga = \frac{1}{100} \frac{\alpha_v C}{3E_g}$$

$$Kp_v = \frac{\alpha_v \hat{C}}{3\hat{E}_g}$$

$$Ki_v = \alpha_v Ga$$

The Simulink diagram is given in APPENDIX F, Figure 0.41.

SIMULATION5 – ESTIMATED PARAMETERS $\hat{R}, \hat{L}, \hat{C}$

For simulation5, we now assume that $\hat{R} \neq R; \hat{L} \neq L; \hat{C} \neq C$. One by one, we modify (increase and decrease) the estimated value and verify the effect on the waveforms.

➤ Resistance influence $\hat{R} \neq R$

A couple of tests have been done and we didn't see any problem due to a bad estimation of the line resistance.

Tests with \hat{R} equal to...	Comments
$R + 3R$	No visible influence
$R - 3R$	$R < 0$, instability
$R - 0.9R$	No visible influence

Table 3.11 : Resistance influence

➤ Inductance influence $\hat{L} \neq L$

Tests with \hat{L} equal to...	Comments
$L + 3L$	See Figure 0.30 in APPENDIX F. - Distorted reference voltage - Vdc oscillations
$L - 0.9L$	See Figure 0.31 in APPENDIX F. - Distorted reference voltage - Vdc oscillations - Distorted line current

Table 3.12 : Inductance influence

➤ Capacitor influence $\hat{C} \neq C$

Tests with \hat{C} equal to...	Comments
$C - 0.9C$	See Figure 0.32 in APPENDIX F. - Line current oscillation - Vdc oscillation
$C + 3C$	No visible influence

Table 3.13 : Capacitor influence

➤ Conclusion

As we can see in the previous tables, inductance and capacitor estimation are more critical than resistance estimation. Nevertheless, we saw in simulation that a bad estimation with an error about 20-40% is not problematic. The waveforms are pretty similar.

SIMULATION 6 – LOAD STEP

Simulation 6 is done by modifying the load resistance from 150Ω to 30Ω, that corresponds, to a load asking suddenly for 16kW (30Ω) instead of 3kW (150Ω).

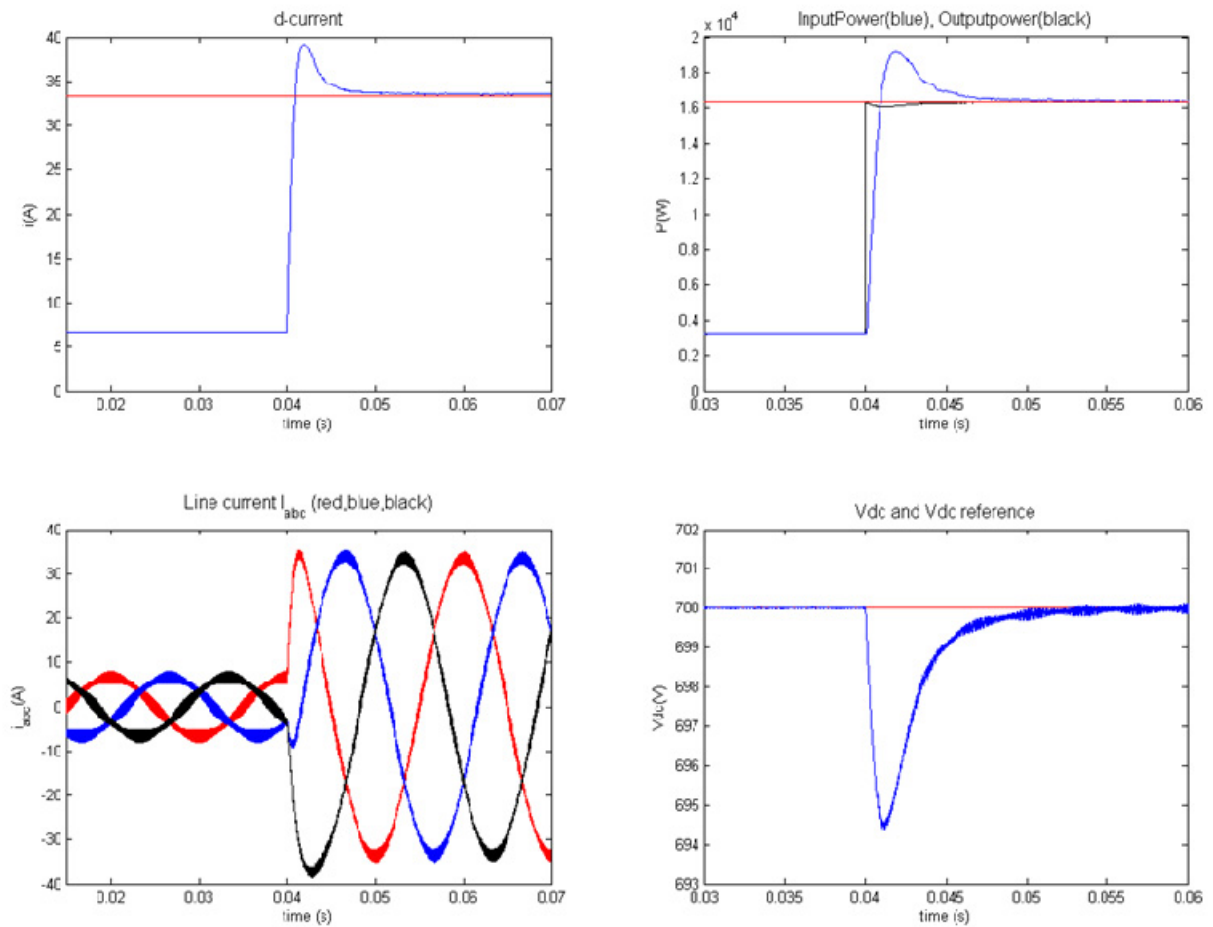


Figure 3.53 : Simulation6 results

The input power (blue) is calculated with the following equation (3.18) :

$$P_g = \frac{3}{2} E_g i_d$$

The output power (black) as below (equation (3.62)) :

$$P_{load} = \frac{v_{dc}^2}{R_{load}}$$

As we can see in the previous figure (Figure 3.53), an overshoot appears in the d-components of the current (6A overshoot). Nevertheless, this overshoot is not so visible on the 3-phase current.

Regarding the DC-link voltage, we observe a small drop (5.5V, 0.7%). The controller is acting and after a couple of millisecond, the error is set to zero again. The controller performance seems to good for disturbance rejection.

4 VOLTAGE ORIENTED CONTROL – IMPLEMENTATION

4.1 Block diagram

The set-up present in the lab can be represented with the following block diagram. It shows one power stage, electronic stage, and software stage.

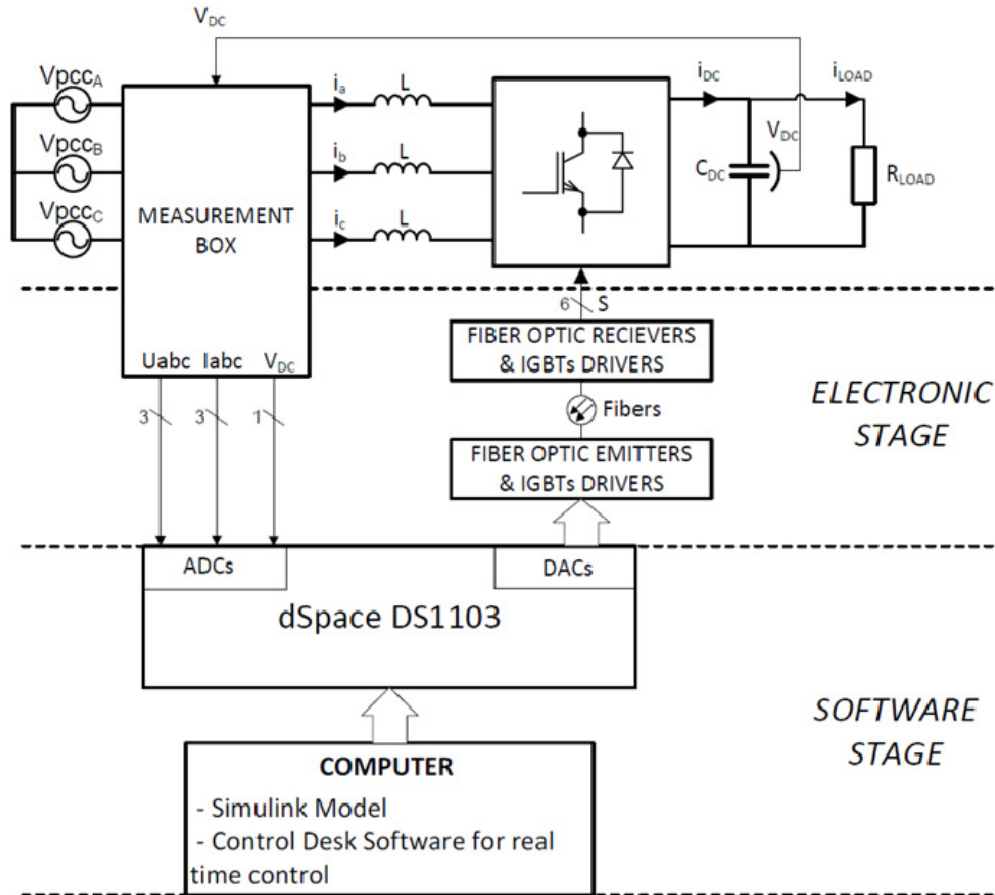


Figure 4.1 : Laboratory set-up

MATERIAL	COMMENTS
dSpace system	DS1103
Computer	PC
Matlab / Simulink	Real Time Workshop library and dSpace library
Control Desk software	Used for real time control
Measurement box	Voltage and current
Emitter card	Optical emitters
Receiver card and IGBT drivers	Optical receivers

Table 4.1 : Lab material

This set-up is not running yet. No experiments have been done in this thesis.

4.2 Principle

From your Simulink model (see next section), Matlab generates a C-code and send it to the hardware (dSpace DS1103) connected to the PC.

Then, using Control Desk software, you can build an interface with control panel : knobs, control buttons. You can also add visualizations : led, gauge, graph and so on.

To be able to run our system, some modification need to be done on our Simulink model.

4.3 Simulink model modification

The top level Simulink model for implementation is show in Figure 4.2.

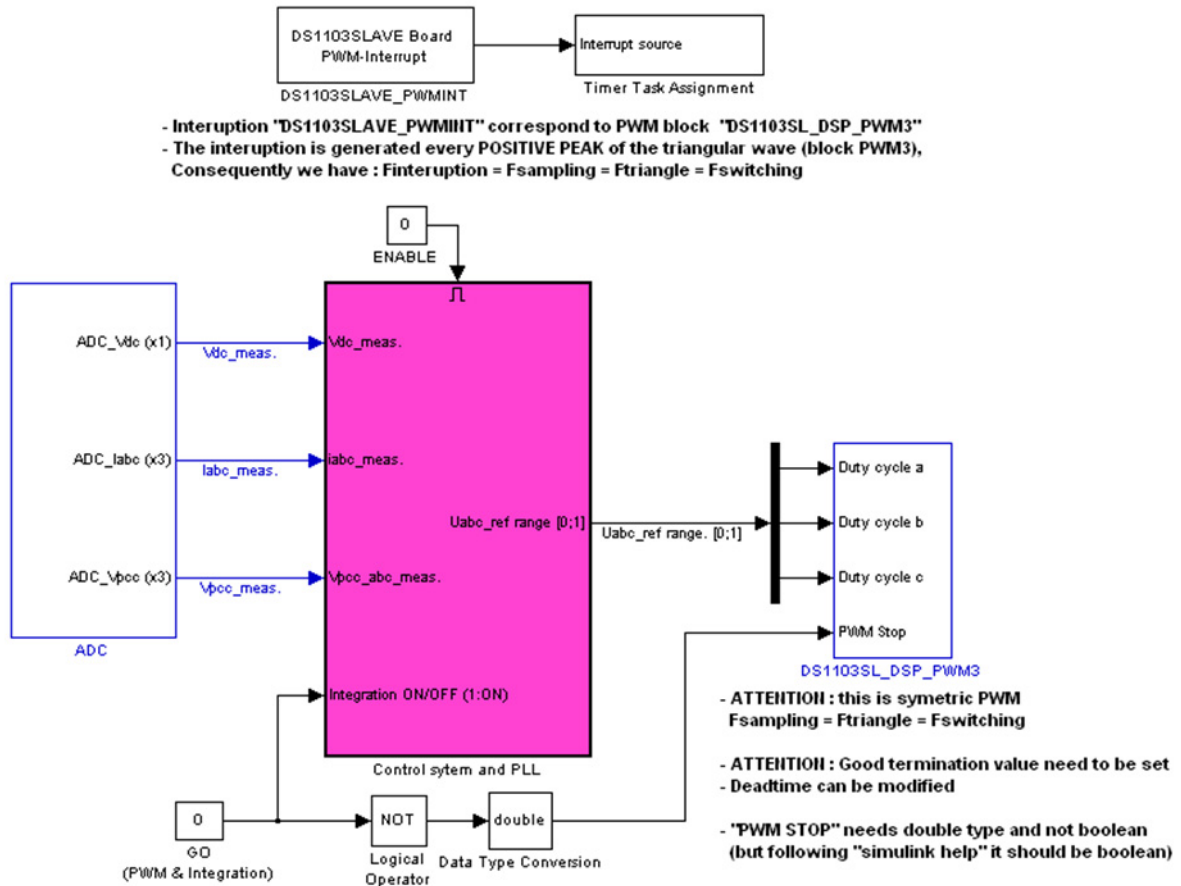


Figure 4.2 : Top level Simulink model for dSpace implementation

ADC

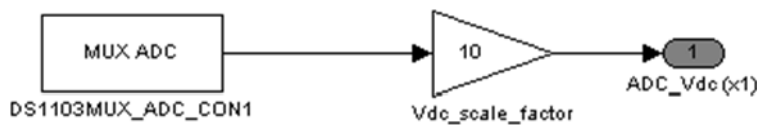


Figure 4.3 : ADC example (see APPENDIX G. Figure 0.42)

The important information using ADC and DAC is shown in the following table. You need to multiply by 10 a value from ADC, and divide by 10 before sending to DAC.

ADC		DAC	
Input voltage range	Correspondance in Simulink	Simulink value	Output voltage range
-10V...+10V	-1...+1	-1...+1	-10V...+10V

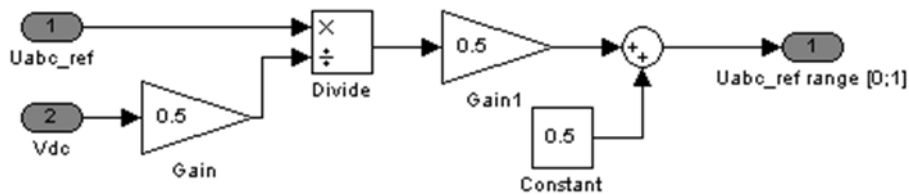
Table 4.2 : ADC/DAC value range

PWM

The PWM block have been replaced by the dSpace PWM block “DS1103SL_DSP_PWM3”. This is a sinusoidal symmetric PWM (Ftriangle = Fswitching = Fsampling). You can modify the carrier wave (triangle) and the deadtime duration.

“PWM stop” allows to enable(PWM stop = 0) or disable(PWM stop = 1) the PWM block. This signal needs double type and not Boolean (but following “Simulink help” it should be Boolean). The **Termination and Initialization** values of the block should be set (see next section for explanation about *Termination* and *Initialization*).

The input range for “duty cycle abc” is [0;+1]. Finally, we have to send our three-phase reference voltage to this block but a scaling block is needed. This block is included to the control block and shown in Figure 4.4.



- **Uabc_ref is divide by Vdc/2 to have a range [-1 ; +1]**
- **Then divide by 2 and one is added to have a range [0 ; +1] to send it to dSpace PWM block**
- **dSpace PWM block include a triangular wave to built the switching pattern**

Figure 4.4 : Scaling block

CONTROL SYSTEM AND PLL

You can find the detail of this block in APPENDIX G. Figure 0.43. You can see that the scaling block presented above is included to this block. The control is totally similar to the one presented in Chapter 3 except that :

- All the sample & hold block have been removed but the system is still discrete.
- The sample time "Ts" is replaced by "-1" (inherited).

The enable signal is maybe not useful. It could be removed. It depends how will be run the system. But if it's used, the output port “Uabc_ref range [0;1]” should be set to the following characteristics :

- Reset when disabled
- Initial output = 0.

In this configuration, when the block is disabled, the output will be zero and the PWM block will see zero duty cycle and will open the switches.

TRIGGER SIGNAL, SYNCHRONIZATION

The sample & Hold have been removed. Now, we need to specify when acquire a sample. We know that we need to sample on the peak of the triangular wave of the PWM, ideally, on every peak that is the asymmetric PWM.

We guess that more than one solution is possible to run the system. But for simplicity, as we said above, we decided to use the PWM block “DS1103SL_DSP_PWM3” using a symmetric PWM.

Furthermore, this block is link to an interruption “DS1103SLAVE_PWMINT”. The interruption is generated every POSITIVE PEAK of the triangular wave of block PWM3 as shown in Figure 4.5. Consequently we have : Finterruption = Fsampling = Ftriangle = Fswitching.

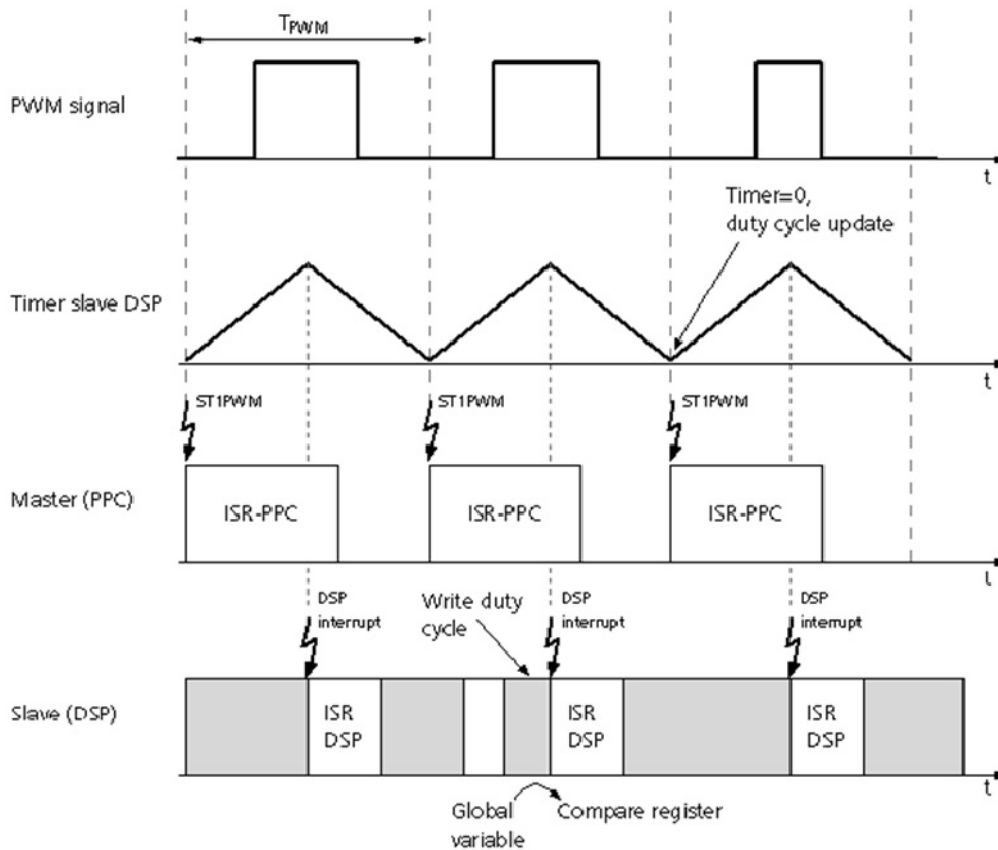


Figure 4.5 : Matlab Help from dSpace, PWM interruption [33]

The interrupt is generated that can be shifted nearly over the whole PWM period by specifying the interrupt alignment (Source : dSpace Help in Matlab [33]).

In Simulink, a block “DS1103SLAVE_PWMINT” is available. To trigger the whole Simulink model, we have to link this block to another block called “Timer Task Assignment” as shown in the top-level model Figure 4.2. Finally, every interruption signal, ONE sample will be acquired.

Nevertheless, the “overrun” condition should be checked. We need to be sure that the calculation (in the controller) is finished before a new sample is acquired.

CONTROL SIGNAL “GO”

The “GO” signal (Figure 4.2) is used to activate the integrator part of the controller (see section “3.9.1 Simulation steps, Simulink block diagram” for explanation). It is also used to enable or disable PWM block.

HOW TO FORCE IGBTs OFF

It’s possible to force IGBTs OFF disabling the block “Control system and PLL” since the output will be zero when disable (if set correctly...). A zero value will be sent to the PWM block and the switches will be open.

Another solution is presented in Figure 4.6 and is present in the main block diagram in APPENDIX G. Figure 0.43.

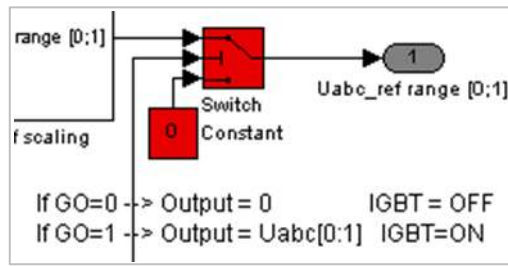


Figure 4.6 : How to force IGBTs OFF (complete diagram : APPENDIX G. Figure 0.43)

The switches are activated by the “GO” signal in our model.

- If GO = 0 ➔ Output = 0 ➔ IGBT = OFF
- If GO = 1 ➔ Output = Uabc range [0;1] ➔ IGBT = ON

4.4 Running an experiment

To run an experiment we need to introduce some important points that are : STOP/PAUSE/RUN mechanism, *simState* variable, *Initialization* and *Termination* value, how to *build* a model and which parameters should we used, and how to use Control Desk software.

A tutorial is also available in [37] , and we also advice to use the dSpace Help in Simulink (more useful than the dSpace books).

SIMSTATE VARIABLE

The *simState* variable is an internal variable that allows to read or set the simulation state of the application [33] . This variable is created when the system is built (see how to *build* a model in the following).

It can take the following value (Table XXX).

Simulation State	simState variable
STOP	0
PAUSE	1
RUN	2

Table 4.3 : *simState* values

STOP/PAUSE/RUN MECHANISM

The STOP/PAUSE/RUN mechanism depends on the *simState* variable. By controlling it, you can stop, pause or run your experiment.

In our case, we chose to control it via Control Desk. When your system is built and your variable description file (“.sdf”) is opened in Control Desk (see next paragraph), you can find this variable in the main group of variable.

The following figure shows a part of control panel in Control Desk, the *simState* is linked to “Push Buttons”.

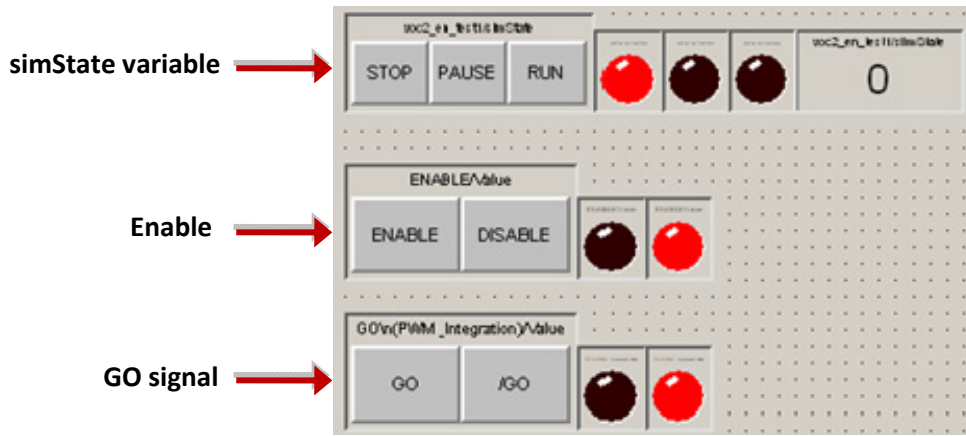


Figure 4.7 : Control Panel in Control Desk

In each Simulink block, you can specify an *Initialization* and *Termination* value. The following table shows the links with the *simState* variable.

STATE	SIMSTATE	RESULT
STOP	0	Termination code executed. Termination value are used.
PAUSE	1	<ul style="list-style-type: none"> If the previous state was in RUN, no Termination values are used, the current outputs are kept. If the system was in STOP mode, the Initialization values are used.
RUN	2	<ul style="list-style-type: none"> If the simulation was previously in the PAUSE mode, the execution of the application is re-enabled. If the previous state was STOP, the states of the model are reset to their initial values and the execution of the application is restarted.

Table 4.4 : Relation between application state and Initialization and Termination values

SIMULATION PARAMETERS AND “BUILD MODEL”

When your Simulink model is modified, you can *BUILD* the model from Simulink using :

//Tools/Real Time Workshop/Build Model (or CTRL+B)

But before that, you may need to modify the *Configuration Parameters* as follow :

PARAMETERS	VALUE
Solver/Step	Fixed
Solver/Stop Time	INF
Optimization/block reduction	Disable
Real Time Workshop/System Target File	rti1103.tlc

Table 4.5 : Configuration Parameters before BUILD

Before pressing “CTRL+B” (*build*), we advice to open Control Desk software. In this case, Control Desk will automatically detect that a new file have been built (variable description file with extension “.sdf”).

Then, a “new experiment” should be created, and the “.sdf” file should be “added to experiment”. You can now create a new “layout”. Since you have the layout open, you can add buttons, knobs, display, gauge, numeric input (to write a value) and so on. After that, you can link your Simulink variables (or labels) to graphical instruments, for example, a button to control this variable or a

graph for visualization. The variables are visible in the “Tool Window” in the bottom part of the Control Desk interface.

ATTENTION !

When you *build* the model, the C-code generated is automatically sent to your hardware and the application **START TO RUN** (*simState* = 2). So, as you can see in the Figure 4.2, the signal GO and the Enable are set to zero. Consequently, when our system is built and start running, the PWM is OFF and the controller is disabled.

5 CONCLUSIONS AND FUTURE WORK

Controller lab-tests

In the Chapter 3, some simulations were presented. The controller seems to be correct and stable. We suppose that some lab-tests can now be achieved with a grid-connected converter with simple resistive load.

The Simulink file prepared for implementation may need to be slightly modified but the idea was presented in Chapter 4 with some key point to run an experiment with dSpace. A tutorial is available at the reference [37].

Stability analysis

In this report, a simple stability analysis has been done. Nevertheless, this analysis is quite simplistic (with approximations) and has been realized in continuous time only. It should be also complete in discrete time because the controller is implemented in discrete time.

Deadtime

As we explain in the first part (2.4.3 *Dead time effect*), the performances of the converter are affected by injection of deadtime in the PWM signals to avoid short circuit of the DC-link. We suppose that some simulations of this deadtime and some compensation should be done before testing the controller in the laboratory.

Modulation method

The modulation method could be improved. In our system, we decided to implement a sinusoidal Pulse Width Modulation mainly for its simplicity and acceptable performances. We advise to test it in the lab. Nevertheless, a simulation with Space Vector Modulation (SVM) should be also simulated and a deep comparison to sinusoidal PWM could be done. The SVM is known for its effectiveness, simplicity for implementation, harmonics reduction.

Control method

A last possible improvement could be done by implementing a Virtual Flux Oriented Control (VFOC). It could improve the performance under non-ideal line voltage conditions. Furthermore, this method could be useful if a machine is added to the model (AC side) because machine models are generally done with flux-oriented reference.

We also advise to implement a load current controller. Reading some papers, we saw some battery charger configuration with another stage after the rectifier (on more leg with two IGBTs for DC-DC conversion). A load current controller was responsible of the switches for this stage ([3]).

REFERENCES

Control and Modeling of PWM rectifiers

- [1] BLASKO V., KAURA V. "A New Mathematical Model and Control of a Three-Phase AC–DC Voltage Source Converter". IEEE Transactions on Power Electronics, 1997. Vol.12 , issue: 1. Pages: 116 – 123.
- [2] BO YIN, ORUGANTI R., PANDA S.K., BHAT A.K.S. "A Simple Single-Input-Single-Output (SISO) Model for a Three-Phase PWM Rectifier". IEEE Transactions on Power Electronics, 2009. Vol.24, issue: 3. Pages: 620 – 631.
- [3] BOJRUP MARTIN. "Advanced Control of Active Filters in a Battery Charger Application". Phd Thesis, Department of Industrial Electrical Engineering and Automation (IEA), Lund Institute of Technology (LTH), Lund, Sweden. 1999. 124p. ISBN 91-88934-13-6.
- [4] HARNEFORS LENNART. "Control of Variable-Speed Drives". Applied Signal Processing and Control, Department of Electronics, Mälardalen University, Västerås, Sweden, 2002. 194p.
- [5] HENGCHUN MAO, BOROYEVICH D., LEE F.C.Y. "Novel Reduced-Order Small-Signal Model of a Three-Phase PWM Rectifier and Its Application in Control Design and System Analysis". IEEE Transactions on Power Electronics, 1998. Vol.13 , issue: 3. Pages: 511 – 521.
- [6] HITI S., BOROYEVICH D., CUADROS, C. "Small-signal modeling and control of three-phase PWM converters". Industry Applications Society Annual Meeting, IEEE 1994. Vol.2, pages: 1143 – 1150.
- [7] H.S. KIM, H.S. MOK, G.H. CHOE, D.S. HYUN, S.Y. CHOE. "Design of Current Controller for 3-Phase PWM Converter with Unbalanced Input Voltage". Power Electronics Specialists Conference, IEEE 1998. Vol.1. Pages: 503 – 509.
- [8] JASINSKI M., ANTONIEWICZ P., KAZMIERKOWSKI M.P. "Vector control of PWM rectifier - inverter fed induction machine - a comparison". Compatibility in Power Electronics, IEEE 2005. Pages: 91 – 95.
- [9] KASMIERKOWSKI MARIAN P., BLAABJERG F., KRISHNAN R.- "Control in power electronics, selected problem". Elsevier Science, USA. 2002. 518p. ISBN : 0-12-402772-5.
- [10] KASMIERKOWSKI MARIAN P. "Current Control Techniques for Three-Phase Voltage-Source PWM Converters: A Survey". IEEE Transactions on Industrial Electronics. Vol.45 , issue: 5. 1998. Pages: 691 – 703.
- [11] KNAPCZYK MICHAŁ, PIENKOWSKI KRZYSZTOF. "High Performance decoupled control of PWM rectifier with load compensation". Politechnika Wrocławska, Instytut Maszyn, Napędów i Pomiarów Elektrycznych. 2007. 11p. Available at :
<http://www.imne.pwr.wroc.pl/Wydawnictwa/PNIMNIPEnr60/Napedy/pdf/4%20Michal%20KNAPCZYK%20Krzysztof%20PIENKOWSKI%202.pdf>
- [12] LUNDBERG STEFAN. Lecture slides : ENM075 Electric Drives II. Department of Energy and Environment, Chalmers University of Technology, Göteborg, Sweden. 2009.
- [13] MALINOWSKI MARIUSZ. "Sensorless Control Strategies for Three-Phase PWM Rectifiers". Phd Thesis, Warsaw University of Technology, Faculty of Electrical Engineering, Institute of Control and Industrial Electronics. Warsaw, Poland. 2001. 128p.

-
- [14] OTTERSTEN ROLF. *“On Control of Back-to-Back converters and Sensorless Induction Machine Drives”*. PhD Thesis, Department of Electric Power Engineering, Chalmers University of Technology, Göteborg, Sweden. 2003. 165p. ISBN : 91-7291-296-0.
- [15] RODRIGUEZ J.R., DIXON J.W., ESPINOZA J.R., PONTT J., LEZANA, P. *“PWM Regenerative Rectifiers: State of the Art”*. IEEE Transactions on Industrial Electronics, 2005. Vol.52, issue: 1. Pages: 5 – 22.
- [16] RUNXIN WANG, JINJUN LIU. *“Redefining a New-Formed Average Model for Three-Phase Boost Rectifiers/Voltage Source Inverters”*. Applied Power Electronics Conference and Exposition, 2009. Pages: 1680 – 1686.
- [17] WANG XU, HUANG KAIZHENG, YAN SHIJIE, XU BIN. *“Simulation of Three-phase Voltage Source PWM rectifier Based on Space Vector Modulation”*. Control and Decision Conference, Chinese, IEEE 2008. Pages: 1881 – 1884.
- [18] WEI KE-XIN, WANG SHUI-MING. *“Modeling and Simulation of Three-Phase Voltage Source PWM Rectifier”*. International Conference on Advanced Computer Theory and Engineering, IEEE 2008, Pages: 982 – 986.
- [19] YU FANG, YONG XIE, YAN XING. *“Study on control strategy of three phase high power factor PWM rectifier”*. International Conference on Electrical Machines and Systems, IEEE 2008. Pages: 1832 – 1837.

Power Electronics

- [20] ERIKSON ROBERT W., MAKSIMOVIĆ D. *“Fundamentals of Power Electronics”*. Second Edition. Springer Science, USA. 2001. 883p. ISBN : 978-0-7923-7270-7.
- [21] MOHAN N., UNDELAND T., ROBBINS W. *“Power Electronics, Converters, Applications and Design”*. Second Edition. John Wiley & Sons, Inc. USA. 1995. 802p. ISBN : 0-471-30576-6.
- [22] MUHAMMAD H. RASHID. *“Power Electronic Handbook, Devices, Circuits, and Applications”*. Second Edition. Burlington, MA : Academic. 2006. 1172p. ISBN: 978-0-12-088479-7.
Available at : <http://www.sciencedirect.com/science/book/9780120884797> (Chalmers library).

PWM

- [23] BONGIORNO MASSIMO, SANINO A. Lecture slides : ENM100 Power Electronic Solutions for Power Systems. Department of Energy and Environment, Chalmers University of Technology, Göteborg, Sweden. 2009.

Carrier-based PWM

- [24] HAVA AHMET M., KERKMAN RUSSEL J., LIPO THOMAS A. *“Carrier-Based PWM-VSI Overmodulation Strategies : Analysis, Comparison, and Design”*. IEEE Transactions on Power Electronics, 1998, Vol.13, issue: 4, pages: 674 – 689.

SVM

- [25] ANALOG DEVICES APPLICATION NOTE AN31-17. *“Implementing Space Vector Modulation with the ADMC331”*. Analog Devices Inc., January 2000.
- [26] DORIN O. NEACSU. *“Space Vector Modulation-An Introduction”*. Tutorial at IECON2001, the 27th Annual Conference of the IEEE Industrial Electronics Society. 2001.
Available at : <http://www.et.upt.ro/admin/tmpfile/fileM1224954797file490353adde0d4.pdf>

-
- [27] JIN-WOO JUNG. "Project #2 Space Vector PWM inverter". Project performed at Mechatronic Systems Laboratory, Department of Electrical and Computer Engineering, The Ohio State University, USA. 2005. Available at :
http://www2.ece.ohio-state.edu/ems/PowerConverter/SpaceVector_PWM_Inverter.pdf

PLL

- [28] AMUDA L.N., CARDOSO FILHO B.J., SILVA S.M., SILVA S.R., DINIZ A.S.A.C. "Wide bandwidth single and three-phase PLL structures for grid-tied PV systems". Photovoltaic Specialists Conference, IEEE 2000. Pages: 1660 – 1663.
- [29] CHUNG S.K. "Phase-locked loop for grid-connected three-phase power conversion systems". Electric Power Applications, IEE Proceedings. 2000. Vol.147 , issue: 3. Pages: 213 – 219.
- [30] SALAMAH A.M. "Three-phase phase-lock loop for distorted utilities". IET Electric Power Applications, 2007. Vol.1, issue : 6, pages: 937–945.

Deadtime

- [31] JONG WOO CHOI, SUNG IL YONG, SEUNG KI SUL. "Inverter output voltage synthesis using novel dead time compensation". IEEE Applied Power Electronics Conference and Exposition, 1994. Vol.1, Pages: 100 – 106.
- [32] SEUNG-GI JEONG, MIN-HO PARK. "The analysis and compensation of dead-time effects in PWM inverters". IEEE Transactions on Industrial Electronics, vol.38, no.2, 1991. Pages: 108 – 114.

dSpace

- [33] dSpace Help in Simulink.
- [34] JUSTIN D. LANGDON. "Design and Adaptive Control of a Lab-based, Tire-coupled, Quarter-car, Suspension Test Rig for the Accurate Re-creation of Vehicle Response". MSc Thesis, Virginia Polytechnic Institute and State University, USA. January 31, 2007. Available at:
http://scholar.lib.vt.edu/theses/available/etd-02132007-112050/unrestricted/Langdon_Thesis_Rev_Final_ETD_2007.pdf
- [35] KIRAN KUMAR GUNDA. "Adjustable Speed Drives Laboratory Based on dSpace Controller". MSc Thesis, Department of Electrical & Computer Engineering, Louisiana State University and Agricultural and Mechanical College, USA. 2008.
- [36] Laboratory Tutorial, Massachusetts Institute of Technology, Department of Mechanical Engineering, 2.737 Mechatronics–Spring 2006, February 14, 2006. Available at:
<http://web.mit.edu/2.737/www/labs/General/tutorial.pdf>
- [37] NICANOR QUIJANO, KEVIN PASSINO. "A Tutorial Introduction to Control Systems Development and Implementation with dSPACE". Dept. of Electrical Engineering, The Ohio State University, USA. 2002. Available at : <http://www2.ece.ohio-state.edu/~passino/dSPACEtutorial.doc.pdf>

APPENDICES

A. Three-phase system – Coordinate transformations

A.1 Voltage and current definition

First of all, we can define the voltage and current of a three-phase system :

$$\begin{aligned}v_a(t) &= E_m \cos(\omega t) \\v_b(t) &= E_m \cos\left(\omega t - \frac{2\pi}{3}\right) \\v_c(t) &= E_m \cos\left(\omega t - \frac{4\pi}{3}\right) \\&\text{(positive sequence here)}\end{aligned}$$

$$\begin{aligned}i_a(t) &= I_m \cos(\omega t + \varphi) \\i_b(t) &= I_m \cos\left(\omega t + \varphi - \frac{2\pi}{3}\right) \\i_c(t) &= I_m \cos\left(\omega t + \varphi - \frac{4\pi}{3}\right)\end{aligned}$$

For any three-phase system composed of positive and negative sequence we have

$$v_a(t) + v_b(t) + v_c(t) = 0 \quad \forall t$$

If the system present an asymmetry, a zero sequence appears and is define as the mean value

$$v_0(t) = \frac{v_a(t) + v_b(t) + v_c(t)}{3}.$$

A good thing is that there will never be any zero sequence in the currents, provided that there is no neutral connection.

A.2 Equivalent two-phase system, $\alpha\beta$ -transformation (Clarke)

A three-phase system can be described with only two components α and β (real and imaginary respectively). Furthermore, we call a **space vector** the quantity

$$v^s(t) = v_\alpha(t) + jv_\beta(t) = \frac{2}{3}K \left(v_a(t) + v_b(t)e^{j\frac{2\pi}{3}} + v_c(t)e^{j\frac{4\pi}{3}} \right).$$

where K is a scaling constant. The transformation from ABC-to- $\alpha\beta$ (Clarke transformation) depending on the scaling constant K is :

$$\begin{bmatrix} \alpha \\ \beta \end{bmatrix} = K \begin{bmatrix} \frac{2}{3} & -\frac{1}{3} & -\frac{1}{3} \\ 0 & \frac{1}{\sqrt{3}} & -\frac{1}{\sqrt{3}} \end{bmatrix} \begin{bmatrix} a \\ b \\ c \end{bmatrix}$$

and

$$\begin{bmatrix} a \\ b \\ c \end{bmatrix} = \frac{1}{K} \begin{bmatrix} 1 & 0 \\ -\frac{1}{2} & \frac{\sqrt{3}}{2} \\ -\frac{1}{2} & -\frac{\sqrt{3}}{2} \end{bmatrix} \begin{bmatrix} \alpha \\ \beta \end{bmatrix}.$$

Amplitude invariant	$K = 1$
RMS-value invariant	$K = \frac{1}{\sqrt{2}}$
Power invariant	$K = \sqrt{\frac{3}{2}}$

A.3 Synchronous coordinate, dq-transformation (Park)

We can now define a transformation of the previous space vector $v^s = v_\alpha + jv_\beta$ (we now drop the time argument “(t)” for simplicity) with

$$v_{dq} = v^s e^{-j\theta}$$

where $\theta = \omega t$. This transformation makes v_{dq} similar to fixed complex phasor. This transformation is called dq-transformation and can be regarded as observing the space vector from a coordinate system rotating with the frequency ω (synchronous coordinate or dq-coordinate). We denote the space vector in synchronous coordinates as

$$v_{dq} = vd + jvq.$$

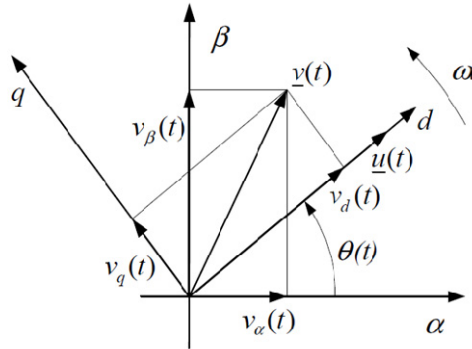


Figure 0.1 : Relation between $\alpha\beta$ -frame and dq -frame (rotating) [23]

Giving dc-steady state quantity, the synchronous coordinates are very useful for analysis, implementation of control algorithm (controller design is easier on dc-quantities).

We can write

$$\begin{aligned} v^s &= v_{dq} e^{j\theta} = (v_d + jv_q)(\cos\theta + jsin\theta) = (v_d \cos\theta - v_q \sin\theta) + j(v_d \sin\theta + v_q \cos\theta) \\ &= v_\alpha + jv_\beta \end{aligned}$$

$$\begin{bmatrix} d \\ q \end{bmatrix} = \begin{bmatrix} \cos\theta & \sin\theta \\ -\sin\theta & \cos\theta \end{bmatrix} \begin{bmatrix} \alpha \\ \beta \end{bmatrix} \text{ and } \begin{bmatrix} \alpha \\ \beta \end{bmatrix} = \begin{bmatrix} \cos\theta & -\sin\theta \\ \sin\theta & \cos\theta \end{bmatrix} \begin{bmatrix} d \\ q \end{bmatrix}.$$

Source : [4]

A.4 Simulation

These transformations and the theta angle (voltage angle) are very critical for all the simulations in the project. To be sure that we have the correct angle, we created this angle first, then, a three-phase voltage system is created according to this angle as we can see in the following block diagram.

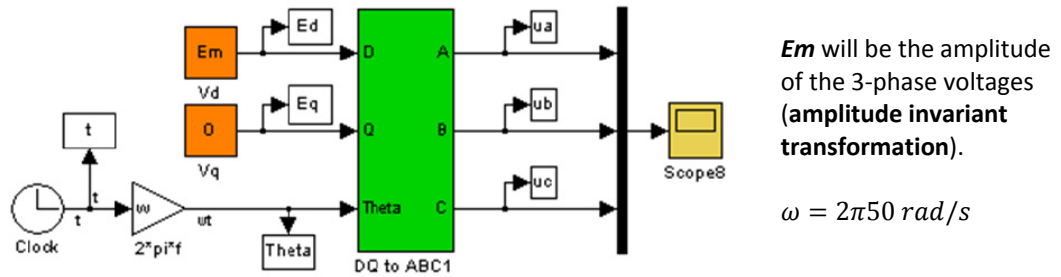


Figure 0.2 : Three-phase system simulation

The transformations are implemented as below.

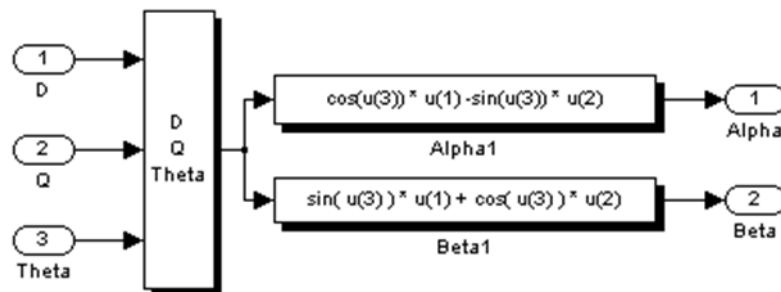


Figure 0.3 : $\alpha\beta$ -transformation

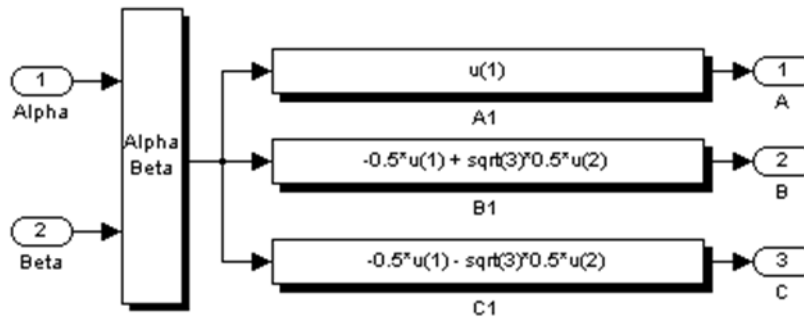


Figure 0.4 : dq-transformation

The simulation results are plotted on the following figure.

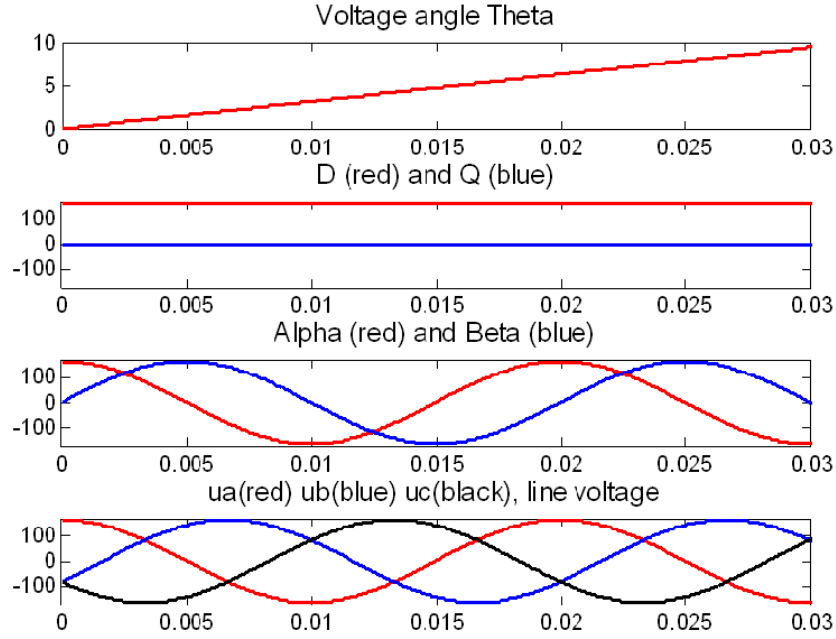


Figure 0.5 : Simulation of coordinates transformations

Simulation comments :

- Theta is positive.
- Voltage is placed on the d-axis.
- Beta signal is delay (lag).
- We verify a direct three-phase system (A first[0 rad], B in second[-2π/3 rad], C third[-4π/3 rad]).

A.5 Impedance in synchronous coordinates

We assume in the report (current controller design) that the impedance is : $Z(s) = (s + j\omega)L$. We can prove this relation with the following.

y^s is a general space vector, its transformation in synchronous coordinates is

$$y_{dq} = y^s e^{-j\theta}$$

and its time derivative is transformed as

$$\frac{dy^s}{dt} = \frac{d(e^{j\theta} y_{dq})}{dt} = e^{j\theta} \left(j\omega y_{dq} + \frac{dy_{dq}}{dt} \right).$$

Then, using the derivative operation $p = d/dt$ we get

$$p y^s = e^{j\theta} (p + j\omega) y_{dq}$$

In the Laplace domain, the following substitution is made : $s \rightarrow s + j\omega$. This implies that the complex impedance of an inductor in synchronous coordinates is

$$Z(s) = (s + j\omega)L$$

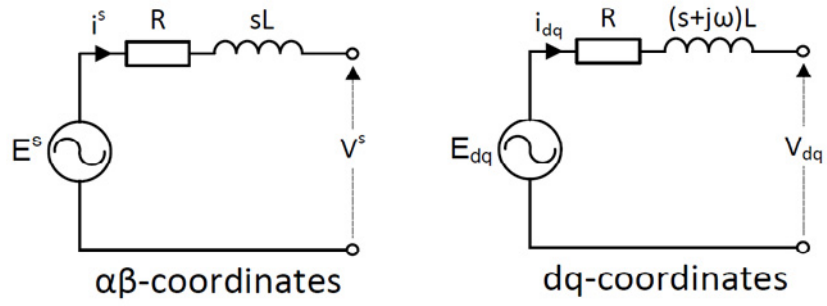


Figure 0.6 : *Illustration $\alpha\beta$ - and dq -impedance*

Source : [4]

B. Voltage and current control, continuous simulation

B.1 Simulink current control tests – Block diagram

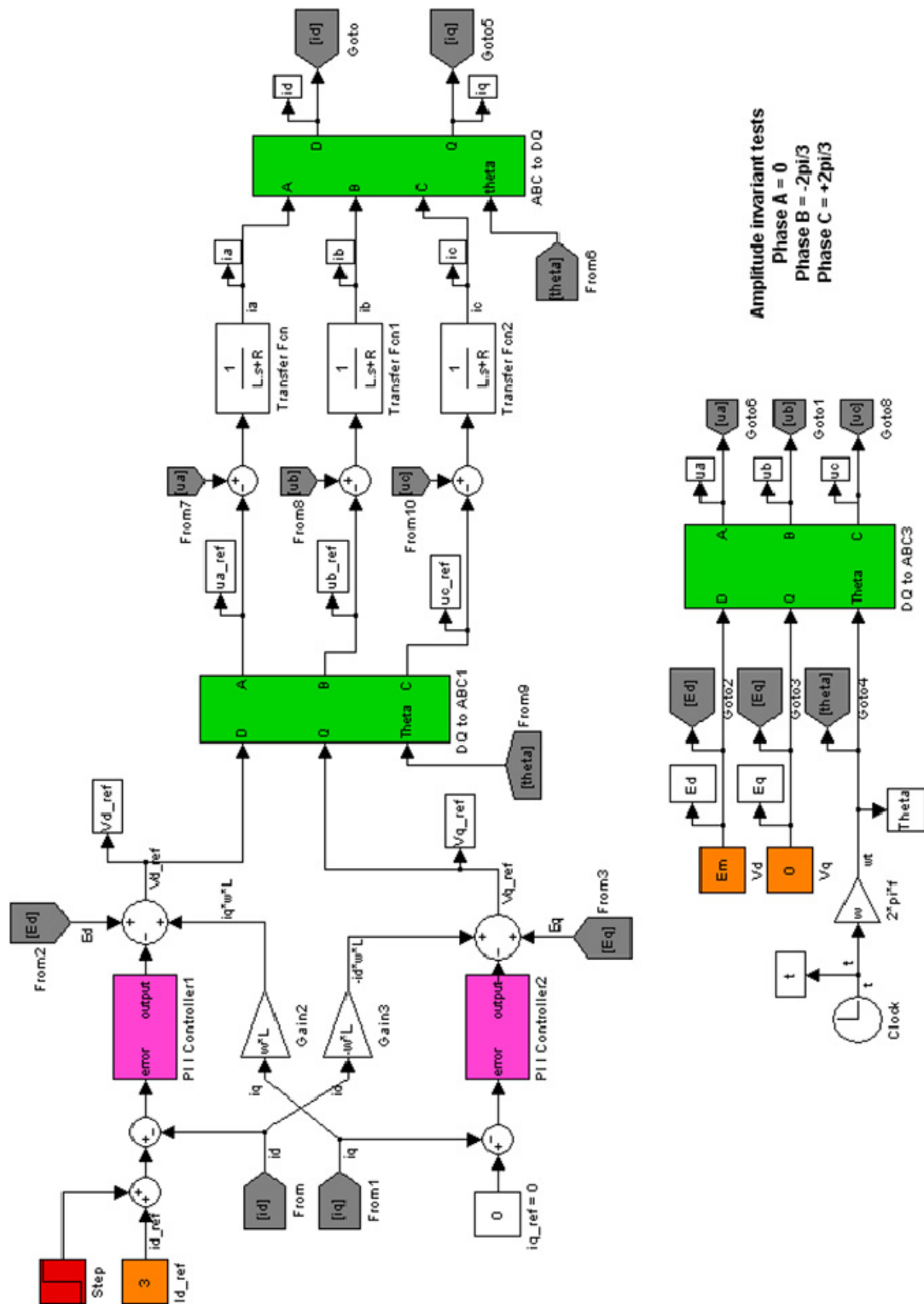


Figure 0.7 : Simulink current control tests – Block diagram

B.2 Continuous voltage controller, simulation with saturation, anti-windup, active damping

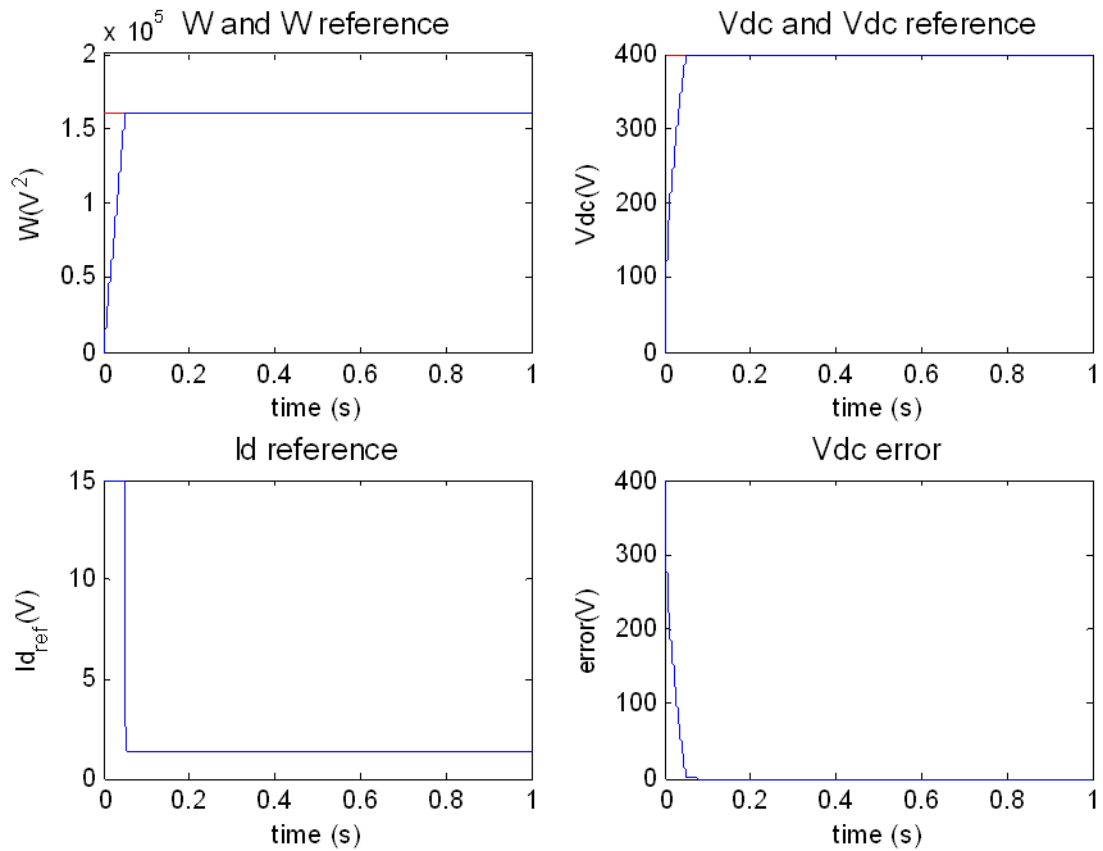


Figure 0.8 : Voltage controller – Simulation with saturation, anti-windup, active damping

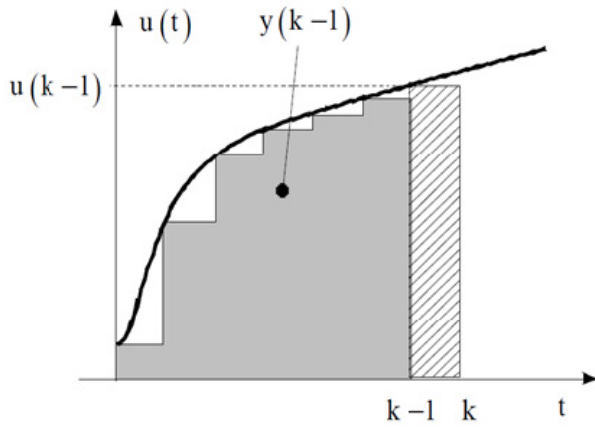
NEW PARAMETERS	VALUE
Ga	0.0057
Kiv	7.1205

Table 0.1 : New parameters for voltage controller with active damping

C. Digital simulation

DISCRETE INTEGRATOR

As the controller will be digital, we decided to simulate the control system in discrete time. The integrator have been implemented as below.



U: input / Y : output

$$y(k) = y(k - 1) + T_s u(k - 1)$$

$$\Leftrightarrow Y(z) = Y(z)z^{-1} + T_s U(z)z^{-1}$$

$$\Leftrightarrow Y(z)(1 - z^{-1}) = T_s U(z)z^{-1}$$

$$\frac{Y(z)}{U(z)} = \frac{T_s z^{-1}}{1 - z^{-1}} = \frac{T_s}{z - 1}$$

We can also draw the block scheme with the following equation :

$$Y(z) = [Y(z) + T_s U(z)]z^{-1}$$

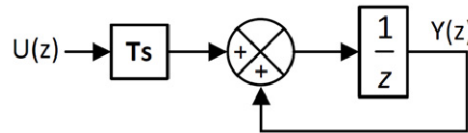


Figure 0.9 : Discrete integrator

REMARK FOR SIMULINK SIMULATION

In a simulation where discrete and continuous blocks are used at the same time, in order to come back from discrete to continuous, we should add a zero to the discrete signal with sampling time "INF" as below. Then, the output signal is treated as continuous by Simulink.

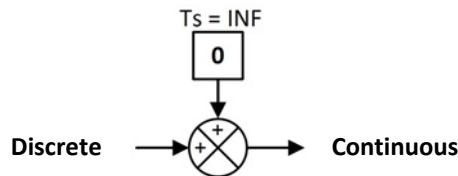


Figure 0.10 : Simulink discrete-to-continuous

D. Voltage and current control, discrete time simulation

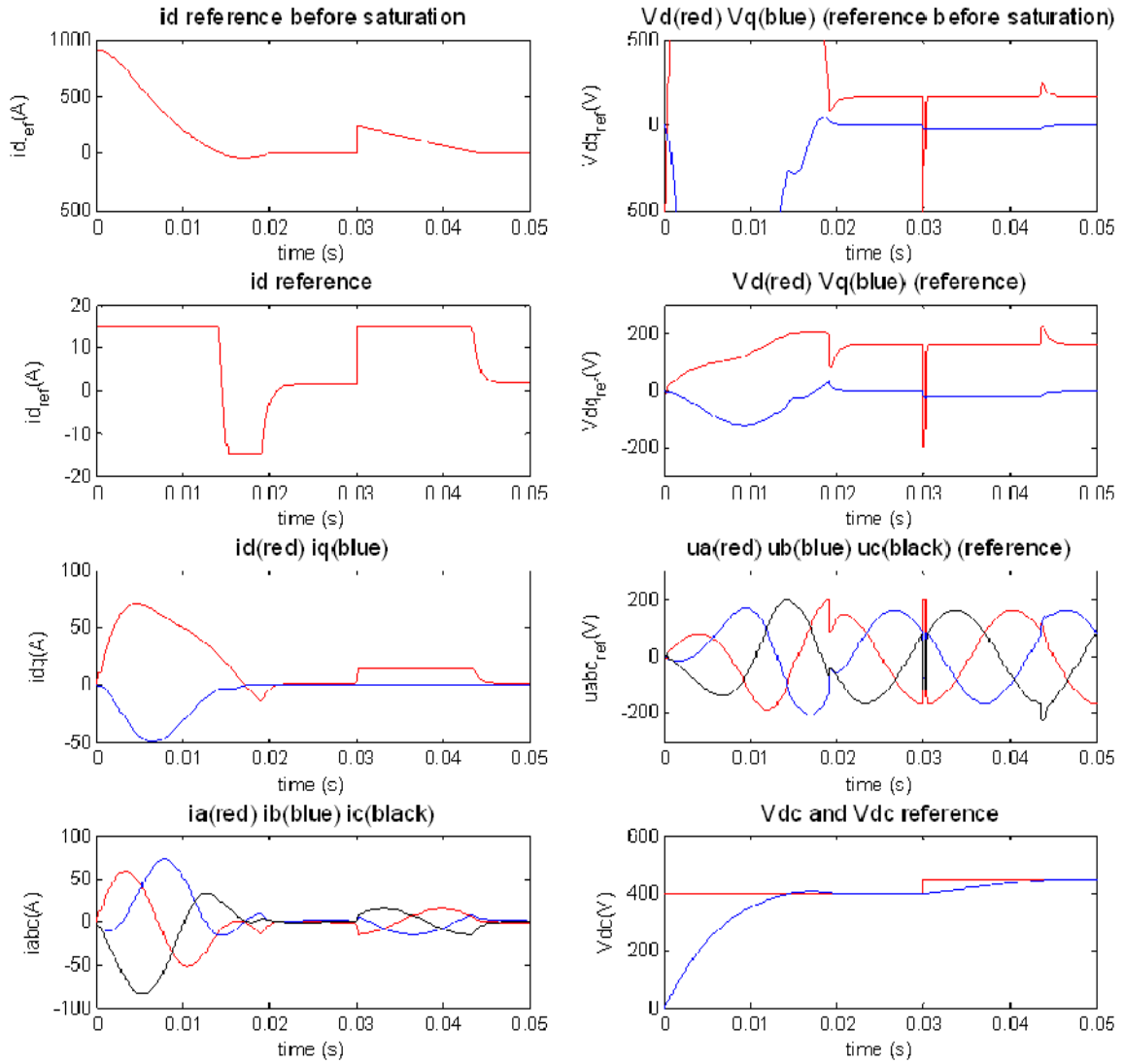


Figure 0.11 : Controller simulation results (discrete)

Table 0.2 : Voltage and current control, discrete time simulation

Parameters	Value		Value
R (Ω)	0.1	$\alpha_v = 2\pi F_{SW}/100$ (rad/s)	1.26e3
L (H)	5e-3	V controller, Kpv	0.0057
C (μF)	2200	V controller, Kiv	0.01
ω (rad/s)	$2\pi 50$	I controller, Kpi	62.8
Em (V), ph-to-gnd amplitude (=Ed)	$115\sqrt{2}$	I controller, Kii	1.26e3
Fsw (kHz), switching frequency	20	I saturation (A)	±15
Rload (Ω)	500	Vdc step at 0.03 (V)	50
Vdc reference (V)	400	Triangular wave Freq. (kHz)	20
$\alpha_i = 2\pi F_{SW}/10$ (rad/s)	1.26e4	Sampling frequency (kHz), $F_s=2 F_{tri}$	40

E. Stability analysis cont.

E.1 Simulations

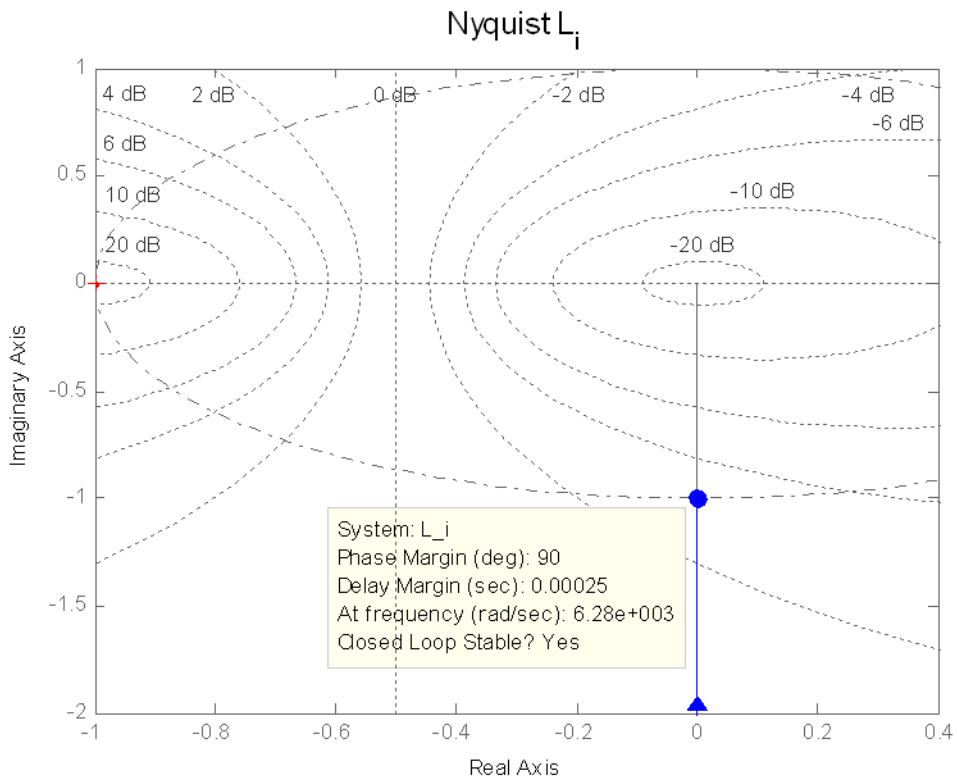


Figure 0.12 : Nyquist of L_i

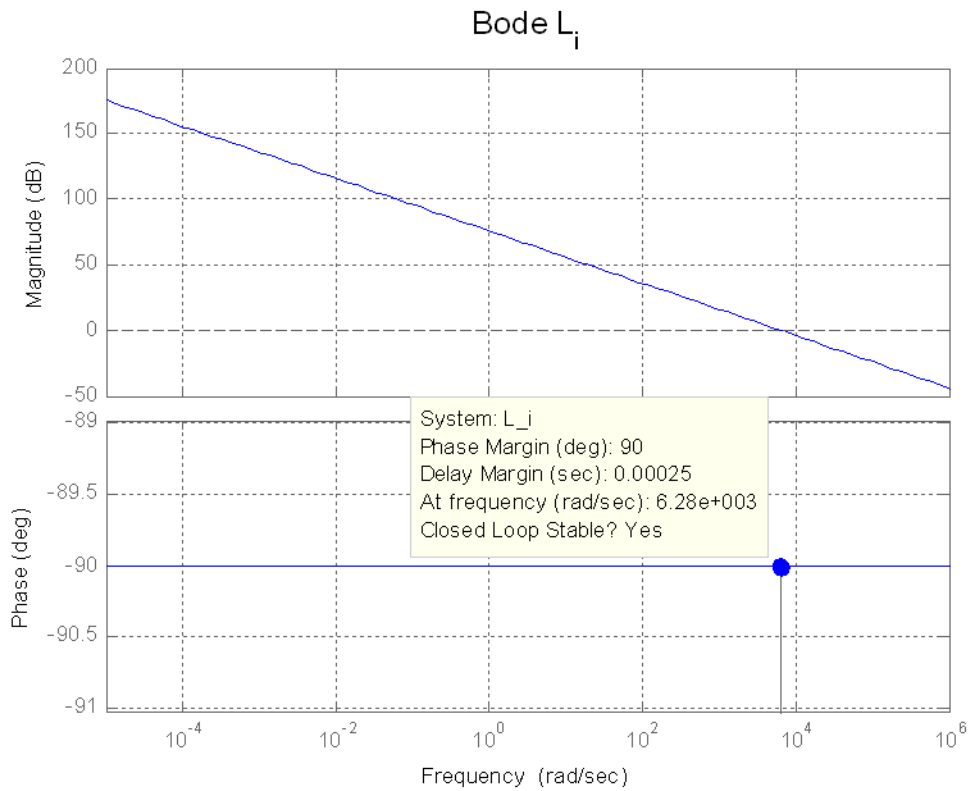


Figure 0.13 : Bode of L_i

Bode diagram S_i

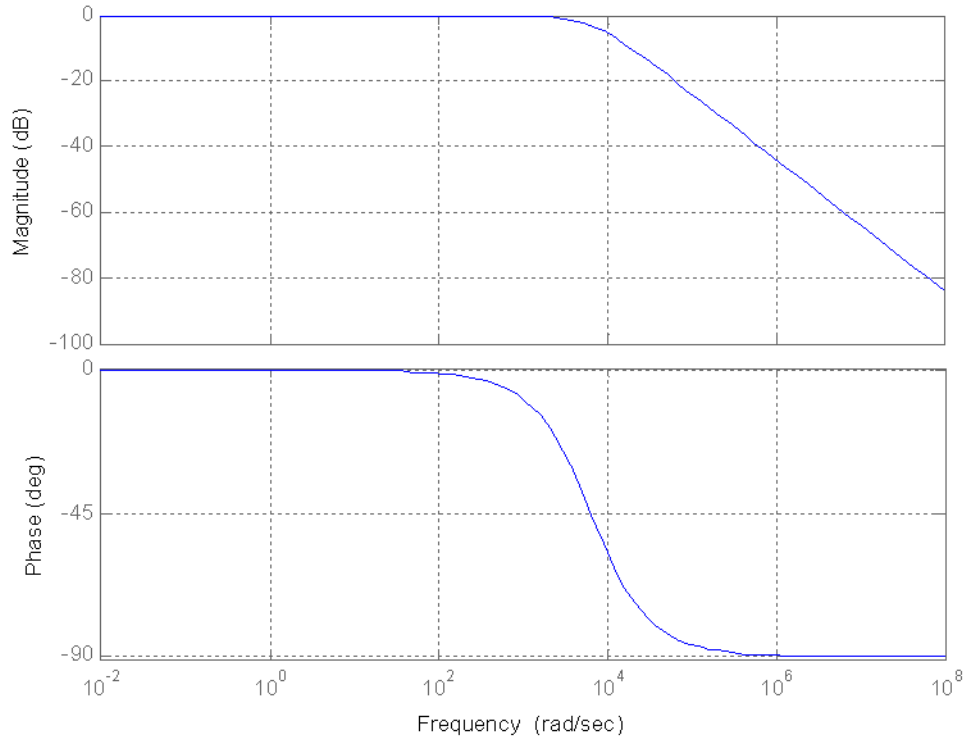


Figure 0.14 : Bode of S_i

PROPORTIONAL CONTROL ONLY

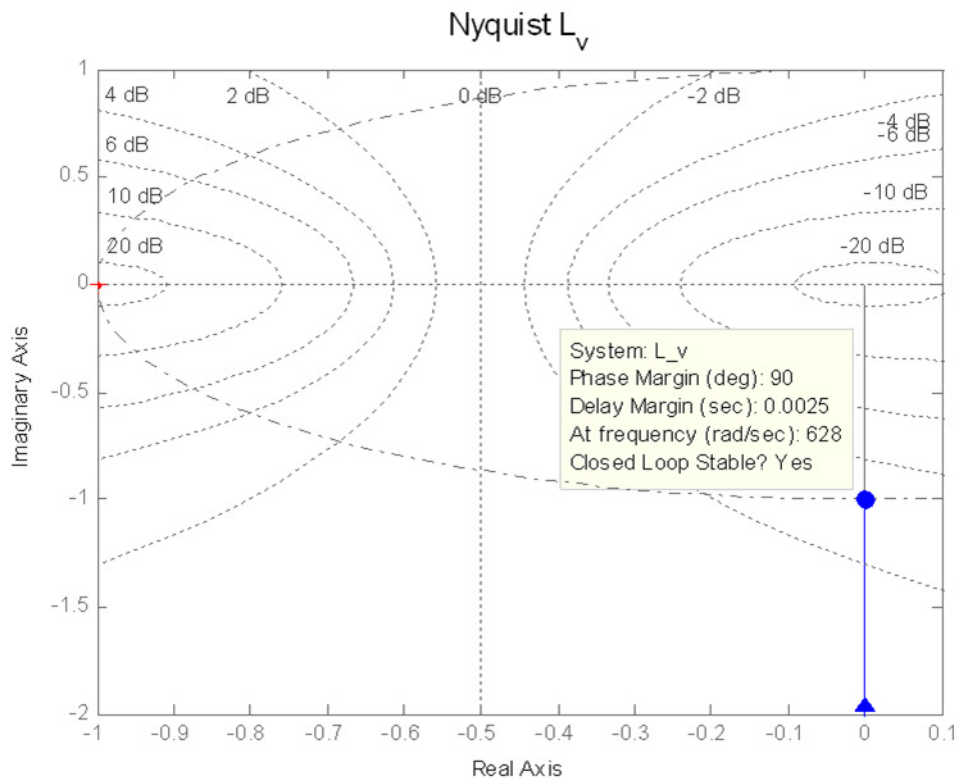


Figure 0.15 : Nyquist of L_v (P only)

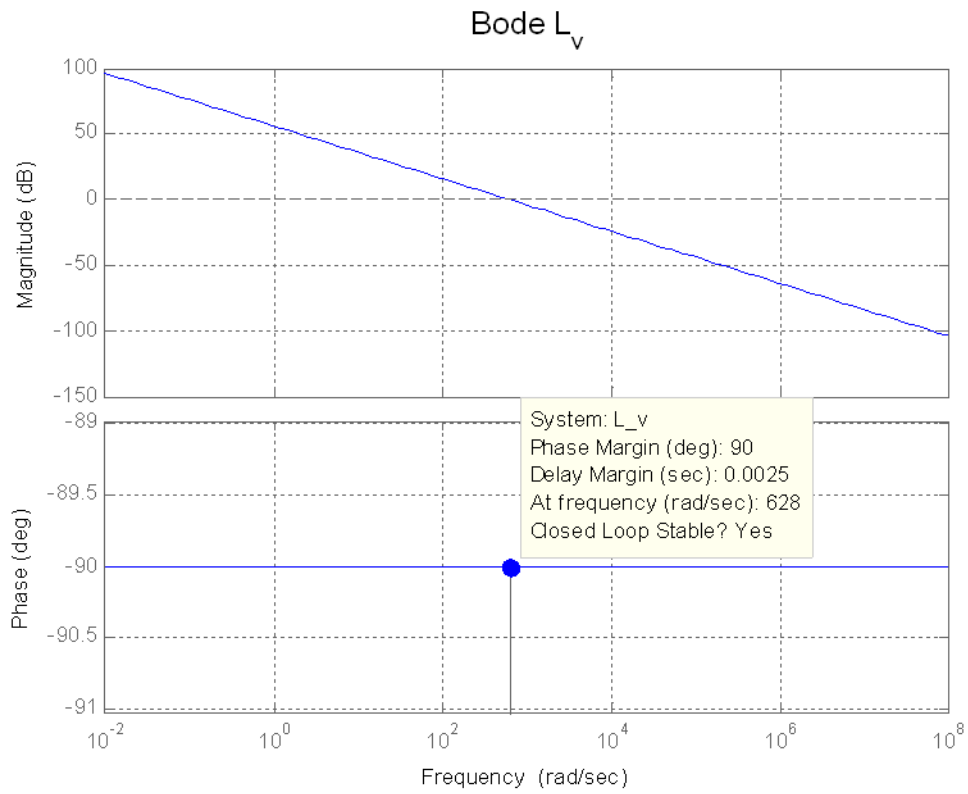


Figure 0.16 : Bode of $L_v(P$ only)

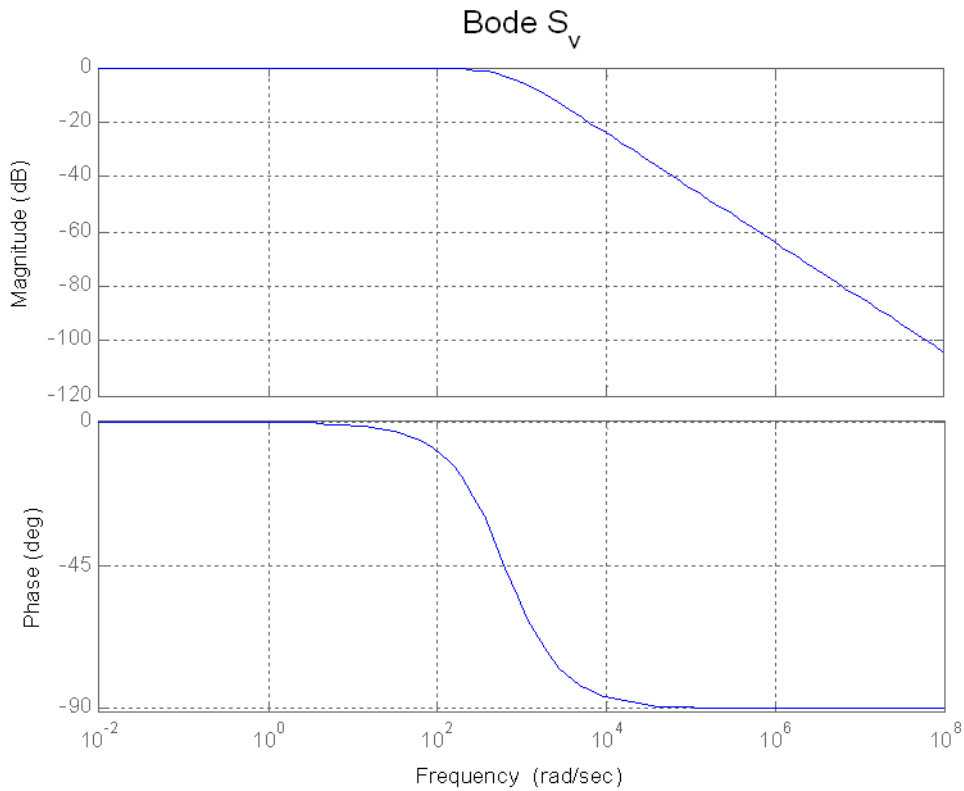


Figure 0.17 : Bode of $S_v(P$ only)

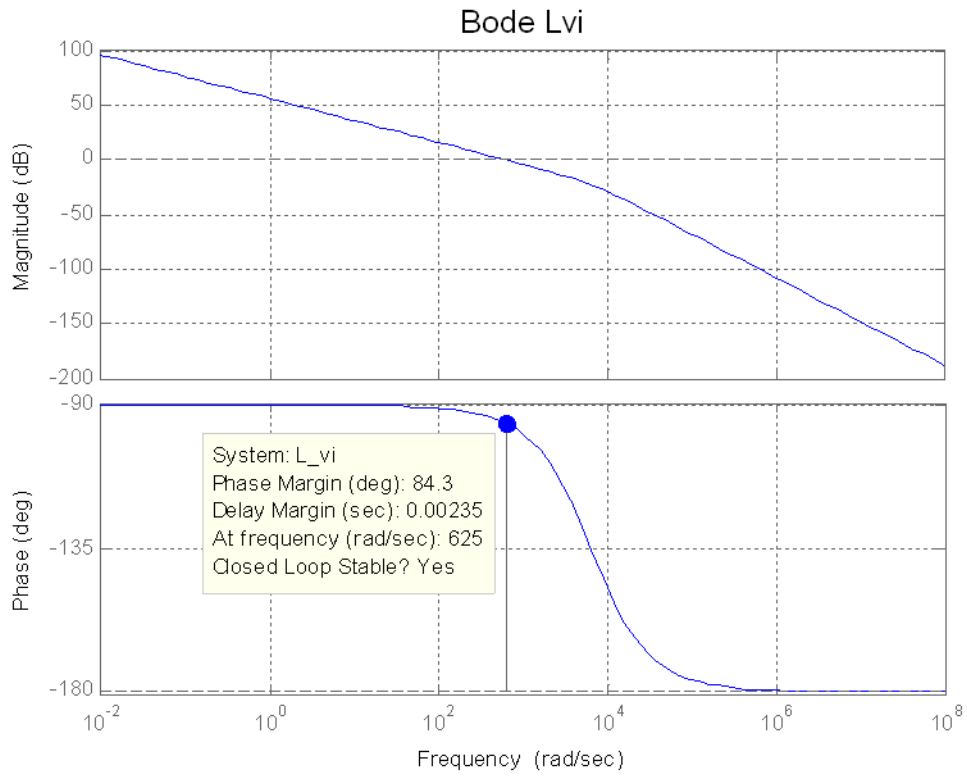


Figure 0.18 : Bode of $L_v(P)$ only

PROPORTIONAL AND INTEGRAL CONTROL

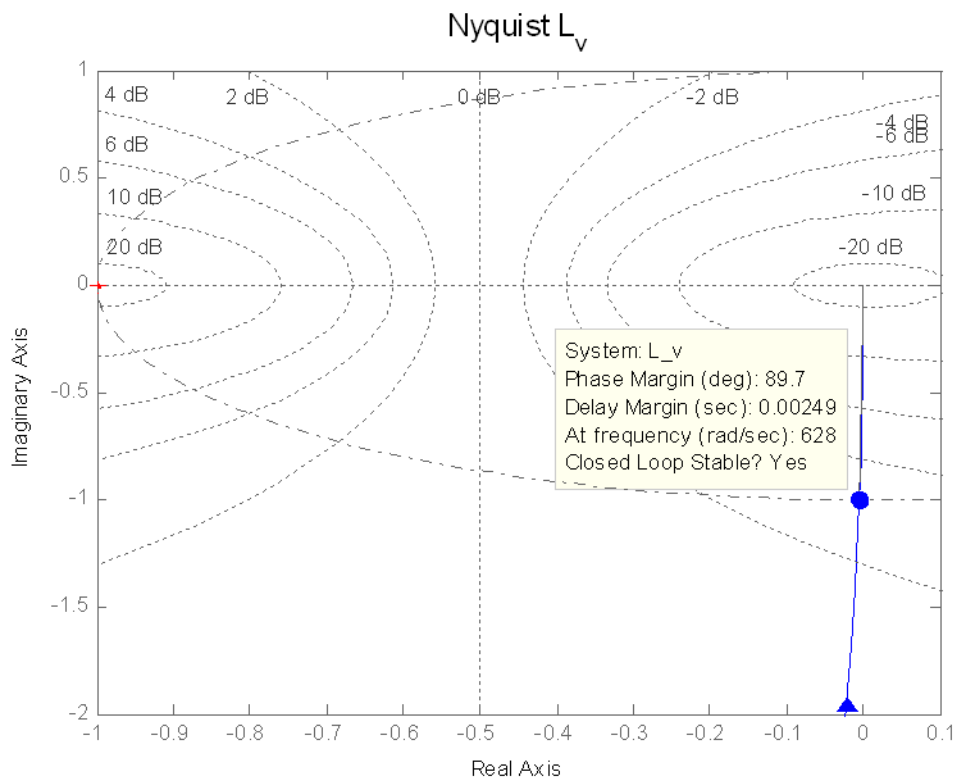


Figure 0.19 : Nyquist of $L_v(PI)$

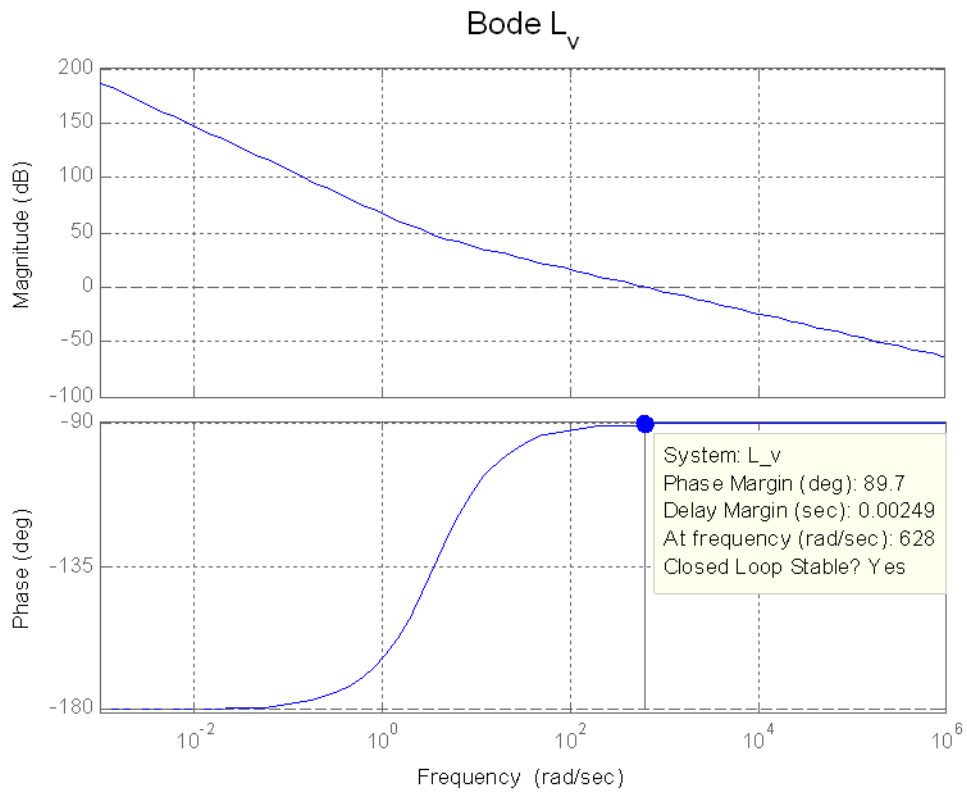


Figure 0.20 : Bode of L_v (PI)

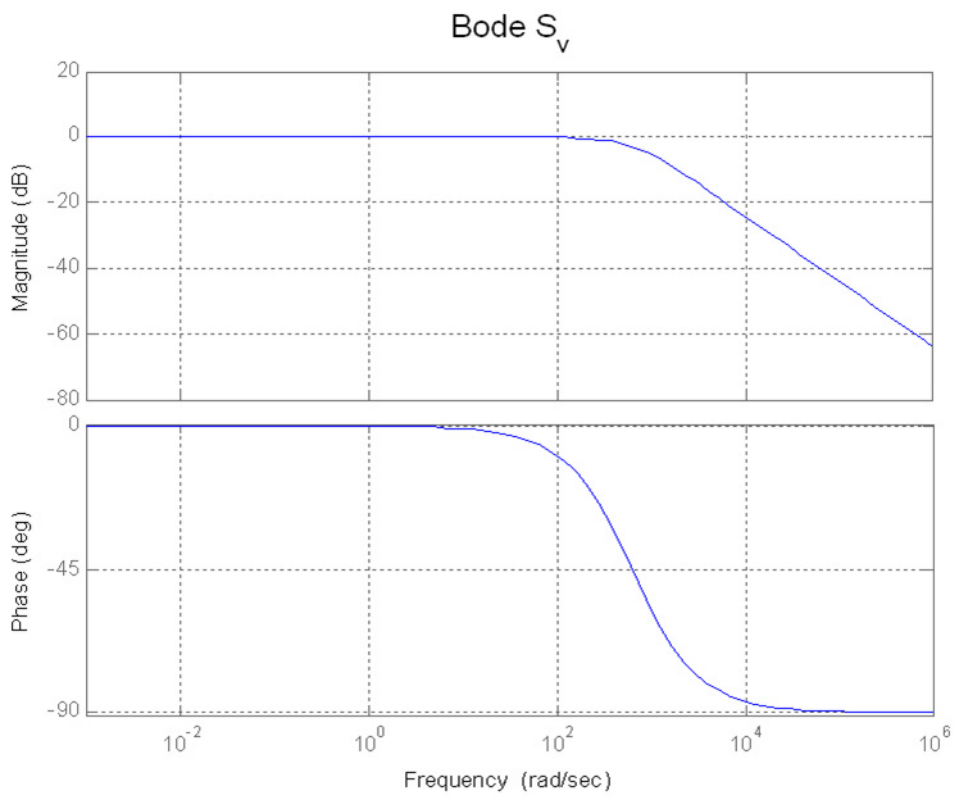


Figure 0.21 : Bode of S_v (PI)

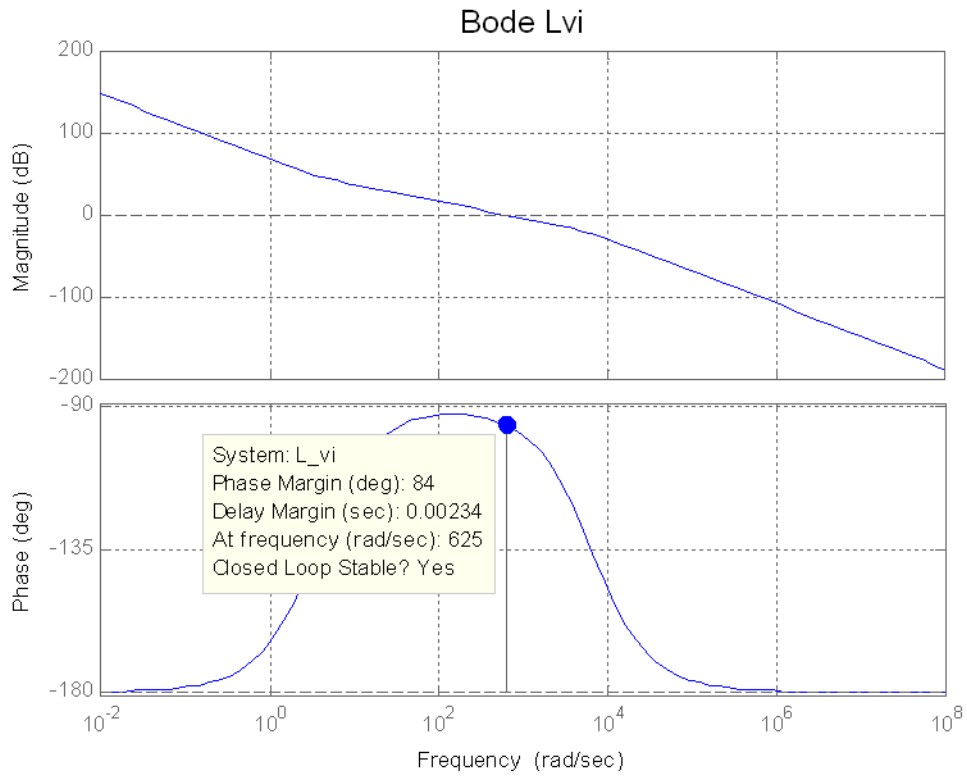


Figure 0.22 : Bode of Lvi (PI)

WITH ACTIVE DAMPING GA

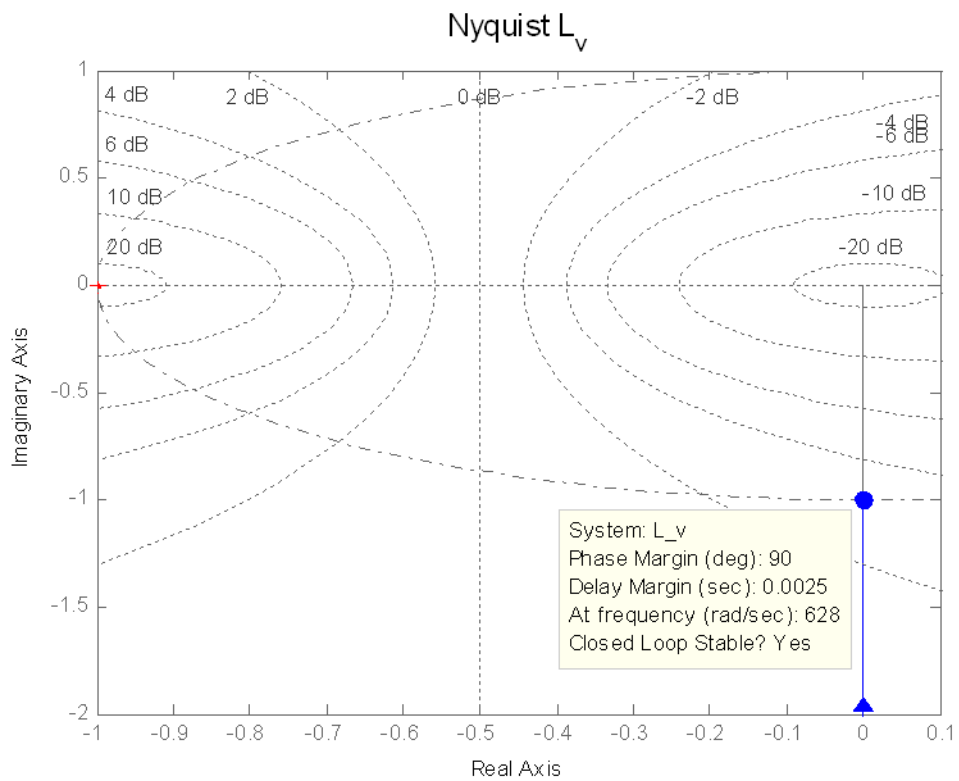


Figure 0.23 : Bode of Lv (PI Ga)

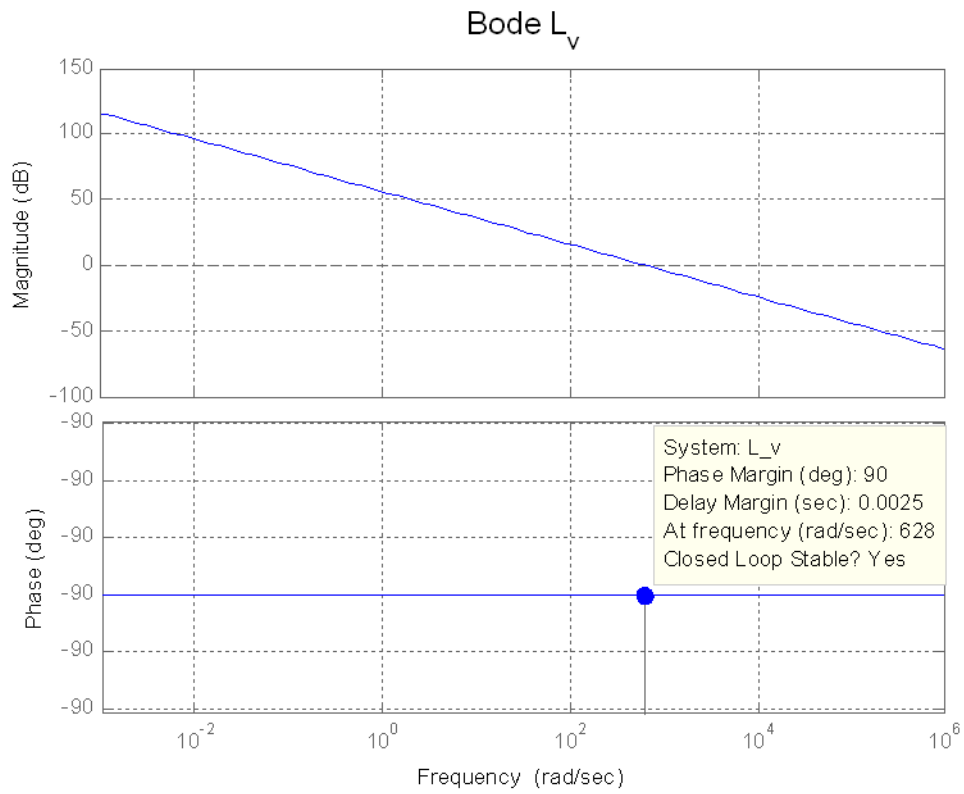


Figure 0.24 : Bode of L_v (PI Ga)

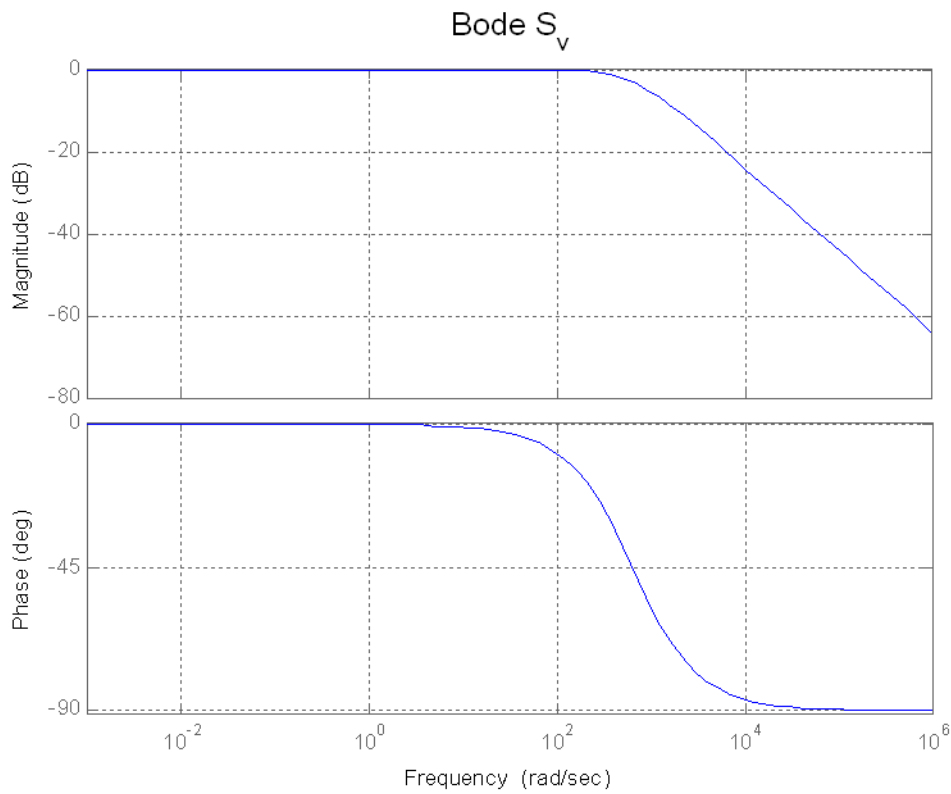


Figure 0.25 : Bode of S_v (PI Ga)

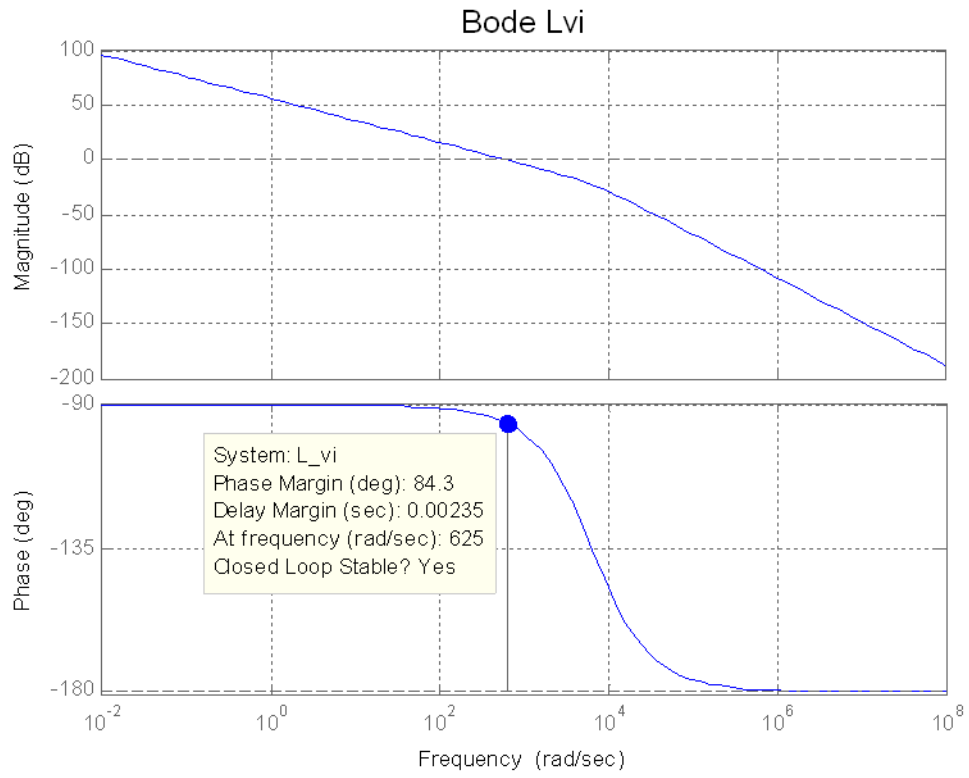


Figure 0.26 : Bode of Lvi (PI Ga)

F. Grid connected converter simulation cont.

F.1 Data and simulations

GRID	VALUE	PWM	VALUE
Frequency (Hz)	50	Triangular freq. F_c (kHz)	10
U_{RMS} (V), line-to-line RMS	400	Mode	Asymmetric
V_{RMS} (V), line-to-neutral RMS	230		
E_g (V), line-to-neutral amplitude	327	CONVERTER	VALUE
R_g (Ω), grid resistance	1e-3	R (Ω)	0.05
L_g (H), grid inductance	1e-5	L (H)	3e-3
		C (F)	2200e-6
BREAKER SW1	VALUE	F_{SW} (kHz), switching freq.= F_c	10
Rb_open (Ω)	1e5	R_{LOAD} (Ω)	150
Rb_close (Ω)	0.01	R_{LOAD_TEMP} (Ω)	1e5
Cac (nF)	1	V_{DCref} (V)	700
Closing at time... (s)	0.005	V_{DCref} STEP (V)	30
		Step at... (s)	0.025
IGBTs ON/OFF SIGNAL	VALUE	Power V_{DCref}^2/R_{LOAD} (W)	3267
IGBTs ON at time... (s)	0.01		
ON-state	1	CONTROLLER	VALUE
OFF-state	0	\hat{R} (Ω)	R
		\hat{L} (H)	L
PLL	VALUE	\hat{C} (F)	C
Bandwidth (Hz)	20	$\alpha_i = 2\pi F_S/10$ (rad/s)	1.2566e+004
Bandwidth ρ (rad/s)	125.6637	$\alpha_v = 2\pi F_S/100$ (rad/s)	1.2566e+003
γ_1	48.3510	Kp_i , current controller	37.6991
γ_2	0.7695	Ki_i , current controller	628.3185
		Kp_v , voltage controller	0.0028
DISCRETE SYSTEM	VALUE	Ki_v , voltage controller	0.01
Sample freq. $F_S = 2F_c$ (kHz)	20	Saturation current control (A)	± 15
Sample time T_S (s)	5e-005	Filter $\alpha_{ff} = \alpha_i/10$ (rad/s)	1.2566e+003
SIMULATION	VALUE		
Solver Step	Variable		
Step max	$1/(10F_{SW})$		
Faster solver	Ode23tb		
Tolerance	1e-3		

Table 0.3 : Parameters of simulation1

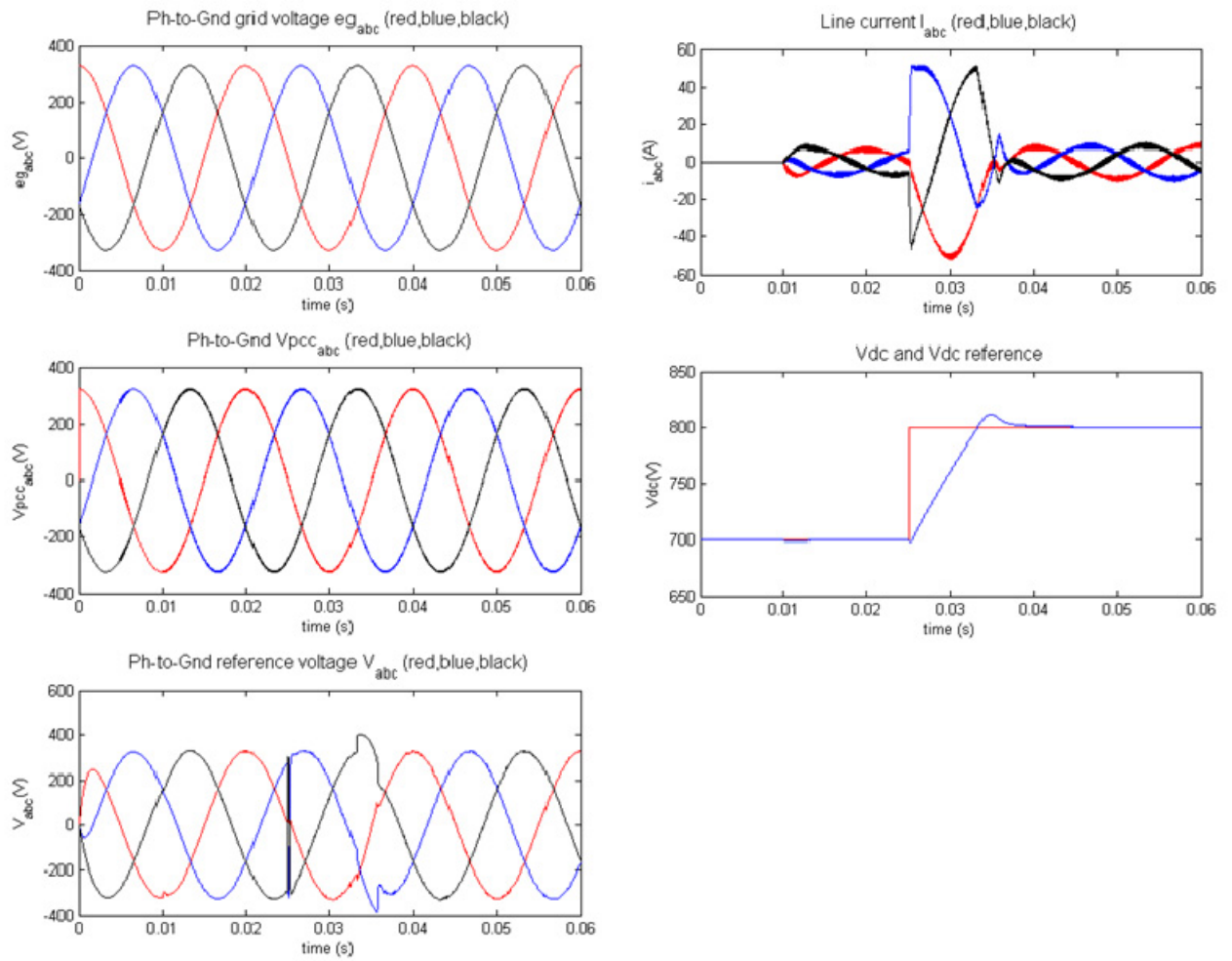


Figure 0.27 : Simulation1 – 100V Step on V_{Dcref} , saturation limit $\pm 50A$ (current controller)

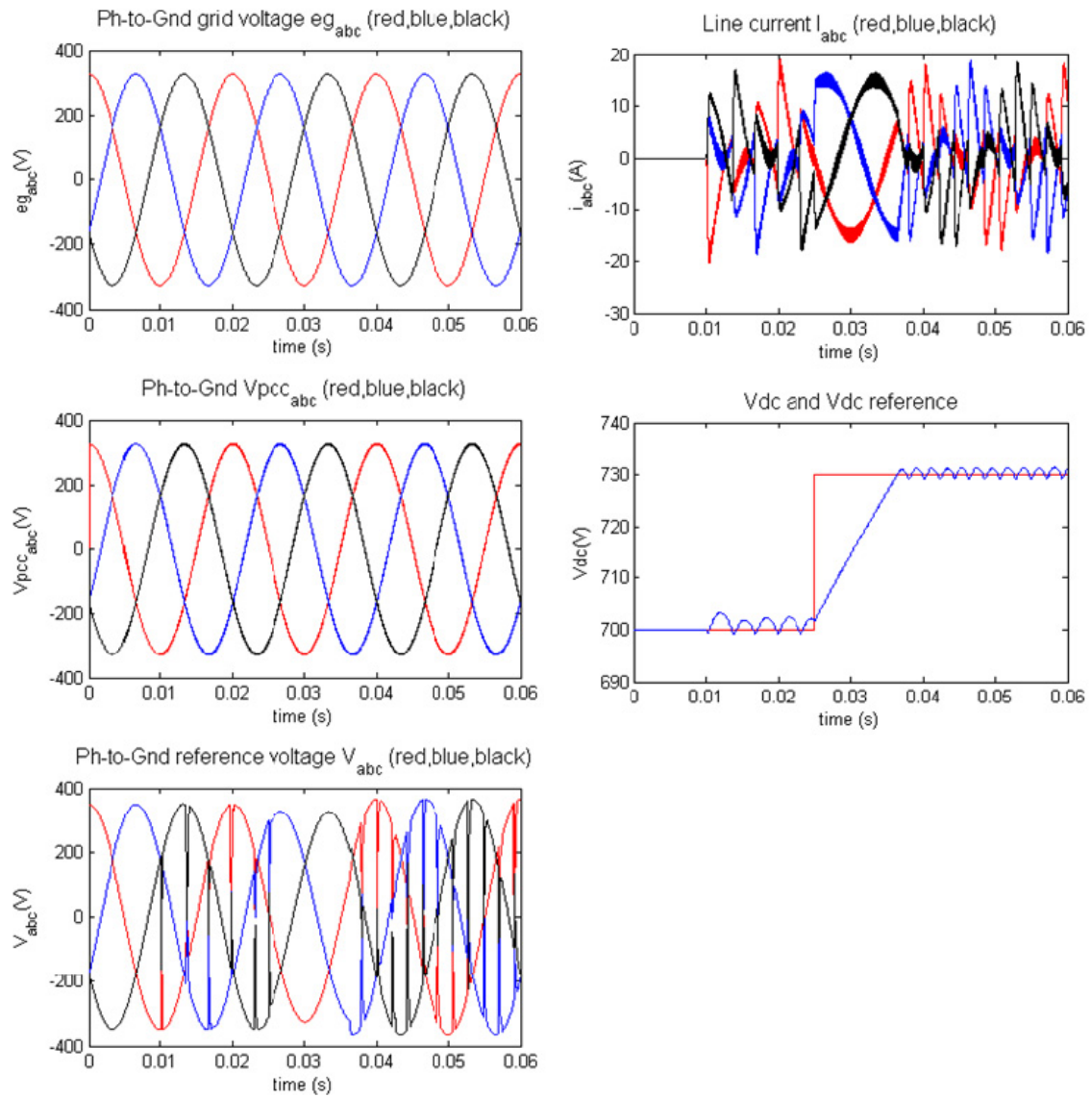


Figure 0.28 : Simulation4 with active damping

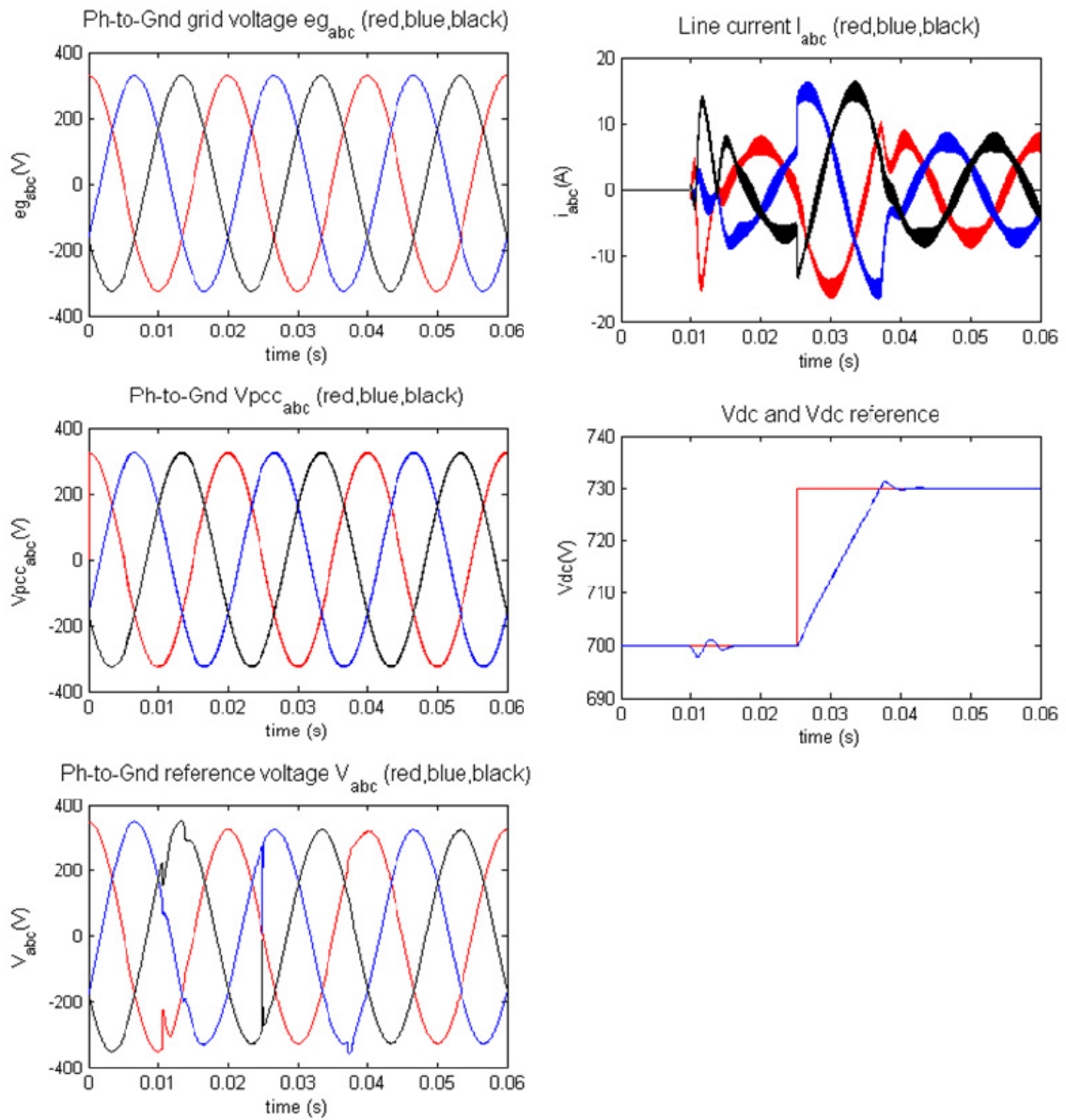


Figure 0.29 : *Simulation4 with active damping, modified controller parameters*

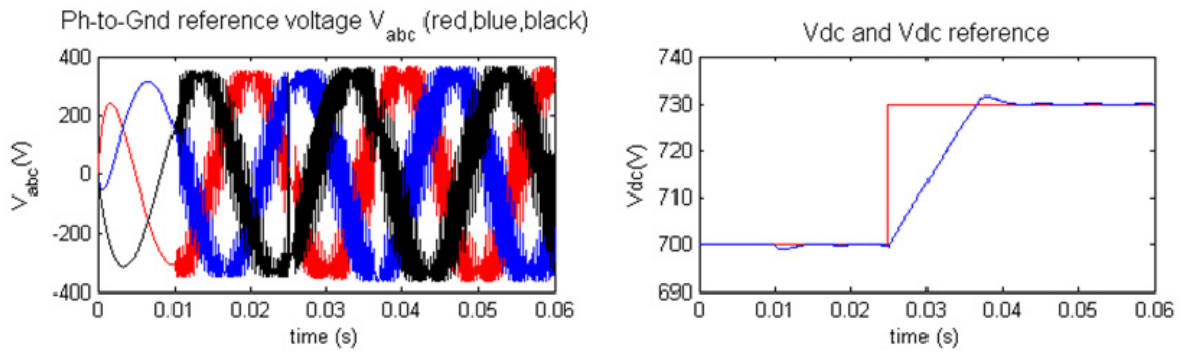


Figure 0.30 : Inductance influence – Test : $\hat{L} = L + 3L$

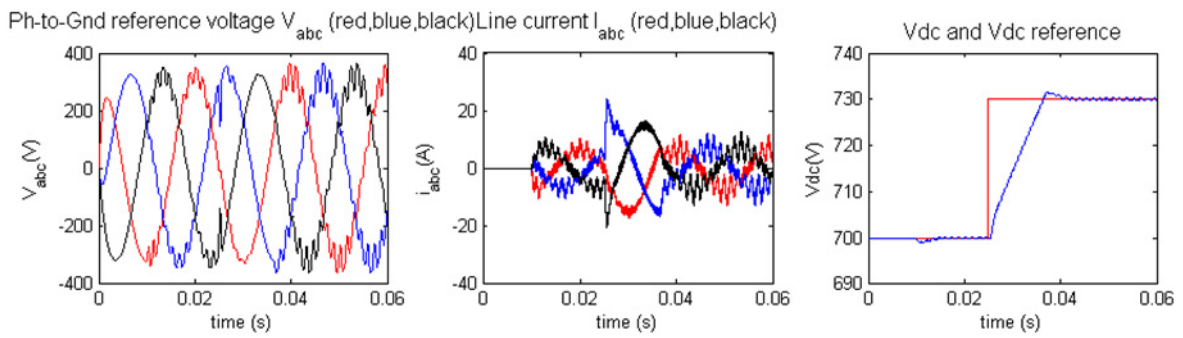


Figure 0.31 : Inductance influence – Test : $\hat{L} = L - 0.9L$

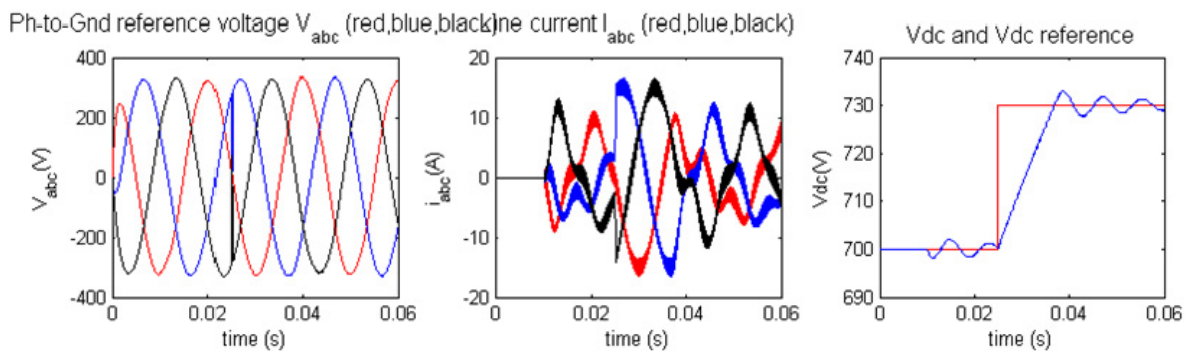


Figure 0.32 : Capacitor influence – Test : $\hat{C} = C - 0.9C$

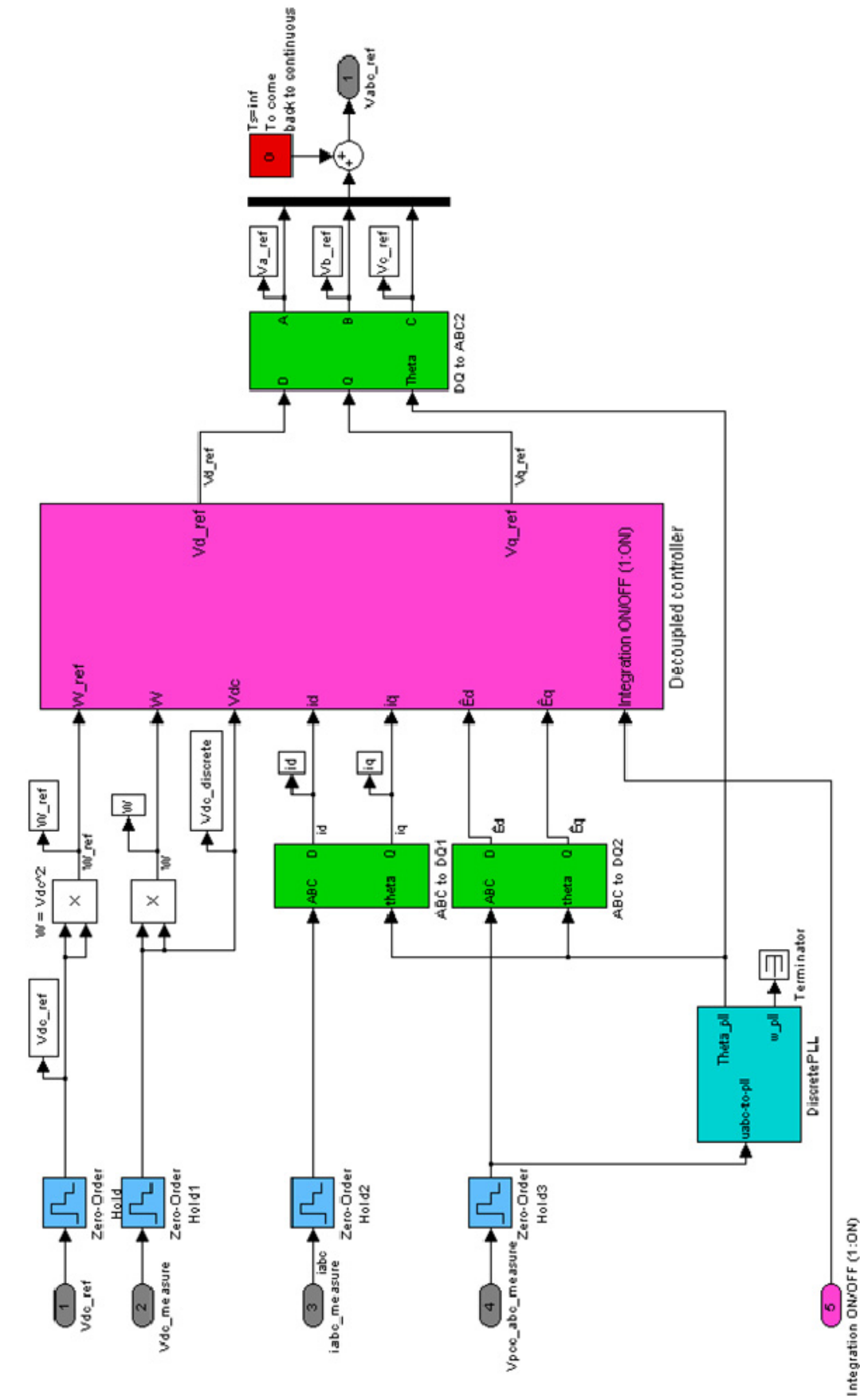


Figure 0.33 : Simulink – DISCRETE BLOC

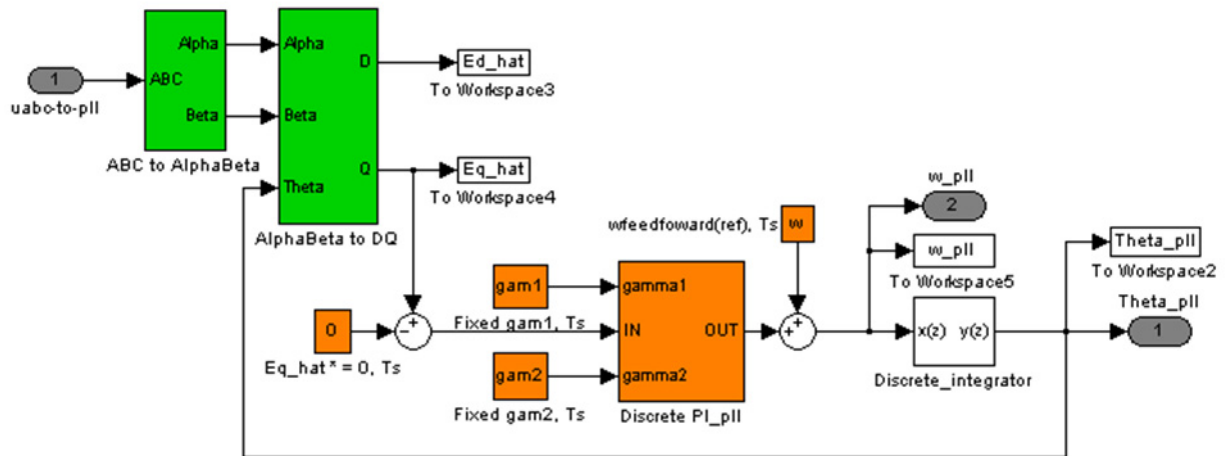


Figure 0.34 : Simulink – DISCRETE BLOCK / PLL

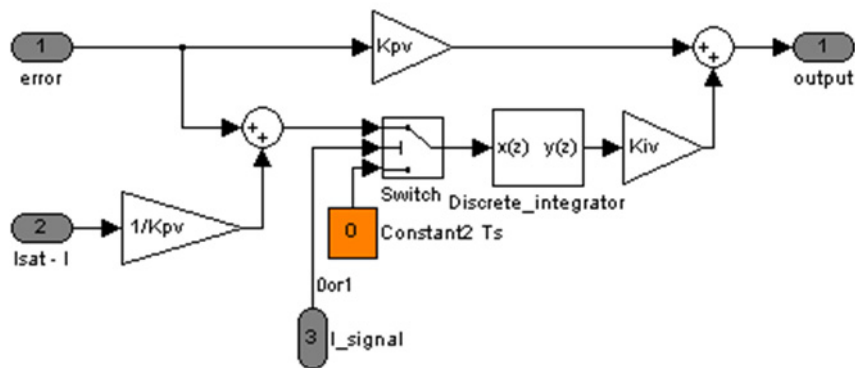


Figure 0.35 : Simulink – DISCRETE BLOCK / DECOUPLED CONTROLLER / Discrete PI V Controller

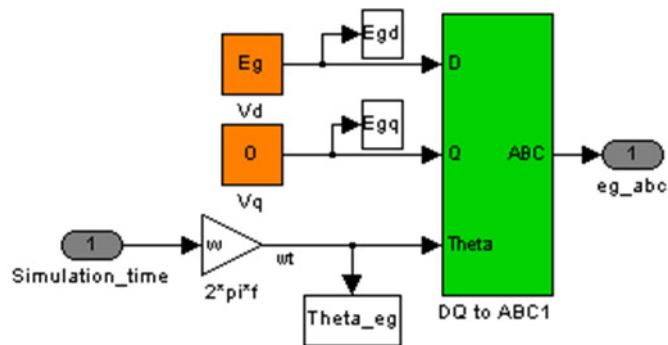


Figure 0.36 : Simulink – GRID AND RECTIFIER MODEL / eg_abc

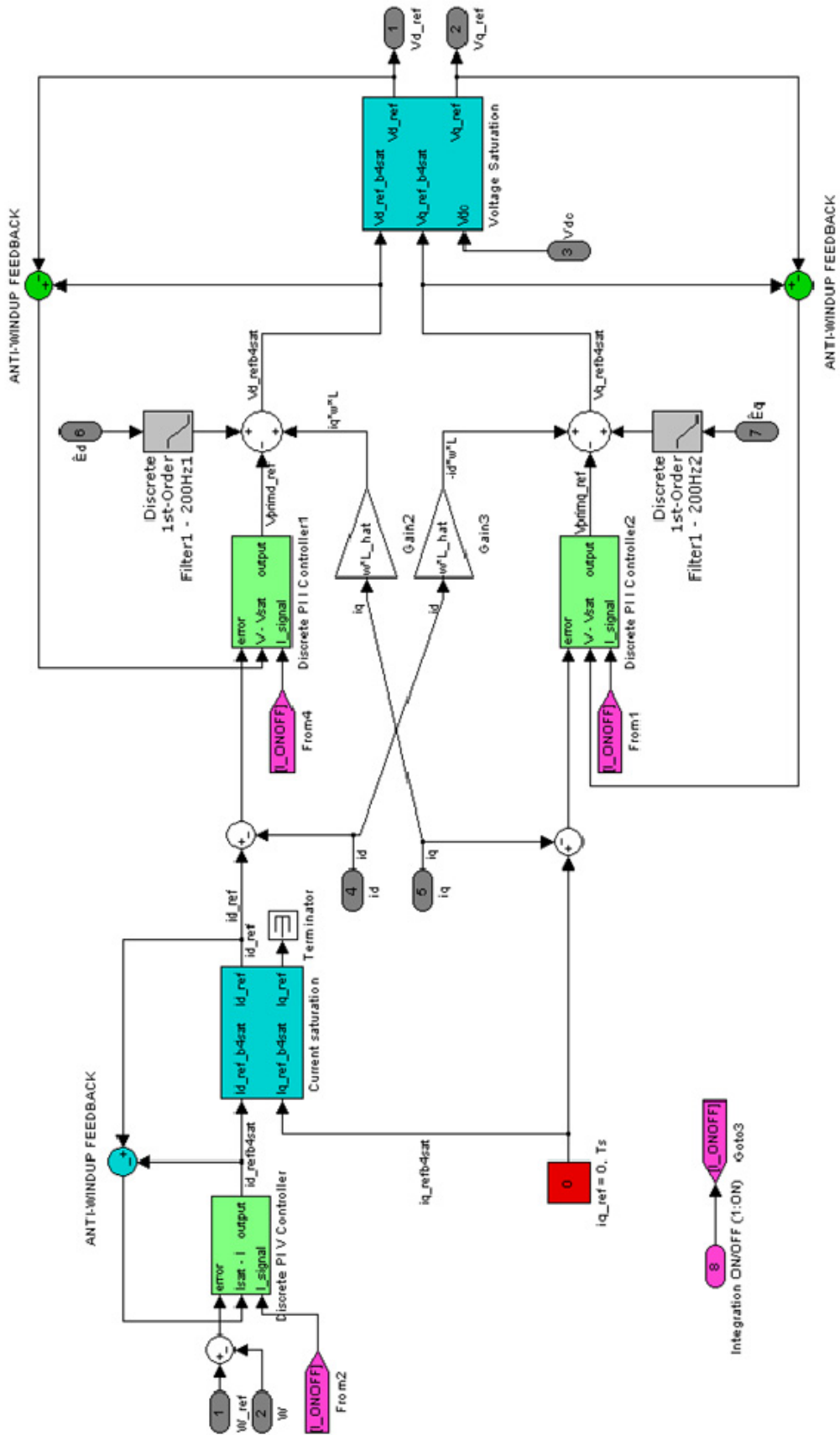


Figure 0.37 : Simulink – DISCRETE BLOCK / Decoupled Controller

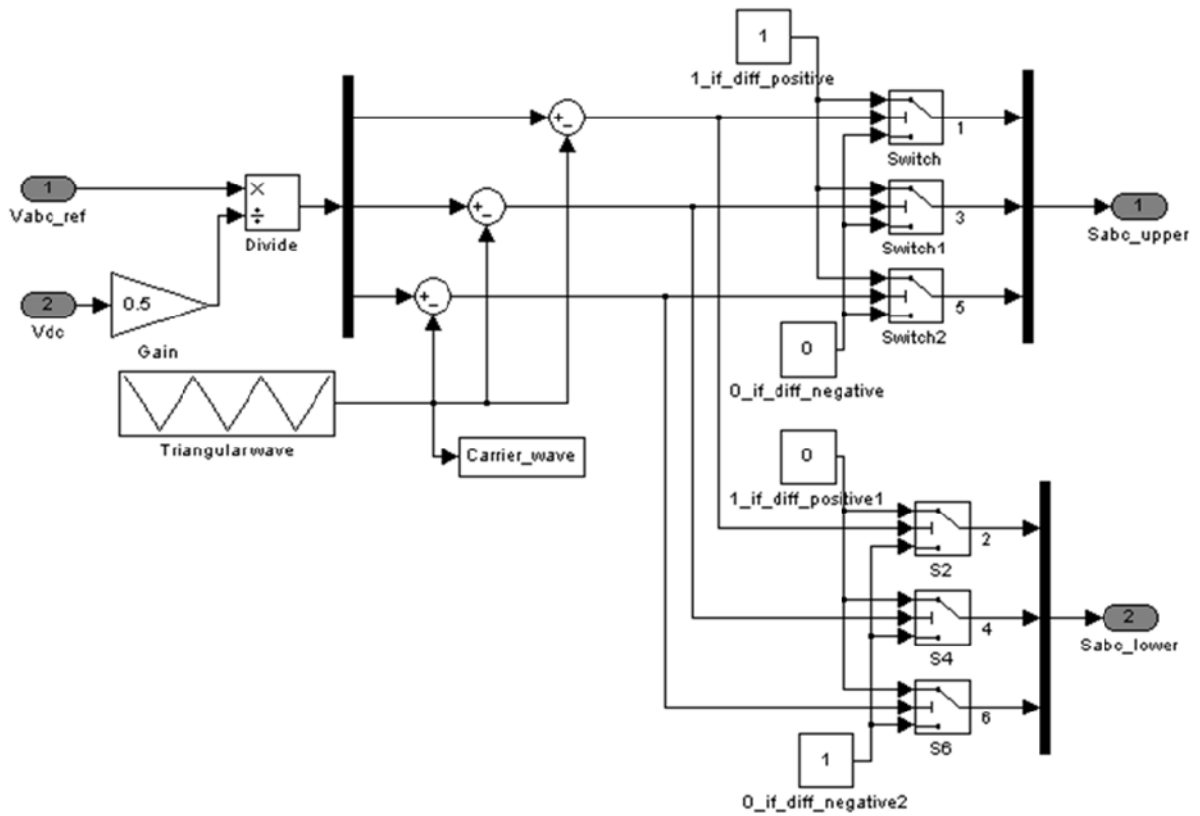


Figure 0.38 : Simulink – PWM block

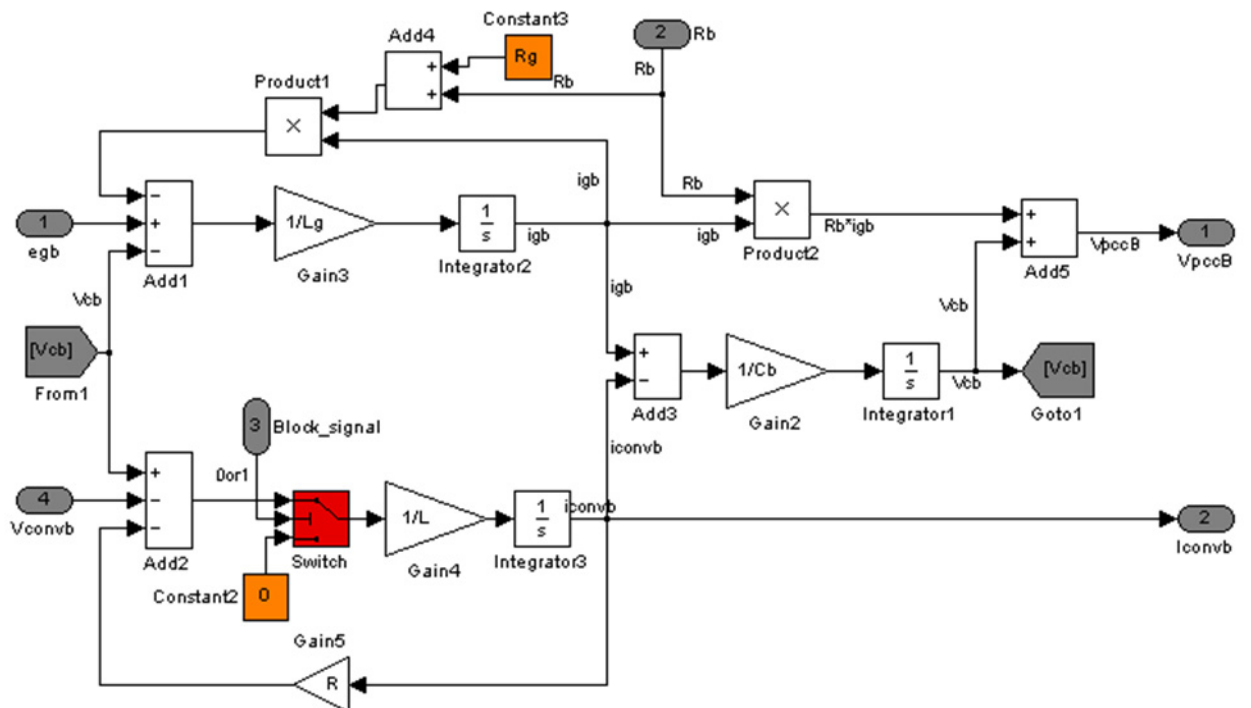


Figure 0.39 : Simulink – GRID AND RECTIFIER MODEL / GridPhaseB

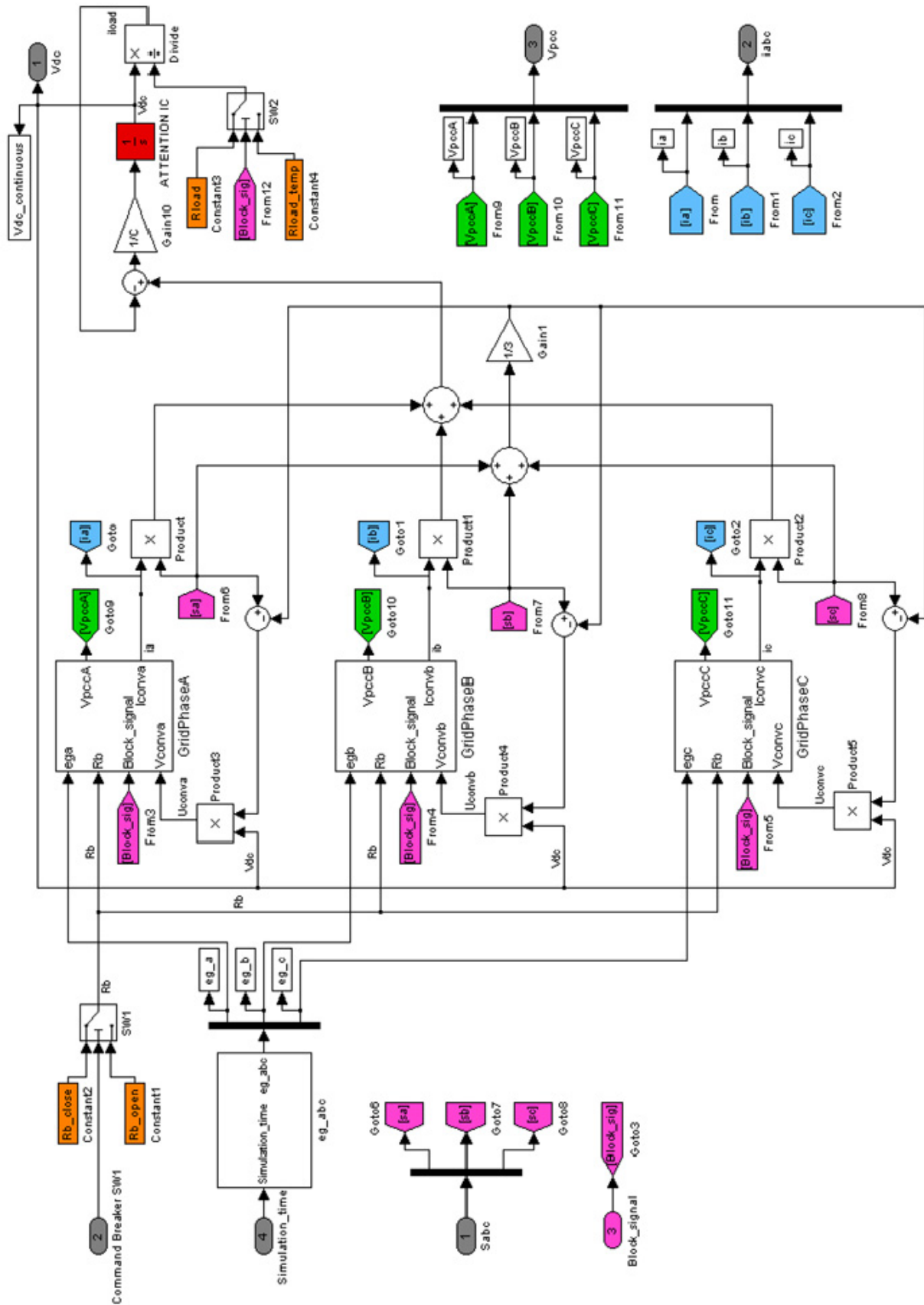


Figure 0.40 : Simulink – GRID AND RECTIFIER MODEL

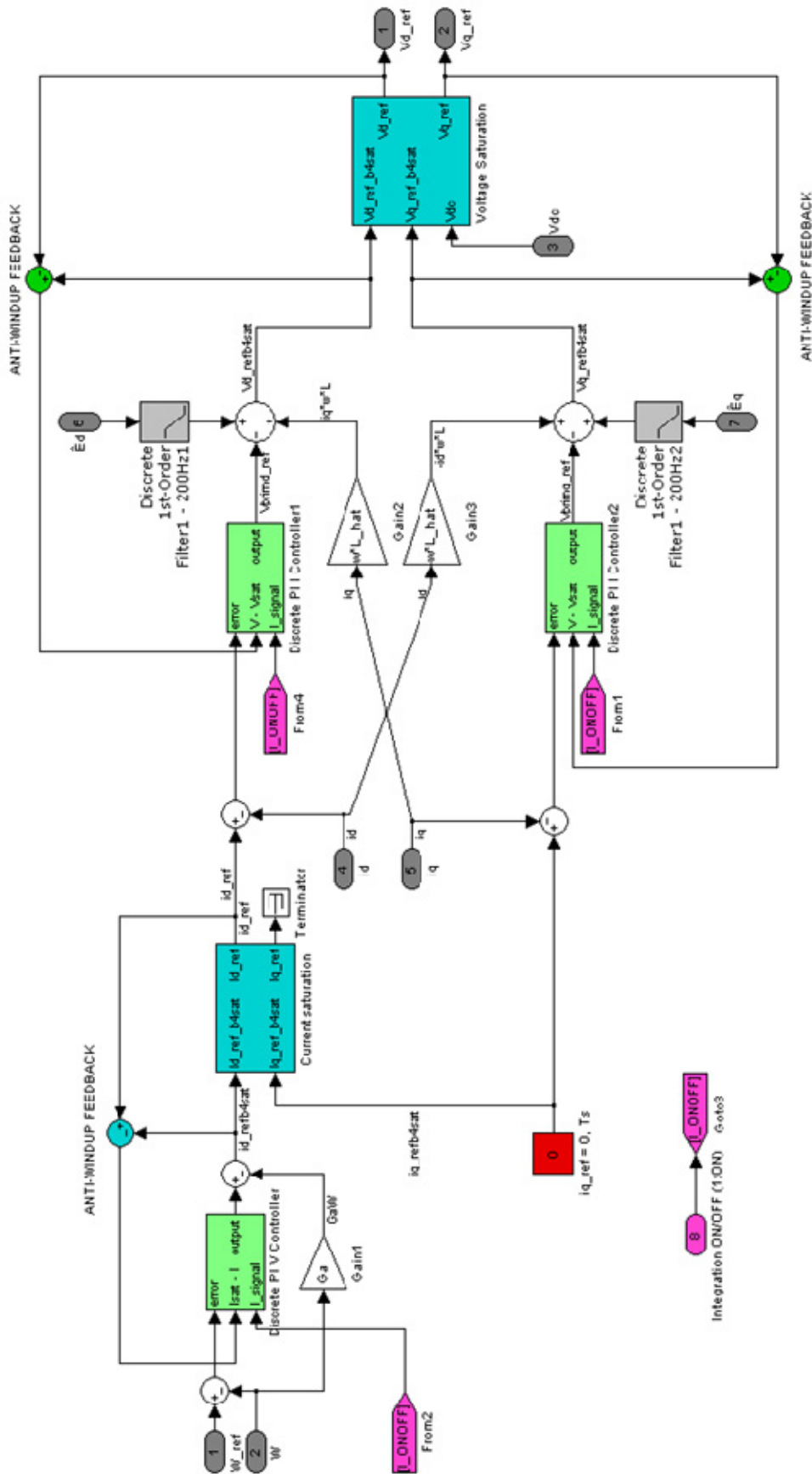


Figure 0.41 : Simulink – DISCRETE BLOCK / Decoupled Controller with active damping

F.2 Matlab Script (Vdc Step)

```

close all; clear all; clc

%*****
% GRID / BREAKER / COMMAND
%*****
grid_f = 50;
w = 2*pi*grid_f;    % Line frequency
Urms = 400;         % Line-to-line RMS voltage
Vrms = 400/sqrt(3); % Line-to-ground RMS voltage
Eg = Vrms*sqrt(2)   % Phase-to-ground voltage amplitude
Rg = 1e-3;          % 1e-2
Lg = 1e-5;          % 1e-4

%BREAKER
Rb_open = 1e5;      %ATTENTION VALUE
Rb_close = 0.01;
Cb = 1e-9; %Cac - ATTENTION VALUE (NEED DESIGN FILTER, avoid resonance
frequency)

%STEP breaker SW1 command : 0/1
breaker_step_time = 0.005; %Close switch at...
breaker_initial_value = 0;
breaker_final_value = 1;    %Or more than 0

%IGBTs ON/OFF SIGNAL (To activate switching)
IGBTONOFF_step_time = 0.01;
IGBTONOFF_initial_value = 0;
IGBTONOFF_final_value = 1;

%*****
% CARRIER BASED PWM PARAMETERS
%*****
Carrier_amp = 1;    % Triangular wave Amplitude
Carrier_f = 10e3;   % Triangular wave frequency = Fsw
Tc = 1/Carrier_f;   % Triangular wave period

%*****
% CONVERTER PARAMETERS
%*****
R = 0.05;           % Line Resistance
L = 3e-3;           % Line inductance
C = 2200e-6;        % DC bus capacitor
Fsw = Carrier_f;    % Converter switching frequency = Triangular wave f
Rload = 150;         % Output load, Pout about 800W
Rload_temp = 1e5;   % Temporary output load to avoid discharge of C
Vdc_ref = 700;      % Output voltage reference
initial_condition_integrator = Vdc_ref; % IC model integrator

```

```

%*****
% CONTROLLER PARAMETERS
%*****
Ts = 0.5*Tc; % Sample time, half of triangular wave period, Fs = 2*Fc
Fs = 1/Ts;

%ESTIMATED PARAMETERS
R_hat = R;
L_hat = L;
C_hat = C; % probably, C_hat = C OK
Vpcc_hat = Eg ; % Ph-to-gnd - Possible for stiff grid, otherwise, Vpcc <
Eg

%CURRENT PI Regulator (thesis, state-variable W=Vdc^2)
alphaI = Fs/10*2*pi; % Bandwidth in rad/s
Kpi = alphaI*L_hat
Kii = alphaI*R_hat

%VOLTAGE PI Regulator (thesis, state-variable W=Vdc^2)
alphaV = Fs/100*2*pi; % Bandwidth in rad/s
Kpv = alphaV*C_hat/(3*Vpcc_hat)
Kiv = 0.01

%SATURATION (TO MODIFY, depends on rectifier limit)
Isaturation_upper_limit = 50; %saturation on Iref, V PI controller
Isaturation_lower_limit = -50;

%FEEDFOWARD Ed_hat/Eq_hat FILTER
alphaf_ff = alphaI/10;

%*****
% PLL PARAMETERS
%*****
%Gain gammal&2 : calculated in simulink (we assume Ed_hat and Eq_hat can
change)
Fbandwidth_pll = 20; %bandwidth in Hz
rho_pll = 2*pi*Fbandwidth_pll; %bandwidth in rad/s
gam1 = (rho_pll^2)/Vpcc_hat
gam2 = 2*rho_pll/Vpcc_hat

%*****
% TESTS
%*****
%INPUT STEP
input_step_time = 0.025;
input_step_value = 100;

```


G. Implementation

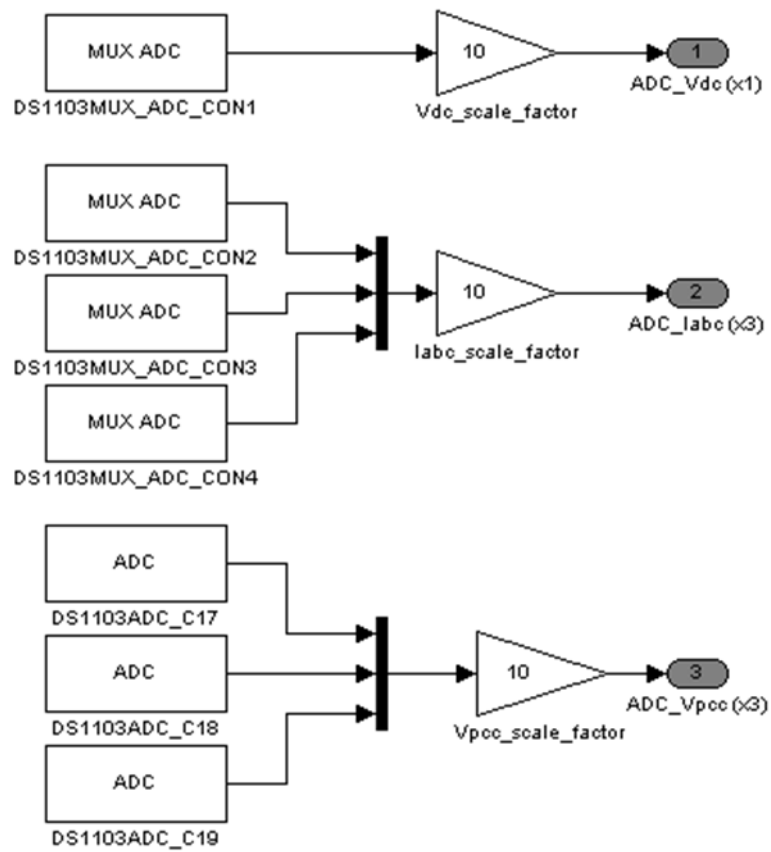


Figure 0.42 : ADC block

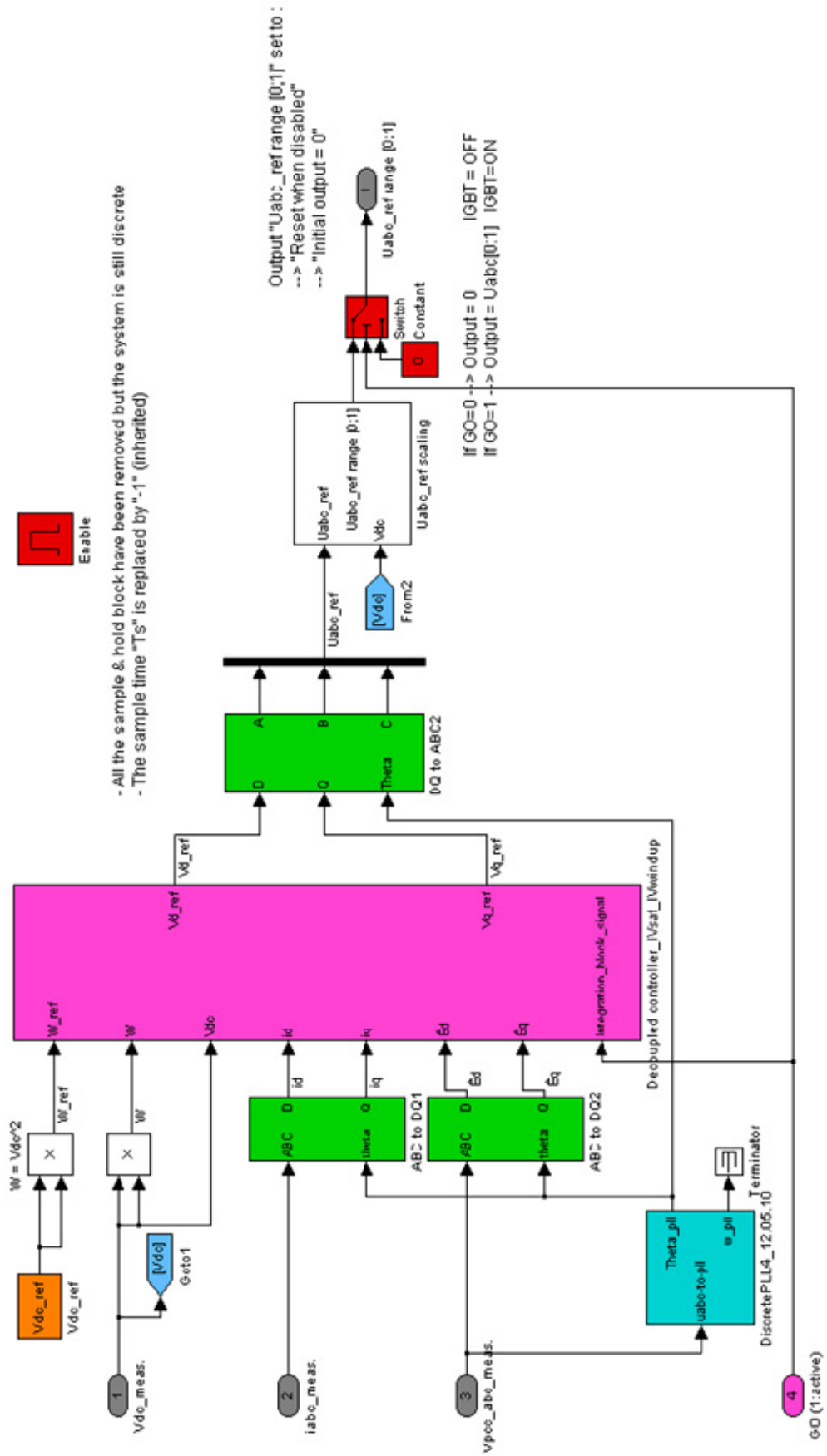


Figure 0.43 : Control block